COO-2250-26
MITNE-200

RESONANCE REGION NEUTRONICS OF UNIT CELLS IN FAST AND THERMAL REACTORS

by

A. A. Salehi
M. J. Driscoll
O. L. Deutsch

May 1977

Massachusetts Institute of Technology
Department of Nuclear Engineering
Cambridge, Massachusetts

ERDA Research and Development

Contract E(11-1)-2250
UC-79P LMFBR - Physics

U. S. Energy Research and Development Administration

Massachusetts Institute of Technology
Department of Nuclear Engineering
Cambridge, Massachusetts

RESONANCE REGION NEUTRONICS OF UNIT CELLS IN FAST AND THERMAL REACTORS

by

A.A. Salehi
M.J. Driscoll
O.L. Deutsch

May 1977

COO-2250-26

MITNE-200

ERDA Research and Development

Contract E(11-1)-2250

UC-79P LMFBR - Physics

U.S. Energy Research and Development Administration

"This report was prepared as an account of Government-sponsored work. Neither the United States, or the Energy Research and Development Administration nor any person acting on behalf of the Commission

A. Makes any warranty or representation, expressed or implied, with respect to the accuracy, completeness or usefulness of the information contained in this report, or that the use of any information, apparatus method, or process disclosed in this report may not infringe privately owned rights; or

B. Assumes any liabilities with respect to the use of, or for damages resulting from the use of, any information, apparatus, method, or process disclosed in this report.

As used in the above, 'person acting on behalf of the Commission' includes any employee or contractor of the Administration or employee of such contractor, to the extent that such employee or contractor prepares, disseminates, or provides access to, any information pursuant to his employment or contract with the Administration or his employment with such contractor."

DISTRIBUTION

COO-2250-26 MITNE-200

ERDA Research and Development Contracts

E(11-1)-2250

UC-79P LMFBR - Physics

Copies

1-3 U.S. Energy Research and Development Administration
Division of Reactor Development and Technology
Reactor Physics Branch
Washington, D.C. 20545

4-9 U.S. Energy Research and Development Administration
Chicago Operations Office
9800 South Cass Avenue
Argonne, Illinios 60439
(for distribution in accordance with Category UC-79P)

10 Director, Nuclear Power
Electric Power Research Institute
Post Office Box 10412
Palo Alto, California 94303

ABSTRACT

A method has been developed for generating resonance-self-shielded cross sections based upon an improved equivalence theorem, which appears to allow extension of the self-shielding-factor (Bondarenko f-factor) method, now mainly applied to fast reactors, to thermal reactors as well.

The method is based on the use of simple prescriptions for the ratio of coolant-to-fuel region-averaged fluxes, in the equations defining cell averaged cross sections. Linearization of the dependence of these functions on absorber optical thickness is found to be a necessary and sufficient condition for the existence of an equivalence theorem. Results are given for cylindrical, spherical and slab geometries. The functional form of the flux ratio relations is developed from theoretical considerations, but some of the parameters are adjusted to force-fit numerical results. Good agreement over the entire range of fuel and coolant optical thicknesses is demonstrated with numerical results calculated using the ANISN program in the S_8P_1 option. Wider application of these prescriptions, to fast and thermal group applications, is suggested.

The present results are shown to include the Dancoff approximation and Levine factor results, developed previously for thermal reactors, as limiting cases. The theoretical desirability of correcting for the effects of neutron moderation in the fuel region of fast reactor unit cells is demonstrated: a refinement not required in thermal reactors.

The method is applied to U-238 self-shielding in thermal and fast reactor applications. Heterogeneity corrections in fast reactors are so small that the method is not severely tested. Calculations of PWR unit cells are compared with LEOPARD program calculations. Epithermal group cross sections for U-238 calculated from the LIB-IV fast reactor cross section set using the present method agree with the LEOPARD results within about $\pm 1\%$ for typical PWR lattices; and while disagreement is larger for larger and smaller unit cells, all of the qualitative features of group cross section dependence are in agreement.

ACKNOWLEDGEMENTS

The work described in this report has been performed primarily by the principal author, A. Salehi, who has submitted substantially the same report in partial fulfillment of the requirements for the Ph.D. degree at MIT.

The work was performed under two ERDA sponsored projects: one involving work on fast reactor blanket physics, Contract E(11-1)-2250, under which it is being published, and the other involving assessment of the use of thorium in improved PWR's, being carried out at MIT through block grant funding provided via the MIT Energy Laboratory. Computer calculations were carried out at the MIT Information Processing Center and at the Laboratory for Nuclear Science. Ms. R. Morton provided assistance and advice on computational problems.

Typing of this manuscript has been very ably handled by Ms. Maggie Houghton.

TABLE OF CONTENTS

LIST OF TABLES

LIST OF FIGURES

Chapter 1

INTRODUCTION

1.1 FOREWORD

An essential step in most reactor physics calculations is the replacement of heterogeneous regions by equivalent homogeneous regions, one of the more important examples being unit cell homogenization. The method most widely applied for use in the homogenization process is the well-known "equivalence theory" approach in which prescriptions for obtaining heterogeneous results from the corresponding homogeneous resonance integrals are defined (D2, H1, L4, M2). The results of applying this technique to the strong resonance absorption in fertile species are, however, still not satisfactory, and state of the art LWR computer methods, such as LEOPARD, presently rely upon normalization to an experimental base (L5). Past work at MIT on conventional and moderated LMFBR blanket designs motivated concern over the adequacy of both fast and thermal reactor based methods to deal with this problem. Recently initiated work on tight-pitch PWR lattices has increased the priority assigned to resolution of this uncertainty. Very little work has been done on strongly epithermal systems of the above types since the Naval Reactors efforts of the early 1950's (S8). Furthermore, in the work completed by Kadiroglu (K1) (and prior to him by Gregory (G1)) at MIT, the general groundwork for a new approach has been

laid down. The purpose of the research reported herein is, therefore, to extend, to evaluate and to fully exploit this new methodology. A secondary objective will be to unify the hitherto separate approaches developed for fast and thermal reactor applications.

1.2 BACKGROUND AND PREVIOUS WORK

Development of the method of equivalence theory was a major step towards facilitating the process of unit cell homogenization. The method is based on the following two theorems (D1, D2, F6, to cite a few):

(i) Heterogeneous systems with the same σ_0' have equal resonance integrals.

(II) A heterogeneous system will have the same resonance integral as a homogeneous system evaluated at σ_0'.

where

$$\sigma_0' = \frac{\bar{\Sigma}_{tnf}}{\bar{N}_f} + \frac{1}{1+\frac{1}{a}\tau_{tm}} \frac{\bar{\Sigma}_{tm}}{\bar{N}_f}, \qquad (1.1)$$

is the modified constant "background" cross section per target nucleus f

$\bar{\Sigma}_{tnf}$ = volume-homogenized total cross section of the non-resonance elements admixed with the fuel

$\bar{\Sigma}_{tm}$ = volume-homogenized total cross section of the nuclides in the moderator/coolant region

$\bar{N}_f$ = volume-homogenized number density of the resonance absorber nuclei

a = is the Levine correction factor (L2)

τ_{tm} = total optical thickness of the moderator - see Eq. (1.7)

The key to this method is the use of the concept of collision or escape probabilities - that is, the probability that a neutron originating in one region will make its next collision in another region; this, in effect, allows one to separate the treatment of the spatial and energy variables in the study of neutron slowing down in the cell. Furthermore, to correct for the effect of absorber lump interferences, it is necessary to use the concept of rod shadowing (D1, D2) - that is, fewer neutrons are incident on the part of the lump that faces another lump than on the part that faces only moderator. To account for this fact an effective surface area S_{eff} is introduced and defined as (F6):

$$S_{eff} = S(1-\mathbf{c}) \tag{1.2}$$

where

(1-**c**) is the "Dancoff-correction"

c is the Dancoff-Ginsberg factor

S is the lump surface area.

The inability of the method, however, to predict sufficiently accurate equivalent homogenized cross sections was immediately apparent. As a result, there has been a continuing effort aimed at improvement (B1, C2, F3, G3, G4, K2, K3, L3, S1, S2, S3, T1), concentrating mainly on developing more accurate expressions for the required escape probabilities and the associated Dancoff factor. Although substantial improvements have been incorporated into the method, the desired accuracy has yet to be achieved (F3, K3, L2, L3, S2). Among recent investigations, the work of Kirby and Karam (K2) is of interest here, as they have shown that the long-standing and controversial flat-flux assumption is not the source of the discrepancy between the conventionally-predicted and experimentally-obtained results. This in turn emphasizes the need for a somewhat different and more fundamental approach.

In what follows, we will have to preview certain expressions and some results developed in more detail in later chapters, for the purpose of explaining the features of the new approach, and contrasting them to the corresponding features of the conventional approach. Let us, therefore, start with the hopefully familiar, and rigorous, definition of the equivalent homogenized cross section (H1).

$$\sigma_{xg}^{\ j} = \frac{\int_{\Delta Eg} \sigma_x^{\ j}(E,T)\bar{\phi}_f(E,T,\sigma_0)dE}{\int_{\Delta Eg}\left[\frac{V_f}{V_{cell}}\bar{\phi}_f(E,T,\sigma_0)+\frac{V_m}{V_{cell}}\bar{\phi}_m(E,T,\sigma_0)\right]dE} \qquad (1.3)$$

or

$$\sigma_{xg}^{j} = \frac{\int_{\Delta Eg} \sigma_x^j(E,T)\bar{\phi}_f(E,T,\sigma_0)dE}{\int_{\Delta Eg} [\frac{V_f}{V_{cell}} + \frac{V_m}{V_{cell}} R]\bar{\phi}_f(E,T,\sigma_0)dE} \qquad (1.4)$$

where

x = particular process (e.g. capture, fission, scattering);

j = isotope index;

g = energy group index;

T = temperature;

ΔEg = energy group width; here chosen so as to contain but a single resonance

$$\sigma_0 = \frac{\bar{\Sigma}_{tnf}}{\bar{N}_j} + \frac{\bar{\Sigma}_{tm}}{\bar{N}_j} \qquad (1.5)$$

is the constant "background" cross section per target nucleus j

$\bar{\Sigma}_{tnf}$, $\bar{\Sigma}_{tm}$, $\bar{N}_j$ are as previously defined

$R \equiv \frac{\bar{\phi}_m(E,T,\sigma_0)}{\bar{\phi}_f(E,T,\sigma_0)}$, is what we have defined as the flux ratio

To be able to evaluate Eq. (1.3) rigorously one would need to have the correct expressions for $\bar{\phi}_f$ and $\bar{\phi}_m$. Although approximate forms for the above fluxes are available in terms of escape probabilities (H1), their direct use in Eq. (1.3) is an extraordinarily complicated prospect. Instead, what

is conventionally done for the purpose of obtaining "equivalent homogenized" cross-sections is as follows:

(1) first a homogeneous version of Eq. (1.3) is considered:

$$\sigma_{xg}^{j} = \frac{\int_{\Delta Eg} \sigma_x^{j}(E,T)\phi^{hom}(E,T,\sigma_0)dE}{\int_{\Delta Eg} \phi^{hom}(E,T,\sigma_0)dE} \qquad (1.6)$$

(2) next the "second equivalence theorem" - which basically involves replacing σ_0 by a properly modified value, σ_0', is applied to Eq. (1.6) to obtain the required "equivalent homogenized" cross section.

The practice of replacing the true integrated heterogeneous flux, as given by the denominator of Eqs. (1.3) and/or (1.4), by a homogeneous flux evaluated at σ_0' is at best a very crude and approximate approach.

In the present work a different approach, aimed at evaluating Eq. (1.2) as it stands, is proposed. The key to practical exploitation of this approach is development of a simple prescription for the flux ratio, R(E); this task will constitute a major portion of the present study.

As will be shown later, the above flux ratio has the following form:

$$R \equiv \frac{\bar{\phi}_m(E)}{\bar{\phi}_f(E)} = \frac{1+F(\tau_{af},\tau_{am},\tau_{sf},\tau_{sm})\cdot\tau_{af}(E)\ Q_m}{1+F(\tau_{am},\tau_{af},\tau_{sm},\tau_{sf})\cdot\tau_{am}(E)\ Q_f} \qquad (1.7)$$

where

$\tau_{xi} = \Sigma_x(E) \cdot \ell_i$, the optical thickness for process x in region i

ℓ_i = mean Dirac penetration chord length through region i

$\Sigma_x = \sum_j \Sigma_x^j$ macroscopic cross section summed over all j isotopes in the region i (fuel, f, or moderator, m)

$Q_m(E)$ = fraction of neutron source originating in the moderator

$Q_f(E)$ = fraction of neutron source originating in the fuel

Analytic expressions for R have been derived for cylindrical unit cells for small τ_{af} and τ_{am} by Gregory (G1); and for large τ_{af} by Kadiroglu (K1): they obtained for the function F lower and upper asymptotic values of 1/3 and 2/3, respectively. A major contribution of the present work will be development of an expression for F which accurately joins the two asymptotic values [1/3,2/3]. Similar analyses will also be carried out for other unit cell geometries of interest: the sphere and the slab.

A key feature of the present methodology is that it handles cases not easily dealt with conventionally - e.g. when fuel moderation is not negligible compared to that of the coolant and/or moderator (i.e. $Q_f \neq 0$), as is true in fast reactor applications. This permits satisfaction of one goal of the present work, which is the development of a unified method, both simple and accurate, for treating the heterogeneity corrections pertaining to both fast and thermal reactors.

1.3 OUTLINE

The body of the report which follows parallels in its organization the sequence suggested by the preceding discussion. In Chapter 2 simple analytic expressions for R, the ratio of the spatially-averaged coolant-to-fuel fluxes, suitable for future applications, are developed. Next in Chapter 3, so-called homogeneous self-shielding is reviewed to develop the basic concepts necessary for subsequent extension of the methodology to heterogeneous media to obtain a new equivalence relation (see Sections 3.3.2 and 3.3.3). Finally, results obtained using the new methodology are checked against the results of the LEOPARD Code (L5) when applied to U-238 capture in a typical PWR unit cell. In Chapter 4 the far less prominent effects of heterogeneity in fast reactors are investigated. An approximate equivalence relation is derived which explicitly accounts for the effect of moderation in the fuel; this expression is essentially identical to the one derived by Kadiroglu (K1) via basically different arguments. The concluding chapter, 5, summarizes the work and proposes follow-on research. Finally, there are appendices which contain tabulated results, subsidiary derivations, discussions, and numerical examples.

Chapter 2

FLUX RATIOS IN UNIT CELLS

2.1 INTRODUCTION

As noted in Chapter 1, the key to the approach analyzed in the present work is the use of simple analytic expressions for the ratio of coolant/moderator to fuel fluxes suitable for our future applications. In this chapter we will develop Flux Ratio Models for three different types of unit cells: cylindrical, slab, and spherical. In developing the models various techniques such as Escape Probability and Integral Transport methods will be used in conjunction with approximations such as those suggested by consideration of high and low optical thickness limits. Finally, the above models will be checked using numerical methods.

2.2 THE UNIT CELL

This section will deal, very briefly, with the definition and description of the three classes of unit cells mentioned above. Almost all reactor cores have a periodic structure in which one particular subelement, namely a fuel element with its adjacent coolant/moderator, is repeated throughout the core. This subelement is commonly called the unit cell. Most reactors, (LWR, LMFBR), have cylindrical fuel elements, hence cylindrical unit cells, but there are other reactors, (Pebble Bed, HTGR), with spherical unit cells. Finally, there are also reactors with thin slab-type fuel elements such as the familiar "Swimming Pool"

and related designs. Although actual cores are not precisely regular, but contain nonuniformities due to the presence of control rods, instrumentation devices, nonuniform fuel loadings and coolant/moderator densities, core boundaries and so on, for the purpose of the present work the core will be represented as an infinite array of identical lattice cells. The ultimate goal here is to obtain "cell-homogenized" equivalent group parameters such as Σ_{af}, Σ_{sf}, ... etc., which may be assumed constant over the volume occupied by any given unit cell. To achieve this goal a detailed calculation of the flux distribution in a given unit cell of the lattice is needed.

Since all unit cells are identical and the lattice infinite, there can be no net flow of neutrons from one cell to another, i.e., the net current vector $J(\underline{r},E)$ perpendicular to the outer surface of the cell vanishes (H1). Mathematically:

$$\vec{n}.\vec{J}(\vec{\underline{r}},E) = 0 \qquad (2.1)$$

for all points $\vec{\underline{r}}$ on the surface of the cell, where $\vec{n}$ is a unit vector normal to the surface of the cell.

To facilitate the flux calculation within a unit cell it is also necessary to replace the actual lattice cell by a simpler geometry - for example by cylindricalizing or sphericalizing the unit cells. The assumption of the zero-net current boundary condition together with the simplification of the cell geometry is known as the Wigner-Seitz method. Figures 2.1 and 2.2

m: moderator and/or coolant region
f: fuel region
c: clad region
g: gap

$r_1 \equiv r_{fuel}$
$r_2 \equiv r_{moderator}$
$r_3 \equiv r_{clad}$
$r_4 \equiv r_{gap}$

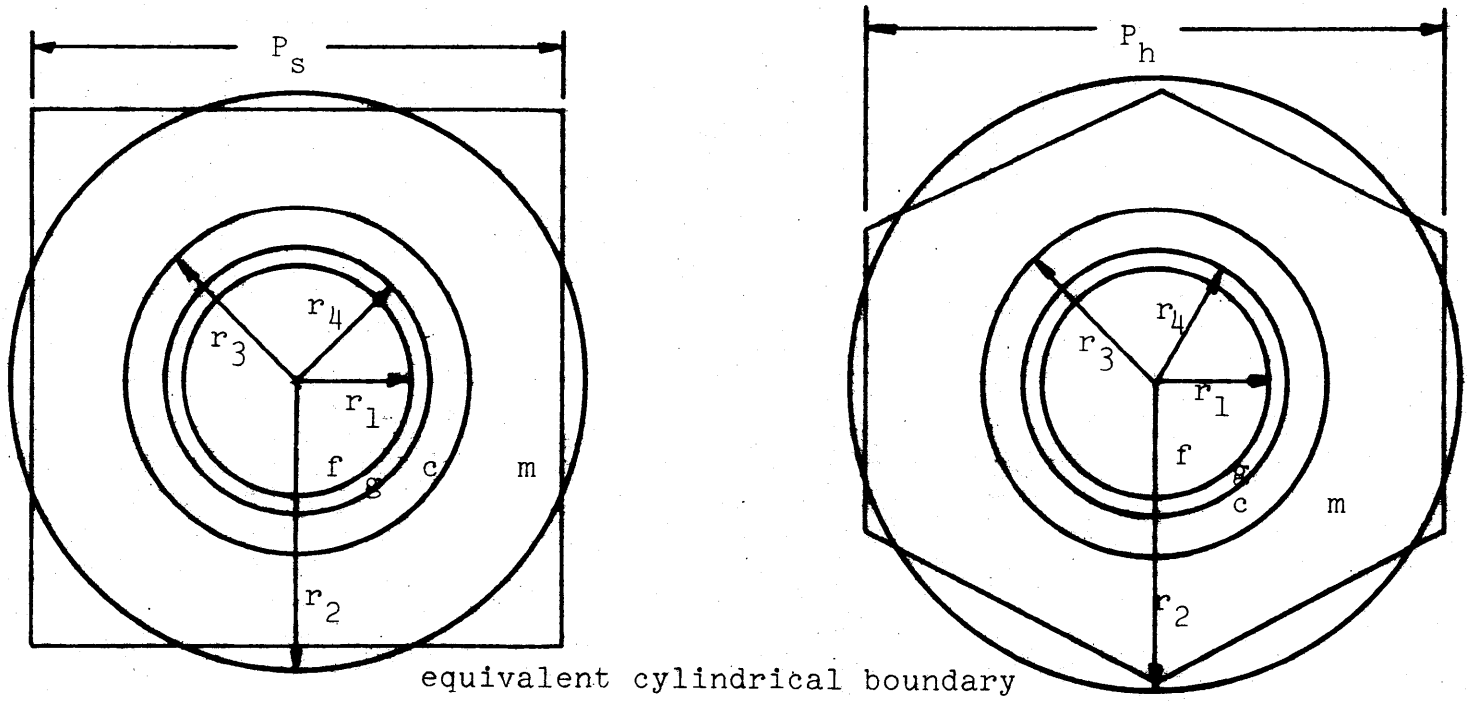

SQUARE LATTICE HEXAGONAL LATTICE

FIG. 2.1 STANDARD CYLINDRICAL UNIT CELL

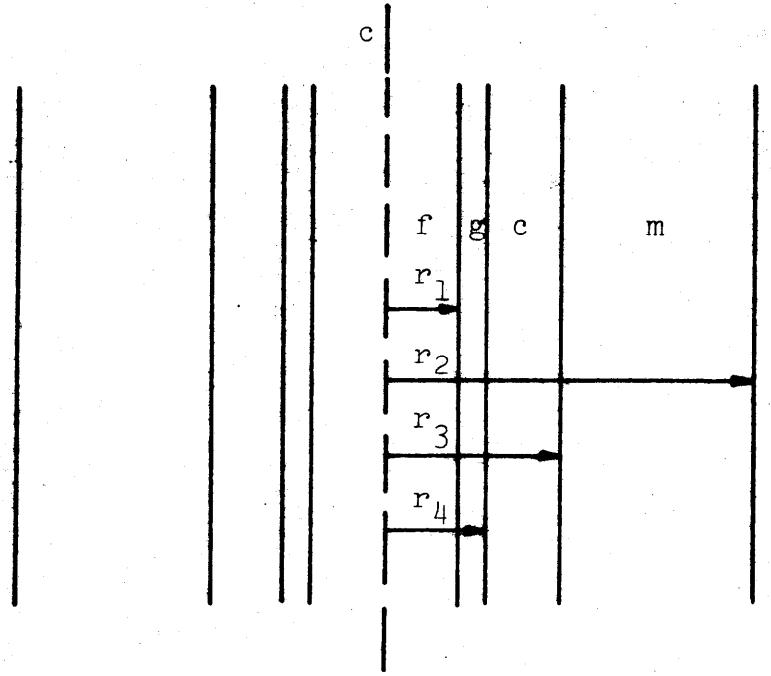

m: moderator and/or coolant region

f: fuel region

c: clad region

g: gap

$r_1 \equiv r_{fuel}$

$r_2 \equiv r_{moderator}$

$r_3 \equiv r_{clad}$

$r_4 \equiv r_{gap}$

FIG. 2.2 STANDARD PLANAR UNIT CELL

illustrate several unit cell configurations (in two dimensions sphericalized and cylindricalized unit cells look alike).

A square lattice with a given pitch, P_s, has its equivalent outer cell radius given by:

$$R_m = \frac{P_s}{\sqrt{\pi}} \qquad (2.2)$$

For a hexagonal lattice the equivalent outer cell radius is given by:

$$R_m = \left(\frac{\sqrt{3}}{2\pi}\right)^{1/2} P_h \qquad (2.3)$$

Throughout our work we will be working with two-region, heterogeneous, unit cells. The three regions, gap, clad, and coolant/moderator are homogenized into one region called the "moderator" region, producing a two-region unit cell with the fuel comprising the interior region and the moderator the outer region. It will be shown later that the above homogenization can be done without introducing appreciable error, as also reported in Ref. (H2). Appendix B, however, will discuss an interface flux prescription which would allow approximate inclusion of the clad as a separate region for situations in which it is deemed necessary.

At this point some unit cell related parameters needed in the succeeding sections will be introduced - the fuel and moderator penetration chord lengths, (M2), defined as:

$$\ell_f = \frac{4V_f}{S_f} \qquad (2.4)$$

$$\ell_m = \frac{4(V_{cell} - V_f)}{S_f} \qquad (2.5)$$

Applying the above definitions we get:

Cylindrical unit cell: $\ell_f = 2r_f \quad \ell_m = \frac{2(r_m^2 - r_f^2)}{r_f}$ (2.6)

Spherical unit cell: $\ell_f = \frac{4}{3} r_f \quad \ell_m = \frac{4}{3} \frac{(r_m^3 - r_f^3)}{r_f^2}$ (2.7)

Slab unit cell: $\ell_f = 4d_f \quad \ell_m = 4\,(d_m - d_f)$ (2.8)

2.3 PROPOSED FLUX-RATIO MODEL

As already noted, a model describing the detailed flux distribution in the unit cell is essential. Since each region of the cell is homogeneous, a simple model will suffice: one which expresses the ratio of the average moderator flux to that in the fuel as a function of various parameters, the most important of which are the fuel optical absorption thickness, the moderator optical absorption thickness, and the fractional neutron source in both the moderator and the fuel regions. As will be shown, the proposed model has the following form

$$\frac{\bar{\phi}_m(E)}{\bar{\phi}_f(E)} = \frac{1+F[\tau_{af}(E),\tau_{am}(E),\tau_{sf}(E),\tau_{sm}(E)]\cdot\tau_{af}(E)\cdot Q_m(E)}{1+F[\tau_{am}(E),\tau_{af}(E),\tau_{sm}(E),\tau_{sf}(E)]\cdot\tau_{am}(E)\cdot Q_f(E)} \qquad (2.9)$$

where:

$\tau_{xi}(E) = \Sigma_x(E)\ell_i$, the optical thickness for process x in region i

ℓ_i = mean Dirac penetration chord length through region i

$\Sigma_x = \sum_j \Sigma_x^j$ macroscopic cross section summed over all j isotopes in the region i (fuel, f, or moderator, m)

Q_m = fraction of neutron source originating in the moderator

Q_f = fraction of neutron source originating in the fuel

Analytic expressions have in the past been derived for the cylindrical case of low τ_{af} and τ_{am} by Gregory (G1); and for large τ_{af} by Kadiroglu (K1): they obtained for $F(\tau_{af},\tau_{am},\tau_{sf},\tau_{sm})$ values of 1/3 and 2/3, respectively. A major contribution of the present work will be development of an expression for $F(\tau_{af},\tau_{am},\tau_{sf},\tau_{sm})$, and its symmetrical counterpart in the denominator of Eq. (2.9), which accurately joins the two asymptotic values [1/3,2/3]. We have also carried out an analysis paralleling that of Gregory and Kadiroglu for the other common geometries - spherical and slab - and determined their asymptotic values: [9/32,9/16], and [1/4,1/2] respectively.

In the next several sections several methods will be analyzed to develop a rationale for specifying the functional form of the smoothing function, $F(\tau_{af},\tau_{am},\tau_{sf},\tau_{sm})$. Since sufficiently simple exact solutions are not obtainable, approximate methods will be adopted and their adequacy evaluated by subjecting the final form of the model to numerical verification.

2.4 ESCAPE PROBABILITY MODEL

The method of escape probabilities is frequently employed in problems of this type. Here we follow an illustrative example - tested by Gregory (G1) - his report may be referred to for a more detailed exposition. Let us assume a two-region cylindrical unit cell as shown in Fig. 2.3.

The objective is to derive an expression for the ratio of the average fluxes in the cylindrical unit cell; the following parameters are defined:

S_i = isotropic, uniformly distributed, source in region i (neutrons/cm^3)

p_i = escape probability: fraction of <u>source</u> neutrons escaping region i

P_i = escape probability for neutron <u>entering</u> region i

In what follows the key assumption is made that P_i applies to neutrons of all generations. Consider successive events for a neutron born in the fuel, region 1: $S_1 p_1 \frac{r_1}{2}$ neutrons per cm^2 of surface per second escape the fuel initially, $(S_1 p_1 \frac{r_1}{2})(P_2 P_1)$ escape the fuel after returning, $(S_1 p_1 \frac{r_1}{2})(P_2 P_1)^2$ do so after a second return to the fuel, and so on. Summing all the escapes from the fuel one gets:

$$\frac{S_1 p_1 \frac{r_1}{2}}{(1-P_1 P_2)}$$

which is the current leaving the fuel. In the same manner one can obtain a similar expression for the moderator, region 2:

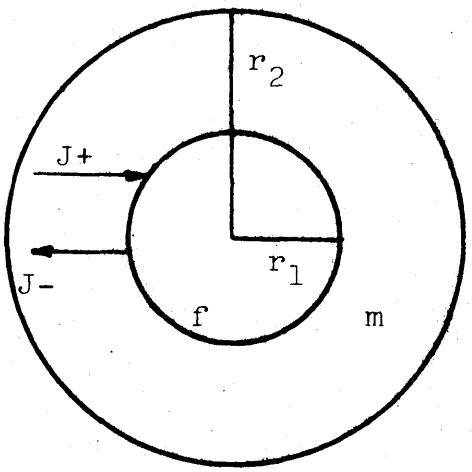

f: fuel

m: moderator

J+: partial current entering the fuel rod

J-: partial current leaving the fuel rod

FIG. 2.3 STANDARD, TWO-REGION CYLINDRICAL UNIT CELL

$$\frac{S_2 p_2 \frac{r_2^2 - r_1^2}{2r_1}}{(1 - P_1 P_2)}$$ current leaving the moderator

Consider neutrons returning to each region: $S_1 p_1 \frac{r_1}{2} P_2$ neutrons escape the fuel and return, $(S_1 p_1 \frac{r_1}{2} P_2)(P_1 P_2)$ re-escape and return a second time, and so on. Summing up, one gets

$$\frac{S_1 p_1 \frac{r_1}{2} P_2}{(1 - P_1 P_2)}$$

neutrons per cm^2 per second entering the fuel due to the source S_1 within the fuel. Again, similarly, the current entering the moderator due to sources within the moderator is

$$\frac{S_2 p_2 \frac{r_2^2 - r_1^2}{2r_1} P_1}{(1 - P_1 P_2)}$$

The partial current entering the fuel rod is the sum of entries due to neutrons of both internal and external origin:

$$J_+ = \frac{S_1 p_1 \frac{r_1}{2} P_2}{(1 - P_1 P_2)} + \frac{S_2 p_2 \frac{r_2^2 - r_1^2}{2r_1}}{(1 - P_1 P_2)} \qquad (2.10)$$

the partial current leaving is:

$$J_- = \frac{S_1 p_1 \frac{r_1}{2}}{(1 - P_1 P_2)} + \frac{S_2 p_2 \frac{r_2^2 - r_1^2}{2r_1} P_1}{(1 - P_1 P_2)} \qquad (2.11)$$

and the net current into the rod is:

$$J = J_+ - J_- = \frac{S_2 p_2 \frac{r_2^2 - r_1^2}{2r_1}(1-P_1) - S_1 p_1 \frac{r_1}{2}(1-P_2)}{(1 - P_1 P_2)} \qquad (2.12)$$

A neutron balance on the fuel rod, (region 1), in terms of the average neutron flux is:

$$\Sigma_{a_1} \bar{\phi}_1 \pi r_1^2 = 2\pi r_1 J + \pi r_1^2 S_1 \qquad (2.13)$$

or

$$\bar{\phi}_1 = \frac{2J + S_1 r_1}{\Sigma_{a_1} r_1} \qquad (2.14)$$

For the moderator region, (region 2), one similarly obtains:

$$\Sigma_{a_2} \bar{\phi}_2 \pi (r_2^2 - r_1^2) = -2\pi r_1 J + \pi (r_2^2 - r_1^2) S_2 \qquad (2.15)$$

or

$$\bar{\phi}_2 = \frac{-2J + S_2 \frac{r_2^2 - r_1^2}{r_1}}{\Sigma_{a_2} \frac{r_2^2 - r_1^2}{r_1}} \qquad (2.16)$$

Using Eqs. (2.12), (2.14), and (2.16), we get:

$$\frac{\bar{\phi}_2}{\bar{\phi}_1} = \frac{S_1 r_1 p_1 (1-P_2) - S_2 z_2 p_2 (1-P_1) + S_2 z_2 (1-P_1 P_2)}{S_2 z_2 p_2 (1-P_1) - S_1 r_1 p_1 (1-P_2) + S_1 r_1 (1-P_1 P_2)} \cdot \frac{\Sigma_{a_1} r_1}{\Sigma_{a_2} z_2} \qquad (2.17)$$

where: $z_2 = \frac{r_2^2 - r_1^2}{r_1}$

First and second order approximations are available for the escape probabilities in Eq. (2.17) for the case of uniformly distributed, isotropically oriented sources:

$$p_1 = 1 - \frac{4}{3}\Sigma_{a_1} r_1 \tag{2.18}$$

$$p_2 = 1 - \frac{4}{3}\Sigma_{a_2} z_2 \tag{2.19}$$

$$P_1 = 1 - 2\Sigma_{a_1} r_1 + \frac{8}{3}(\Sigma_{a_1} r_1)^2 \tag{2.20}$$

$$P_2 = 1 - 2\Sigma_{a_2} z_2 + \frac{8}{3}(\Sigma_{a_2} z_2)^2 \tag{2.21}$$

See references (M2,G1) for further explanation.

Substituting the above expressions for the probabilities into Eq. (2.17) we get:

$$\frac{\bar{\phi}_2}{\bar{\phi}_1} \equiv \frac{\bar{\phi}_m}{\bar{\phi}_f} = \frac{1 + \frac{2}{3}\Sigma_{a_1} r_1 \frac{S_2}{S_1+S_2}}{1 + \frac{2}{3}\Sigma_{a_2} z_2 \frac{S_1}{S_1+S_2}} \tag{2.22}$$

Using the expressions obtained for the penetration chord-lengths of cylindrical unit cells obtained at the end of Section 2.2, and also defining:

$Q_m = \frac{S_2}{S_1+S_2}$ fraction of the source originating in the moderator

$$Q_f = \frac{S_1}{S_1+S_2}$$ fraction of the source originating in the fuel

one can now write Eq. (2.22) in a more compact form, as follows:

$$\frac{\bar{\phi}_m}{\bar{\phi}_f} = \frac{1 + \frac{1}{3}\tau_{af}Q_m}{1 + \frac{1}{3}\tau_{am}Q_f} \qquad (2.23)$$

Upon comparing Eq. (2.23) with Eq. (2.9) we find that $F(\tau_{af},\tau_{am},\tau_{sf},\tau_{sm}) = F(\tau_{am},\tau_{af},\tau_{sm},\tau_{sf}) = \frac{1}{3}$, which, as mentioned earlier, is the result obtained by Gregory (G1), for the <u>limits</u> of <u>low</u> τ_{af} and <u>low</u> τ_{am}.

2.5 INTEGRAL TRANSPORT METHOD

In this section we will, very briefly, state and employ the Integral Transport Method to determine the unit cell Flux Ratio Model. More importantly, the final result will be used to investigate the effects of fuel and moderator scattering on the Flux Ratio Model; and to obtain the functional dependence on these parameters. Towards the end of the section the results of various other arguments pertaining to scattering effects will be presented. In what follows we will rely upon the treatment used by Kadiroglu, and his report (K1) should be referred to for additional explicatory material.

The transport equation for the neutron flux anywhere in the cell represented by Fig. 2.3 is given by the Peierls' Equation (C1,G2):

$$\phi(\underline{r}) = \int_V G(\underline{r}/\underline{r}')[q(\underline{r}') + \Sigma_s \phi(\underline{r}')]d\underline{r}' \qquad (2.24)$$

where $\left|\begin{matrix}\phi(\underline{r}) \\ \phi(\underline{r}')\end{matrix}\right|$ are the fluxes at vector points $\underline{r}$ and $\underline{r}'$

$q(\underline{r}')$ is the source at $\underline{r}'$

V is the volume of the cell

$G(\underline{r}/\underline{r}')$ is the first flight kernel giving the uncollided flux at $\underline{r}$ due to a unit isotropic source at $\underline{r}'$.

Under the flat-flux assumption, one can manipulate Eq. (2.24) to obtain the following set of equations for the moderator and fuel average fluxes in terms of volume-average kernels and sources:

$$\bar{\phi}_m = K_{mm}[Q_m + \Sigma_{sm} V_m \bar{\phi}_m] + K_{mf}[Q_f + \Sigma_{sf} V_f \bar{\phi}_f] \qquad (2.25)$$

$$\bar{\phi}_f = K_{fm}[Q_m + \Sigma_{sm} V_m \bar{\phi}_m] + K_{ff}[Q_f + \Sigma_{sf} V_f \bar{\phi}_f] \qquad (2.26)$$

where:

$$Q_i = \frac{\frac{1}{V_i}\int_{V_i} q(\underline{r})d\underline{r}}{Q_T}$$ fraction of neutron source originating in region i

$Q_T =$ total neutron source

Note: under the flat-flux assumption $q(\underline{r}) = q$ which is constant.

$$K_{ij} = \int_{V_i} d\underline{r} \int_{V_j} G(\underline{r}/\underline{r}')d\underline{r}'$$

is the flux produced in region i per unit source in region j and from the reciprocity theorem:

$$K_{ij} = K_{ji}$$

The above approach has been used by a number of investigators (C2,F1,T1) to study planar and cylindrical geometries for small optical thicknesses.

Solving for the flux ratio, $\bar{\phi}_m/\bar{\phi}_f$, from Eqs. (2.25) and (2.26) and rearranging the coefficients one obtains:

$$\frac{\bar{\phi}_m}{\bar{\phi}_f} = \frac{1 + \left| \left| \frac{K_{mm}}{K_{mf}} - 1 \right| + \left| K_{mf} - \frac{K_{mm}K_{ff}}{K_{mf}} \right| \Sigma_{sf} V_f \right| Q_m}{1 + \left| \left| \frac{K_{ff}}{K_{mf}} - 1 \right| + \left| K_{fm} - \frac{K_{ff}K_{mm}}{K_{fm}} \right| \Sigma_{sm} V_m \right| Q_f} \qquad (2.27)$$

The similarity of Eq. (2.27) to Eq. (2.23) is evident; note that in both equations the denominator can be obtained by cyclic permutation of the subscripts in the numerator. Hence in what follows the algebra can be considerably simplified by considering the case $Q_f = 0$ since the general case can be readily recovered.

The effect of moderator and fuel scattering on the flux ratio is to be examined. Certain simplifying assumptions will prove useful for this purpose:

(1) assume: low τ_{af} and τ_{am} (near transparent case)

(2) assume: $\tau_{af} > \tau_{sf}$

(3) observe: $\Sigma_{sf} V_f \propto \Sigma_{sf} \ell_f \propto \tau_{sf}$

(4) assume: $K_{mm} \simeq e^{-\tau_{tm}}$ & $K_{mf} \sim e^{-(\tau_{tf}+\tau_{tm})}$

(5) assume: $(\frac{K_{mm}}{K_{mf}} - 1) \simeq (e^{\tau_{tf}} - 1)$

(6) assume: $(\frac{K_{ff}}{K_{mf}} - 1) \simeq (e^{\tau_{tm}} - 1)$

Using the above we can obtain the following:

(7) $(K_{fm} - \frac{K_{ff}K_{mm}}{K_{mf}}) \simeq [e^{-(\tau_{tf}+\tau_{tm})} - e^{(\tau_{tf}+2\tau_{tm})}] \simeq$

$$1 - \tau_{tf} - \tau_{tm} - (1+\tau_{tf}+2\tau_{tm}) \simeq -(\tau_{tf}+\tau_{tm})$$

(8) assume: $Q_f = 0$; therefore $Q_m = 1$

(9) assume: $\tau_{am} << \tau_{af}$

The multitude of assumptions will not prove limiting because we are not interested in an exact answer; but, rather, in determining how the effects of scattering can be taken into consideration. Accuracy will be recovered by later resorting to force-fitting numerical results.

Using the listed assumptions in Eq. (2.27)

$$\frac{\bar{\phi}_m}{\bar{\phi}_f} \simeq 1 + [\tau_{tf} - \tau_{sf}(\tau_{tf}+\tau_{tm})] \qquad (2.28)$$

and factoring out τ_{af}

$$\frac{\bar{\phi}_m}{\bar{\phi}_f} \simeq 1 + [1 + \frac{\tau_{sf}}{\tau_{af}} - \frac{\tau_{sf}}{\tau_{af}}(\tau_{af}+\tau_{sf}+\tau_{sm})]\cdot\tau_{af} \qquad (2.29)$$

Simplifying further

$$\frac{\bar{\phi}_m}{\bar{\phi}_f} \simeq 1 + (1 + \frac{\tau_{sf}}{\tau_{af}} - \tau_{sf} - \frac{\tau_{sf}}{\tau_{af}}\tau_{sm})\cdot\tau_{af} \qquad (2.30)$$

$$\frac{\bar{\phi}_m}{\bar{\phi}_f} \simeq 1 + [(1-\tau_{sf}) + \frac{\tau_{sf}}{\tau_{af}}(1-\tau_{sm})]\cdot\tau_{af} \qquad (2.31)$$

or:

$$\frac{\bar{\phi}_m}{\bar{\phi}_f} \simeq 1 + [\frac{1}{(1+\tau_{sf})} + \frac{\tau_{sf}}{\tau_{af}}\frac{1}{(1+\tau_{sm})}]\cdot\tau_{af} \qquad (2.32)$$

further:

$$\frac{\bar{\phi}_m}{\bar{\phi}_f} \simeq 1 + (1+\tau_{sf})(1+\tau_{sm})[\frac{1}{(1+\tau_{sf})^2(1+\tau_{sm})} + \frac{\tau_{sf}}{\tau_{af}}\frac{1}{(1+\tau_{sm})^2(1+\tau_{sf})}]\cdot\tau_{af} \qquad (2.33)$$

At this point we choose to replace the term in brackets by a single lumped parameter:

$$\frac{\bar{\phi}_m}{\bar{\phi}_f} \simeq 1 + \Omega\cdot(1+\tau_{sf})(1+\tau_{sm})\cdot\tau_{af} \qquad (2.34)$$

Furthermore, for later convenience, we will want to implement the correction by multiplying both τ_{sf} and τ_{sm} by a parameter, ω'. Hence, Ω will in turn be replaced by ω' so as to yield an equivalent effect. Therefore:

$$\frac{\bar{\phi}_m}{\bar{\phi}_f} = 1 + \frac{1}{3}(1 + \omega'\tau_{sf})(1 + \omega'\tau_{sm})\cdot\tau_{af} \qquad (2.35)$$

The factor of 1/3 has been introduced to make Eq. (2.35) compatible with Eq. (2.23) in the no-scattering limit.

As pointed out in the beginning of the section, there are other methods, such as diffusion theory and/or track length arguments, that can be utilized for studying scattering effects. Let us consider an "inside-out"* cell, a cell similar to that of Fig. 2.3 but with the fuel and the moderator regions interchanged. Assuming that diffusion theory applies, then:

$$-D\nabla^2\phi(r) = q''' \qquad (2.36)$$

where: $q''' = \frac{q_m}{V_m} = \frac{q_m}{\pi r_1^2}$

Equation (2.36) has a solution of the form:

$$\phi(r) = A - \frac{q_m}{4\pi D}\left(\frac{r^2}{r_1^2}\right) \qquad (2.37)$$

We also have the boundary condition of zero return current if the fuel region is black, hence:

---

* The use of the extended reciprocity theorem (G1) permits us to do this.

$$J_- = 0 = \frac{\phi}{4} + \frac{D}{2}\frac{d\phi}{dr} \quad \text{at } r = r_1 \tag{2.38}$$

Thus: $$A - \frac{q_m}{4\pi D} = 2D\,\frac{q_m}{2\pi D r_1} \tag{2.39}$$

or $$A = q_m\left(\frac{1}{\pi r_1} + \frac{1}{4\pi D}\right) \tag{2.40}$$

The average moderator flux is:

$$\bar{\phi}_m = \frac{1}{\pi r_1^{\,2}} \int_0^{r_1} \phi(r)\cdot 2\pi r\, dr = A - \frac{q_m}{8\pi D} \tag{2.41}$$

Using Eq. (2.40) we get:

$$\left(\frac{\bar{\phi}_m}{q_m}\right) = \frac{1}{\pi r_1} + \frac{1}{8\pi D} \tag{2.42}$$

Since flux is track length per unit volume, we can define an effective penetration chord length as:

$$\ell_{eff} = \pi r_1^{\,2}\left(\frac{\bar{\phi}_m}{q_m}\right) \tag{2.43}$$

Substituting Eq. (2.42) into Eq. (2.43) we get:

$$\ell_{eff} = r_1 + \frac{r_1^{\,2}}{8D} \text{ ; and since } D = \frac{\lambda_s}{3}$$

Therefore:

$$\ell_{eff} = r_1 + r_1\cdot\frac{3}{16}\,\tau_{sm} = 2r_1\left(\frac{1}{2} + \frac{3}{32}\tau_{sm}\right) \tag{2.44}$$

But:

$\ell_p = 2r_1$ for a cylindrical unit cell (Section 2.2)

Therefore:

$$\ell_{eff} = \ell_p(\frac{1}{2} + \frac{3}{32}\tau_{sm}) \propto \ell_p(1 + \omega'\tau_{sm}) \qquad (2.45)$$

The result in Eq. (2.45) suggests a multiplicative moderator scattering correction to τ_{af} of the form $(1 + \omega'\tau_{sm})$ in the formula for the Flux Ratio Model, Eq. (2.9). It is encouraging to see that two different methods, namely the Integral Transport Method and the diffusion theory method, yield the same functional form.

Finally consider a track length argument. Let us, again, assume an "inside-out" unit cell.

Define the following parameters;

$\ell_p = 2r_1$ penetration chord length (Section 2.1)

$\ell_e = \frac{4}{3}r_1$ escape chord length for isotropic uniform internal source. This quantity is derived by Gregory in (G1).

Assumptions are: weak absorption & scattering

A neutron entering the inner region of the unit cell will penetrate an average distance proportional to the penetration chord length of the region prior to scattering, hence

$$ds = \omega''' \cdot \ell_p \qquad (2.46)$$

where: ds is the average distance moved by the neutron, on its first flight, prior to scattering

ω''' is a proportionality factor, and is less than unity ($\omega''' < 1$).

The scattered neutron, once in the rod region, will now trace out on the average a distance equal to the escape chord length, i.e., $\ell_e = \frac{4}{3}r_1$. The total distance traveled by the neutron will then be:

$$dt = \omega''' \cdot \ell_p + \ell_e = \omega''' \cdot \ell_p + \frac{2}{3}\ell_p \qquad (2.47)$$

or

$$dt = (\omega''' + \frac{2}{3}) \cdot \ell_p \equiv \omega'' \cdot \ell_p \qquad (2.48)$$

If the neutron had not been scattered it would have traveled an average distance ℓ_p through the rod, thus the extra distance traveled is:

$$d_{extra} = dt - \ell_p$$

or

$$d_{extra} = \omega'' \cdot \ell_p - \ell_p = (\omega'' - 1) \cdot \ell_p \equiv \omega' \cdot \ell_p \qquad (2.49)$$

Therefore to include the effect of the scattering on the penetration chord length, we will have to define a new effective penetration chord length as follows:

$$\ell_{eff} = \ell_p + \omega' \cdot \ell_p \cdot \tau_{sm} \qquad (2.50)$$

or

$$\ell_{eff} = \ell_p(1 + \omega' \tau_{sm}) \qquad (2.51)$$

where: ℓ_p is the penetration chord length without scattering

$\omega' \cdot \ell_p$ is the extra chord length due to scattering

and τ_{sm} = probability of being scattered

Compare Eqs. (2.35), (2.45), and (2.51): having three different approaches yield the same result strengthens our confidence in the choice of the functional form used to correct for moderator (and fuel) scattering.

2.6 ADDITIONAL RESULTS OF THE TRACK LENGTH METHOD

2.6.1 Near-Black Fuel and Near-Transparent Moderator

In the last two sections we were dealing with low optical absorption thicknesses for both the fuel and the moderator regions. The value obtained for the $F(\tau_{af},\tau_{am},\tau_{sf},\tau_{sm})$ of Eq. (2.9) without taking the effects of scattering into consideration was 1/3. We shall now obtain another asymptotic value of F for the limits of high optical absorption thicknesses. Furthermore, we will display parallel results for all unit cell geometries mentioned in Section 2.2.

Consider an "inside-out" cylindrical unit cell with the fuel surrounding a rod of moderator. As already stated the reciprocity principle (G1) permits us to do this without loss of generality. The following assumptions are made:

(a) the moderator contains a spatially uniform source of neutrons and is optically transparent - i.e. has a small optical thickness for both scattering and absorption.

(b) the fuel is very black - i.e. a strong absorber and a weak scatterer.

A neutron born in the moderator will trace out a distance given by the mean escape chord length $\ell_e = \frac{4}{3}r_1$. Then from the definition of flux as track length per unit volume, the moderator flux is:

$$\bar{\phi}_m = \frac{\ell_e}{V_m} = \frac{\frac{4}{3}r_1}{\pi r_1^2} = \frac{4}{3\pi r_1} \tag{2.52}$$

In the fuel each entering neutron completes a track length only one mean free path long - i.e. $\ell_f = \lambda_f = 1/(\Sigma_{af})$. Thus the fuel flux is:

$$\bar{\phi}_f = \frac{\ell_f}{V_f} = \frac{1}{\Sigma_{af} V_f} \tag{2.53}$$

Employing the definition of the penetration chord length for the fuel region we get:

$$\ell_p^{\text{fuel}} = \frac{4V_f}{S_m} = \frac{4V_f}{2\pi r_1}$$

or

$$V_f = \frac{\pi r_1}{2} \cdot \ell_p^{\text{fuel}} \tag{2.54}$$

Substituting Eq. (2.54) into Eq. (2.53)

$$\bar{\phi}_f = \frac{2}{\pi r_1 \ell_p^{\text{fuel}} \cdot \Sigma_{af}} = \frac{2}{\pi r_1 \tau_{af}} \tag{2.55}$$

Upon dividing Eq. (2.52) by Eq. (2.55)

$$\frac{\overline{\phi}_m}{\overline{\phi}_f} = \frac{2}{3}\,\tau_{af} \tag{2.56}$$

Therefore, the other asymptotic value for $F(\tau_{af}, \tau_{am}, \tau_{sf}, \tau_{sm})$ is 2/3, which is the value obtained by Kadiroglu (K1) using essentially the same treatment.

As for the spherical and the planar unit cells, the same steps can be repeated, replacing the cylindrical escape and penetration chord lengths by the associated spherical and planar escape and penetration chord lengths. The spherical and planar escape chord lengths are derived in Appendix A.

Using the spherical escape chord length of $\ell_e = \frac{3}{4}r_1$, and fuel penetration chord length of $\ell_p^{fuel} = (4V_f)/(4\pi r_1^2)$, we get for the ratio of average fluxes:

$$\frac{\overline{\phi}_m}{\overline{\phi}_f} = \frac{9\pi r_1^2 \cdot \ell_p^{fuel} \cdot \Sigma_{af}}{16\pi r_1^2} \tag{2.57}$$

or

$$\frac{\overline{\phi}_m}{\overline{\phi}_f} = \frac{9}{16} \cdot \tau_{af} \tag{2.58}$$

For the slab: $\ell_e = 2d$; $\ell_p^{fuel} = \frac{4V_f}{2}$

Hence:

$$\frac{\overline{\phi}_m}{\overline{\phi}_f} = \frac{\ell_p^{fuel} \cdot \Sigma_{af}}{2} \tag{2.59}$$

or

$$\frac{\bar{\phi}_m}{\bar{\phi}_f} = \frac{1}{2} \cdot \tau_{af} \qquad (2.60)$$

Equations (2.58) and (2.60) indicate that for the spherical unit cell $F(\tau_{af},\tau_{am},\tau_{sf},\tau_{sm}) = 9/16$, and for the planar unit cell $F(\tau_{af},\tau_{am},\tau_{sf},\tau_{sm}) = 1/2$, as mentioned in Section 2.3.

2.6.2 Near-Black Fuel and Near-Black Moderator

As a final case, we shall investigate the effect of two strongly absorbing media adjacent to one another. The following assumptions are made:

(a) "inside-out" unit cell with the source in the interior region (moderator).

(b) no scattering in either medium.

(c) $\lambda_{am} << r_1$

Due to the third assumption, which indicates that the moderator mean free path is much less than the radius of curvature of the rod, the three different geometries - i.e. sphere, cylinder and plane - will look the same to the neutron. Hence, the following analysis and the results will be exactly the same for the three different unit cells.

$$\bar{\phi}_m = \frac{\text{track length}}{\text{unit volume}} = \frac{\lambda_{am}\, q_m}{V_m} \qquad (2.61)$$

where: q_m is the total source in the moderator.
Escapes into the fuel are ignored.

It can be shown for an infinite slab containing a uniformly distributed source, that particles within one fourth of the medium's mean free path, $(\frac{\lambda_t}{4})$, can escape the surface of the slab uncollided. Utilizing this result to obtain the fuel flux:

$$\bar{\phi}_f = S \cdot \frac{\lambda_{am}}{4} \frac{q_m}{V_m} \frac{\lambda_{af}}{V_f} \tag{2.62}$$

where: S = surface area of the interior rod.

Dividing Eq. (2.61) by Eq. (2.62) gives:

$$\frac{\bar{\phi}_m}{\bar{\phi}_f} = \frac{4 \cdot \lambda_{am} \cdot q_m \cdot V_m \cdot V_f}{S \cdot \lambda_{am} \cdot q_m \cdot \lambda_{af}} \tag{2.63}$$

or:

$$\frac{\bar{\phi}_m}{\bar{\phi}_f} = \tau_{af} \tag{2.64}$$

Hence, for the two adjacent highly absorbing media $F(\tau_{af},\tau_{am},\tau_{sm},\tau_{sf}) = 1$, for the three different unit cells.

In the next section results obtained in the Sections 2.4 through 2.6 will be used to formulate a complete Flux Ratio Model.

2.7 FINAL FORM OF THE FLUX RATIO MODEL

So far we have discussed the general form of the Flux Ratio Model and the functional form of $F(\tau_{af},\tau_{am},\tau_{sf},\tau_{sm})$ under the two asymptotic limits of high and low optical thicknesses. Our

task now is to use the results obtained in the preceding sections as guidelines for suggesting an analytic function for $F(\tau_{af}, \tau_{am}, \tau_{sf}, \tau_{am})$, so as to be able to cover the intermediate ranges of optical thicknesses.

Recall Eqs. (2.23) and (2.56), namely:

$$\frac{\bar{\phi}_m}{\bar{\phi}_f} = 1 + \frac{1}{3}\tau_{af} \tag{2.23}$$

which was derived under the assumption of weak absorption and scattering for both the fuel and the moderator region. Note also that we have set $Q_f = 0$.

$$\frac{\bar{\phi}_m}{\bar{\phi}_f} = \frac{2}{3}\tau_{af} \simeq 1 + \frac{2}{3}\tau_{af} \tag{2.56}$$

Since: $\tau_{af} >> 1$

which was derived under the assumption of strong fuel absorption, weak moderator absorption, and, finally, weak scattering for both regions.

There are numerous functions that could smoothly join the lower asymptotic slope of 1/3, (Eq. 2.23), to the upper asymptotic slope of 2/3, (Eq. 2.56). Among them we have chosen the one that is both the simplest in form and best agrees with the numerical results (to be discussed later). This function has the following form:

$$F(\tau_{af}) = \frac{1}{3}\left(1 + \frac{\omega\tau_{af}^{n}}{1 + \omega\tau_{af}^{n}}\right) \tag{2.65}$$

Note that for $\tau_{af} \to 0$ $\quad F(\tau_{af}) \to 1/3$

and when $\tau_{af} \to \infty$ $\quad F(\tau_{af}) \to 2/3$

The constant "ω" is a fitting parameter which we have selected to force agreement with numerical results, and "n" is a positive power to which τ_{af} is raised.

So far weak moderator absorption has been assumed in conjunction with the two cases of weak and strong fuel absorption. Recall that weak scattering has also been assumed for both the fuel and the moderator. Let us now consider the problem of two adjacent black media with weak scattering in both regions. In Eq. (2.64) we have obtained the following result:

$$\frac{\bar{\phi}_m}{\bar{\phi}_f} = 1 \cdot \tau_{af} \simeq 1 + 1 \cdot \tau_{af} \qquad (2.64)$$

Since: $\tau_{af} >> 1$

By comparing Eqs. (2.65) and (2.64) the following function is suggested:

$$F(\tau_{af},\tau_{am}) = \frac{\frac{1}{3}\left(1 + \frac{\omega\tau_{af}^{n}}{1+\omega\tau_{af}^{n}}\right) + \omega\tau_{am}^{n'}}{1 + \omega\tau_{am}^{n'}} \qquad (2.66)$$

where "n'" is a positive power to which τ_{am} is raised.

Note that for $\tau_{af} \to 0$ $\quad F(\tau_{af},\tau_{am}) \to F(\tau_{af}) = \frac{1}{3}\left(1+\frac{\omega\tau_{af}^{n}}{1+\omega\tau_{af}^{n}}\right)$

and when $\tau_{af} \to \infty$ and $\tau_{am} \to \infty$ $\quad F(\tau_{af},\tau_{am}) \to 1.$

As for the effects of scattering, Eqs. (2.51), (2.45), and (2.35) suggested a functional dependence of the following form:

$$F(\tau_{sf}, \tau_{sm}) = (1 + \omega'\tau_{sf})(1 + \omega'\tau_{sm}) \tag{2.67}$$

Combining Eqs. (2.66) and (2.67) we get the following final form:

$$F(\tau_{af},\tau_{am},\tau_{sf},\tau_{sm}) = \frac{\frac{1}{3}\left(1+\frac{\omega\tau_{af}^{n}}{1+\omega\tau_{af}^{n}}\right) + \omega\tau_{am}^{n'}}{1 + \omega\tau_{am}^{n'}} \cdot (1+\omega'\tau_{sf})(1+\omega'\tau_{sm}) \tag{2.68}$$

And using the fact of symmetry, as mentioned in Section 2.5:

$$F(\tau_{am},\tau_{af},\tau_{sm},\tau_{sf}) = \frac{\frac{1}{3}\left(1+\frac{\omega\tau_{am}^{n}}{1+\omega\tau_{am}^{n}}\right) + \omega\tau_{af}^{n'}}{1 + \omega\tau_{af}^{n'}} \cdot (1+\omega'\tau_{sm})(1+\omega'\tau_{sf}) \tag{2.69}$$

Substituting Eqs. (2.68) and (2.69) into Eq. (2.9) there results:

$$\frac{\bar{\phi}_m}{\bar{\phi}_f} = \frac{1 + \frac{\frac{1}{3}\left(1+\frac{\omega\tau_{af}^{n}}{1+\omega\tau_{af}^{n}}\right)+\omega\tau_{am}^{n'}}{1 +\omega\tau_{am}^{n'}} \cdot (1+\omega'\tau_{sf})(1+\omega'\tau_{sm}) \cdot \tau_{af} \cdot Q_m}{1 + \frac{\frac{1}{3}\left(1+\frac{\omega\tau_{am}^{n}}{1+\omega\tau_{af}^{n}}\right)+\omega\tau_{af}^{n'}}{1 +\omega\tau_{af}^{n'}} \cdot (1+\omega'\tau_{sm})(1+\omega'\tau_{sf}) \cdot \tau_{am} \cdot Q_f} \tag{2.70}$$

which is the final form of the Flux Ratio Model for the cylindrical unit cell. As for the planar and the spherical unit cells, similar models can be generated by the same treatment. Therefore it is sufficient here to note that for the slab case the factor 1/3 in Eq. (2.70) should be replaced by 1/4, and for the spherical case it should be replaced by 9/32 . The rest of the equation will look essentially the same as Eq. (2.70); (but see page 62 regarding the slab case).

2.7.1 Flux Ratio Model Cast in Terms of IR Parameters

Up till now no mention has been made of resonance cross-sections, and the way in which the associated WR, IR, and NR approximations are to be incorporated into the Flux Ratio Model. In what follows we shall be assuming resolved (and non self-overlap) resonances of a single resonance absorber - i.e., we assume no other resonance absorber present in appreciable amount. Some of the above assumptions, however, will be relaxed in later chapters.

Consider a flux of neutrons in Energy-space heading towards a single resonance, as shown in Fig. 2.4. The condition for application of the narrow resonance (NR) approximation is that the maximum energy loss in an elastic scattering collision of a neutron with an absorber nucleus, i.e., $(1-\alpha_a)E_i$, in the vicinity of a resonance should be much greater than the practical width, Γ_p, of the resonance. Under this condition both scattering

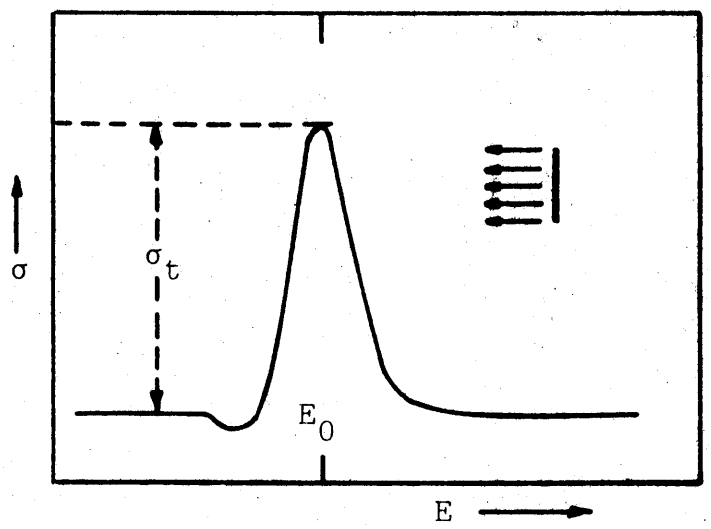

FIG. 2.4 CROSS SECTIONS IN THE VICINITY OF A RESONANCE

and absorption processes will remove neutrons from under the resonance. There are instances, however, when the maximum energy loss is much less than the Practical Width, Γ_p, of the resonance; this condition requires use of the so-called Wide Resonance (WR) approximation. In this case, it is only the absorption process that removes neutrons from under the resonance. Lastly, there is a third approximation intermediate between the two aforementioned, which neither completely denies nor totally admits the role of scattering for removing neutrons. This approximation is called the Intermediate Resonance (IR) approximation and it is implemented through the introduction of three new parameters λ, ν, and $\bar{\mu}$. We shall discuss the IR approximation and its associated parameters further in Section 3.3.1. However, for a more detailed explanation of the above ideas refer to (B2,G3,G4,G5,H3,L4,S3,S4). Therefore, in the IR approximation it is the absorption process plus a fraction of the scattering process which removes neutrons from under the resonance. For a resonance absorber with no admixed moderator the above will mean:

$$\sigma_{\substack{\text{removal of resonance} \\ \text{absorber in fuel}}}(E) \equiv \sigma_f(E) = \sigma_{af}(E)+\lambda\sigma_{sf}(E) \quad (2.71)$$

where λ determines the fraction of the scattering present in the removal cross-section.

Note that for $\lambda=1$:

$$\sigma_f(E) = \sigma_{af}(E) + \sigma_{sf}(E) = \sigma_{tf}(E) \quad (2.72)$$

which is the NR case

and for $\lambda=0$:

$$\sigma_f(E) = \sigma_{af}(E) \tag{2.73}$$

which is the WR case.

Similarly, when moderator is admixed with the resonance absorber:

$$\sigma_{\substack{\text{removal of non-resonance}\\ \text{element in fuel}}}(E) \equiv \sigma_{nf}(E) = \sigma_{anf}(E) + \nu\delta_{snf}(E) \tag{2.74}$$

and for the moderator/coolant in the moderator/coolant region:

$$\sigma_{\text{removal of moderator}}(E) \equiv \sigma_m(E) = \sigma_{am}(E) + \bar{\mu}\sigma_{sm}(E) \tag{2.75}$$

To implement the above ideas in conjunction with the Flux Ratio Model, it is convenient to introduce the following parameters, which greatly simplify the subsequent notation:

$$\delta_f(E) = \tau_{af}(E) + \lambda\tau_{sf}(E) + \tau_{anf}(E) + \nu\tau_{snf}(E) \tag{2.76}$$

$$\delta_m(E) = \tau_{am}(E) + \bar{\mu}\,\tau_{sm}(E) \tag{2.77}$$

$$\beta(E) = 1 + \omega'[(1-\lambda)\tau_{sf}(E) + (1-\nu)\tau_{snf}(E)] \tag{2.78}$$

$$\rho(E) = 1 + \omega'(1-\bar{\mu})\tau_{sm}(E) \tag{2.79}$$

$$\alpha_f(E) = \frac{\frac{1}{3}[1 + \frac{\omega\delta_f^n(E)}{1+\omega\delta_f^n(E)}] + \omega\delta_m^{n'}(E)}{1 + \omega\delta_m^{n'}(E)} \tag{2.80}$$

$$\alpha_m(E) = \frac{\frac{1}{3}[1 + \frac{\omega\delta_m^n(E)}{1+\omega\delta_m^n(E)}] + \omega\delta_f^{n'}(E)}{1 + \omega\delta_f^{n'}(E)} \tag{2.81}$$

Using Eqs. (2.76)-(2.81) in Eq. (2.70) we get:

$$\frac{\bar{\phi}_m(E)}{\bar{\phi}_f(E)} = R(E) = \frac{1 + \alpha_f(E)\beta(E)\rho(E)\delta_f(E)Q_m(E)}{1 + \alpha_m(E)\beta(E)\rho(E)\delta_m(E)Q_f(E)} \tag{2.82}$$

which is the generalized form for the Flux Ratio taking into account the IR parameters. Note that Eq. (2.82) is a continuous function of energy; its discretization into energy groups will be discussed in the next section.

2.7.2 The Flux Ratio in an Energy Group Sense

Although Eqs. (2.70) and (2.82) are exhibited as continuous functions of energy, their mode of derivation did not suggest this fact explicitly. In all the various steps that led to Eq. (2.70) we were, invariably and implicitly, assuming a "one-group" model: that is a neutron balance was performed for a fine energy group of width dE about E. The energy discretization, however, in the sense of going from the fine group to a coarser group structure in Eqs. (2.70) and/or (2.82) is straightforward; and one may refer to any of several references for further details, e.g. (H1, O1); basically it just involves proper definition of the cross sections.

Recall that removal applies to the combination of all processes that remove neutrons from the group into one sum called the total removal cross-section for group g:

$$\Sigma_g \equiv \Sigma_{tg} - \Sigma_{gg} = \Sigma_{ag} + \Sigma_{sg} - \Sigma_{gg} = \Sigma_{ag} + \sum_{g' \neq g} \Sigma_{g'g} \qquad (2.83)$$

and that group scattering is that portion of the scattering cross-section which leaves the neutron within the group - i.e., Σ_{gg}.

Using the above definitions, and following the format of Eqs. (2.76) through (2.81):

$$\delta_{fg} = \tau_{afg} + \tau_{anfg} + \sum_{g' \neq g} \tau_{sfg'g} + \tau_{snfg'g} \qquad (2.84)$$

(g'g includes down-scattering and upscattering if any).

$$\delta_{mg} = \tau_{amg} + \sum_{g' \neq g} \tau_{smg'g} \qquad (2.85)$$

$$\beta_{gg} = 1 + \omega'(\tau_{sfgg} + \tau_{snfgg}) \tag{2.86}$$

$$\rho_{gg} = 1 + \omega'\tau_{smgg} \tag{2.87}$$

$$\alpha_{fg} = \frac{\frac{1}{3}[1 + \frac{\omega\delta_{fg}^{n}}{1+\omega\delta_{fg}^{n}}] + \omega\delta_{mg}^{n'}}{1 + \omega\delta_{mg}^{n'}} \tag{2.88}$$

$$\alpha_{mg} = \frac{\frac{1}{3}[1 + \frac{\omega\delta_{mg}^{n}}{1+\omega\delta_{mg}^{n}}] + \omega\delta_{fg}^{n'}}{1 + \omega\delta_{fg}^{n'}} \tag{2.89}$$

Using Eqs. (2.84)-(2.89) in Eq. (2.70) we get:

$$\left|\frac{\overline{\phi}_m}{\overline{\phi}_f}\right|_g \equiv R_g = \frac{1 + \alpha_{fg}\beta_{gg}\rho_{gg}\delta_{fg}Q_{mg}}{1 + \alpha_{mg}\beta_{gg}\rho_{gg}\delta_{mg}Q_{fg}} \tag{2.90}$$

The discrete energy form of the Flux Ratio Model will prove useful in subsequent chapters. In the following sections numerical results verifying Eq. (2.90) will be presented, and as a result its validity will be established on even firmer grounds.

2.8 COMPARISON OF MODEL RESULTS WITH ANISN CALCULATIONS

In what follows we will be discussing numerical results developed using the ANISN code (A1),* comparing them with our predicted results. The calculations are done for two-region unit cells with the white boundary condition used for the outer region of cylindrical and spherical unit cells to minimize the effects of specular reflections (N1).

2.8.1 Effects of Scattering and Removal

The dependence of the flux ratio on the magnitude of scattering and removal cross-sections in cylindrical unit cells is shown in Figs. 2.5 and 2.6. The numerical values plotted in the figures are tabulated in Appendix B. Similar results for spherical and slab unit cells will be presented in Appendix B. As seen, the predicted results are within a maximum discrepancy of 15%, and an average error of about 5%,of the ANISN results.

---

* Most of the calculations were carried out in the S_8 and P_1 approximations, higher order quadrature sets, i.e. S_{16}, were also used for the slab case.

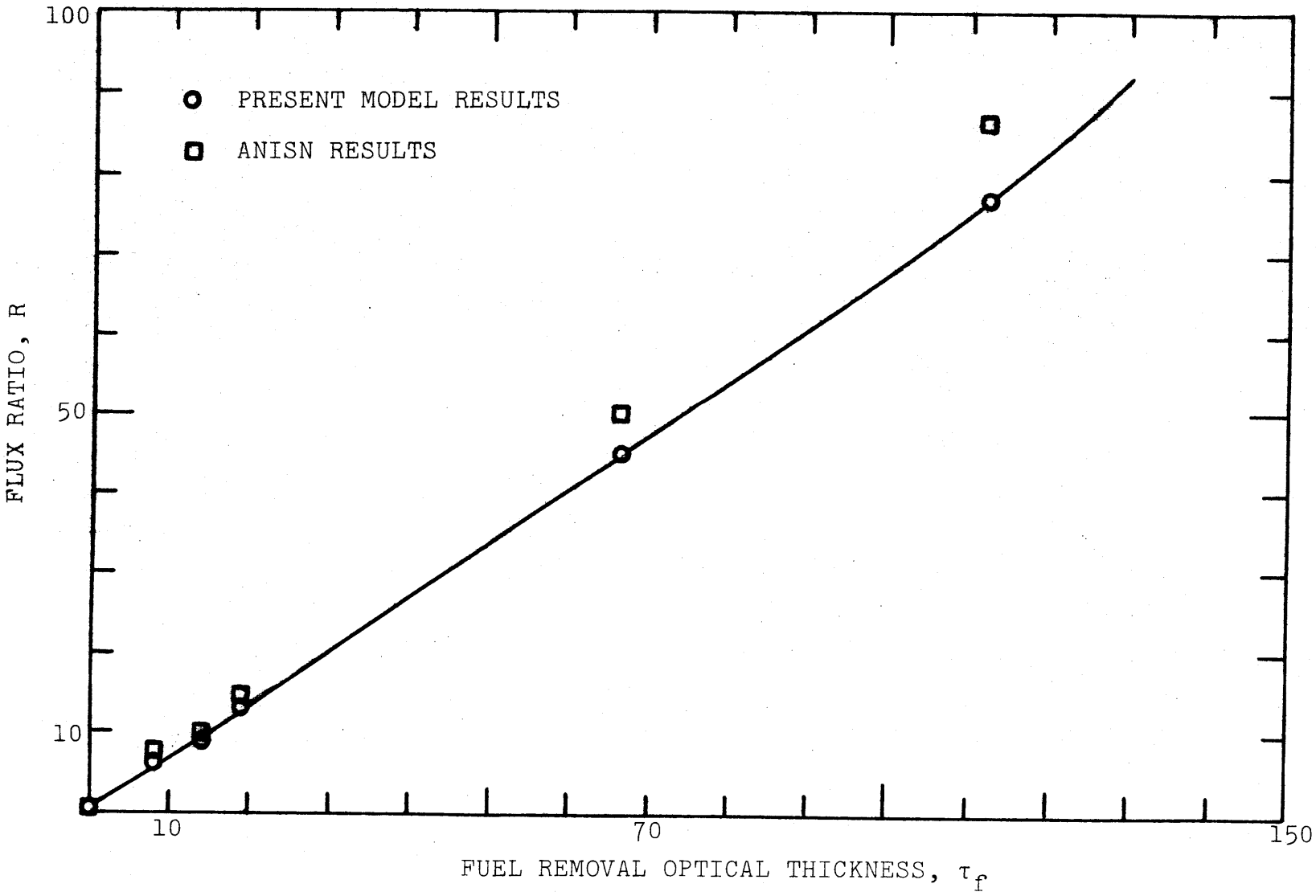

FIG. 2.5 FLUX RATIO AS A FUNCTION OF REMOVAL OPTICAL THICKNESS FOR A TWO-REGION CYLINDRICAL UNIT CELL

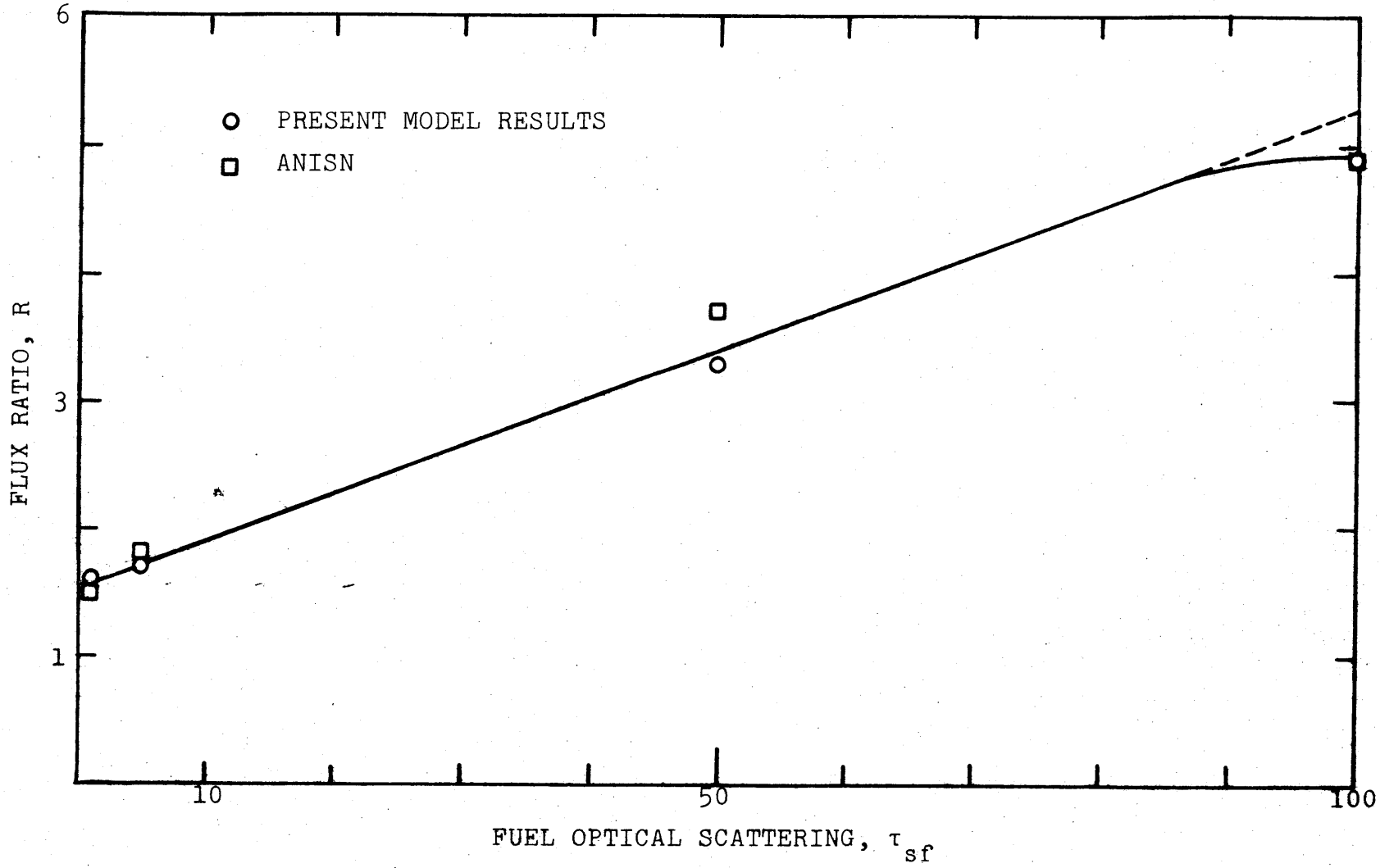

FIG. 2.6 FLUX RATIO AS A FUNCTION OF SCATTERING OPTICAL THICKNESS FOR A TWO-REGION CYLINDRICAL UNIT CELL

The agreement could be improved substantially, if desired, by a different choice of values for the fitting parameters (n,n') and (ω,ω') in the range of maximum interest. The important thing to note, however, is the correct dependence of the Flux Ratio Model on the various optical thicknesses. The above point will be discussed further in Appendix B, and more tabulated results will be given. Moreover, it is important to note that our model was derived on the basis of the flat-source (birth and scattering) approximation while ANISN distributes scattering events according to the local flux shape. Hence the good agreement validates our claim that the flat-source restriction has in fact been partially relaxed.

2.8.2 Effects of Source Distribution

An important and, perhaps, the most unique aspect of the Flux Ratio Model lies in its ability to predict correctly the effects of source distribution; a property which is very important in Fast Reactor calculations. In some literature on fast reactor calculations, it is implicitly assumed that the slowing-down source is entirely in the coolant, an erroneous assumption. Figure 2.7 shows the flux ratio as a function of the source fraction in the fuel, Q_f, for various δ_f. As seen, the predicted and the numerical results are in excellent agreement.

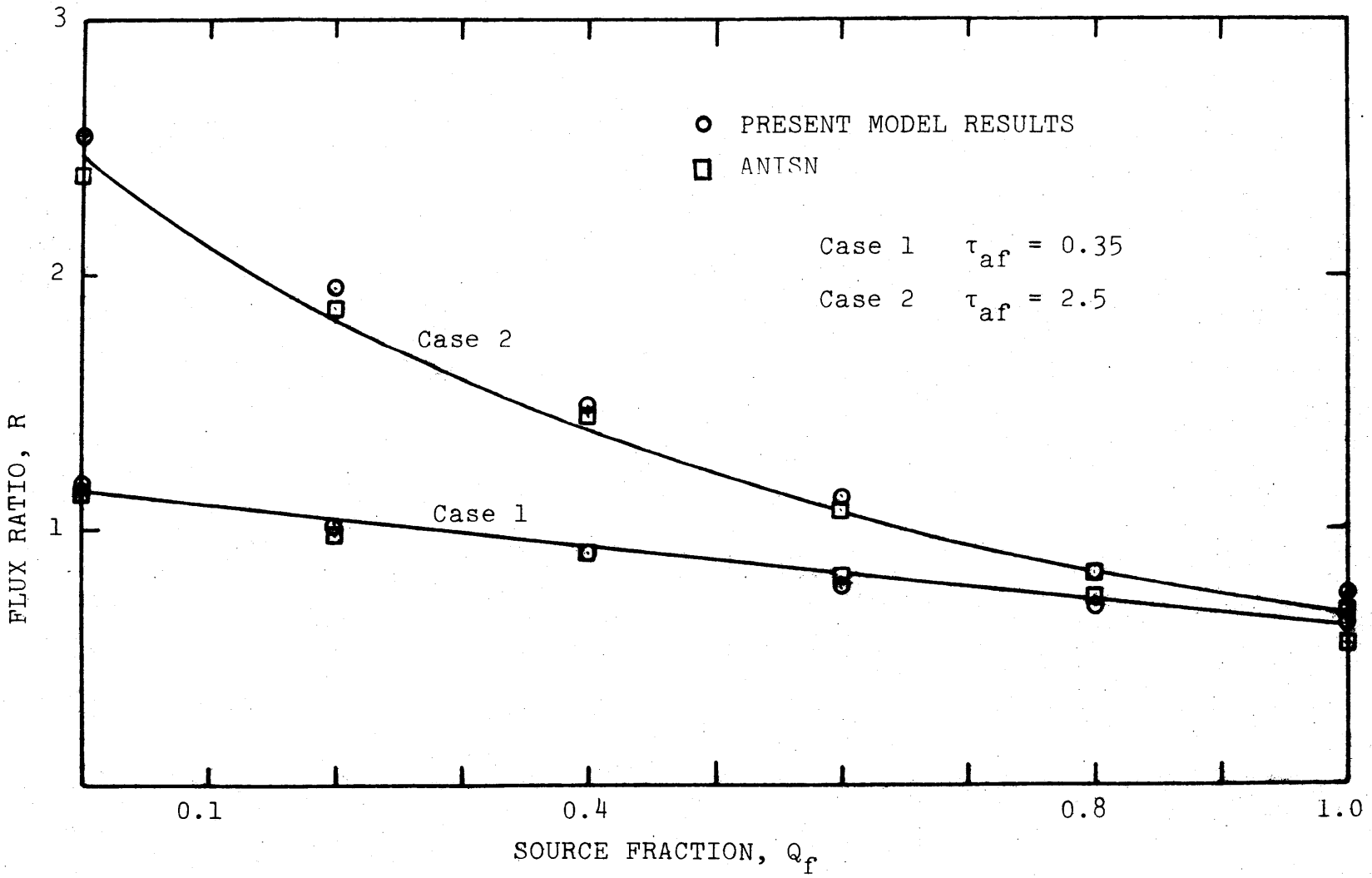

FIG. 2.7 FLUX RATIO AS A FUNCTION OF SOURCE DISTRIBUTION FOR A TWO-REGION CYLINDRICAL UNIT CELL

2.8.3 Further Remarks about the Flux Ratio Model

In Sections 2.6 and 2.7 parameters such as (n,n') and (ω,ω') were introduced, which are found to have the following values for the three different unit cells:

(1) Cylindrical:

$n=1.0$; $n'=0.5$

$\omega=0.24$; $\omega'=0.06$

(2) Spherical:

$n=0.5$; $n'=0.5$

$\omega=0.27$; $\omega'=0.09$

(3) Planar:

$n=1.0$; $n'=0.5$

$\omega=0.15$; $\omega'=0.03$

Cylindrical and spherical unit cells share similar functional forms for the Flux Ratio Model: only the values of (n,n') and (ω,ω') are changed. The planar case, however, required inclusion of an extra term of the form $(1+\omega' \ell n \frac{1}{\delta_m})$, introduced here without proof; interested readers may refer to Ref. (Z1) for justification. Also mentioned in Section 2.7 was the choice of a simple functional form for $F(\tau_{af})$, given by Eq. (2.65), from among many candidate functions that are equally attractive, such as:

$$F(\tau_{af}) = \frac{1}{3}(1 + \text{Tanh}\omega\tau_{af}) \qquad (2.91)$$

or

$$F(\tau_{af}) = \frac{1}{3}(2 - e^{-\omega\tau_{af}}) \qquad (2.92)$$

and, no doubt, many others, Others may select a candidate of their own choosing.

Finally, many other tests of the Flux Ratio Model have been carried out, such as the functional dependence on coolant optical thickness, the effect of lump size at constant optical thickness and the applicability of the extended reciprocity theorem,as documented in Refs. (G1,K1).

2.9 CONCLUSION

In this chapter simple analytic expressions were derived for the ratio of moderator to fuel fluxes in unit cells. Predicted results were shown to be in good agreement with numerical results. A literature search failed to uncover more complete expressions for the disadvantage factor that could reproduce,as accurately ,results over the wide range of optical thicknesses and source distributions covered by the present model. As noted in Section 2.8.3 there is still some room left for fine tuning which could further narrow the gap between the predicted and numerical results. However, the results will be shown to be more than adequate for present purposes: a 6% error in the flux ratio will typically affect homogenized group cross sections in the resonance region by less than 2%, a value which is tolerable in view of the often only modest precision of input data in this region and the consequences of other simplifying assumptions which must be introduced to make the larger problem tractable.

Chapter 3

ENERGY SELF-SHIELDING OF RESONANCES

3.1 INTRODUCTION

In this chapter an expression will be derived for the heterogeneous capture cross-section of a given isotope in the fuel region of a unit cell in an infinite lattice. The key to the above derivation will be the use of the simple flux ratio model developed in Chapter 2. Also, for the sake of generality, the intermediate resonance parameters are introduced to make the above approach applicable to any resonance of any isotope for all energies in the slowing down region. The final expression for the homogenized cross-section is given in terms of homogeneous parameters, hence leading to a new equivalence theorem. Finally, results obtained using the above method will be checked against the results of the LEOPARD code (L5) when applied to U-238 capture in a typical PWR unit cell.

3.2 HOMOGENEOUS SELF-SHIELDING

The discussion which follows is confined to homogeneous systems where the spatial and angular dependence of the flux are suppressed, and only the energy variable, E, is of concern. The reason for starting with homogeneous self-shielding is to introduce the basic concepts necessary for the extension of the methodology to heterogeneous media in later sections. As the name implies, resonance self-shielding occurs as the result

of flux depression under resonance peaks. Since resonance cross-sections are strongly temperature dependent, it therefore follows that self-shielding is a temperature-dependent phenomenon as well. Self-shielding also depends on cell composition and on the geometry of the problem in a complex way. However, all composition and geometry effects can be embodied in one parameter, the total cross-section of non-resonance-absorber-nuclei per absorber nucleus, σ_0. In the subsequent sections we will, briefly, treat some of the above ideas in more detail.

3.2.1 Low Material Concentrations

The fundamental and physically meaningful assumption made in most reactor physics calculations is conservation of total reaction rate. In fact, it is through the utilization of the above assumption that we shall define group-averaged homogeneous cross-sections as:

$$\int_{V_{cell}} \int_{\Delta E_g} \Sigma_x^j(E)\,\phi(E)\,dV\,dE = \Sigma_{xg}^j \cdot \int_{V_{cell}} \int_{\Delta Eg} \phi(E)\,dV\,dE \qquad (3.1)$$

where the quantity on the left of Eq. (2.92) is the true reaction rate, "Σ_{xg}^j" is the macroscopic group-averaged cross-section for the particular process "x" of isotope "j", and the double integral multiplying "Σ_{xg}^j" is the true total flux of neutrons in the energy range ΔEg. If we now assume that an element is present in a medium in low concentration, then its particular resonance structure will not induce any significant effect on the neutron spectrum. As a result, a smooth weighting function

C(E) can be used in the group-averaging process. Hence, Eq. (3.1) in the low concentration limit will be given as:

$$\sigma_{xg}^{\infty} = \frac{\int_{\Delta Eg} \sigma_x(E)C(E)dE}{\int_{\Delta Eg} C(E)dE} \qquad (3.2)$$

where, typically, C(E) is taken to be a Maxwellian spectrum at low energies, a 1/E spectrum in the mid-range, and a fission spectrum at high energies; and σ_{xg}^{∞} is the "infinitely dilute" isotope cross-section for group "g" and process "x".

Here ΔEg is to be interpreted as a fine-width group containing only one resonance.

3.2.2 Higher Material Concentrations

Although the method described in this work can be extended to low and high energy limits as well as to most physical processes such as scattering, fission..., etc., the analysis here will be restricted to the slowing-down range and to the finding of group-averaged homogeneous capture cross-sections for a single dominant resonant isotope. Let us, now, treat the case where the material concentration is not negligible, so that its resonance structure will affect the neutron spectrum in the mixture. Because of this, a proper weighting function (flux) is needed for the purpose of cross-section averaging. The appropriate weighting flux can be found by solving the slowing down equation for a uniform mixture of infinite extent:

$$[\sigma_0+\sigma_{tf}(E,T)]\phi(E,T,\sigma_0) = \int_E^{E/\alpha_m} \frac{\sigma_0}{(1-\alpha_m)}\,\phi(E')\frac{dE'}{E'} +$$

$$+ \int_E^{E/\alpha_f} \frac{\sigma_{sf}(E',T)}{(1-\alpha_f)}\,\phi(E')\frac{dE'}{E'} \qquad (3.3)$$

where

$\sigma_0 = \frac{\Sigma_{tm}}{N_o}$; Σ_{tm} = constant moderator cross-section ($\Sigma_{am} << \Sigma_{sm}$)

N_0 = number of resonance absorber nuclei per unit volume

$\sigma_{af}, \sigma_{rf}, \sigma_{pf}$ = resonance absorption, resonance scattering, potential scattering, cross-sections, respectively, of the resonance absorber

$\sigma_{sf}(E,T) = \sigma_{rf}(E,T)+\sigma_{pf}$

$\sigma_{tf}(E,T) = \sigma_{af}(E,T)+\sigma_{sf}(E,T)$

$\alpha_j = (\frac{A_j-1}{A_j+1})^2$; A_j being the ratio of the mass of isotope j to the mass of the neutron

Note that "moderator" in the above usage refers to <u>all</u> non-resonance-absorber nuclei present. If we use the NR approximation for the moderator and the IR approximation for the absorber (G4), we get:

$$\phi(E,T,\sigma_0) = \frac{\sigma_0+\lambda\sigma_{pf}}{\sigma_{af}(E,T)+\lambda\sigma_{sf}(E,T)+\sigma_0}\,\frac{1}{E} \qquad (3.4)$$

where the source is normalized such that "$\phi=\frac{1}{E}$" will be the off-resonance reference value for the flux per unit energy. Upon substituting Eq. (3.4) into Eq. (3.1) one obtains:

$$\sigma_{cg}(T,\sigma_0) = \frac{\int_{\Delta Eg} \frac{\sigma_0 + \lambda\sigma_{pf}}{\sigma_{af}(E,T)+\lambda\sigma_{sf}(E,T)+\sigma_0} \sigma_c(E,T)\frac{dE}{E}}{\int_{\Delta Eg} \frac{\sigma_0 + \lambda\sigma_{pf}}{\sigma_{af}(E,T)+\lambda\sigma_{sf}(E,T)+\sigma_0} \frac{dE}{E}} . \qquad (3.5)$$

Because σ_0 and σ_{pf} are essentially constant within ΔEg, they can be cancelled-out from the numerator and denominator of Eq. (3.5) to give:

$$\sigma_{cg}(T,\sigma_0) = \frac{\int_{\Delta Eg} \frac{\sigma_c(E,T)}{\sigma_{af}(E,T)+\lambda\sigma_s(E,T)+\sigma_0} \cdot\frac{dE}{E}}{\int_{\Delta Eg} \frac{1}{\sigma_{af}(E,T)+\lambda\sigma_s(E,T)+\sigma_0} \cdot\frac{dE}{E}} \qquad (3.6)$$

which is the effective capture cross-section at temperature T and with the constant background cross-section σ_0.

3.2.3 Definition of Homogeneous Self-Shielding Factor and its Parametrized Forms

The idea and method of self-shielding factors was first popularized in the widely used publication of the so-called "Bondarenko" cross sections in 1964 (B3). Since then, the self-shielding factor approach has become common practice in the fast reactor field, due primarily to its ease of application; there are, however, minor disadvantages in the method, as described in Ref. (K5).

The self-shielding factor, $f_{xg}(T,\sigma_0)$, is defined by the equation:

$$\sigma_{xg}(T,\sigma_0) = f_{xg}(T,\sigma_0)\sigma^{\infty}_{xg} \qquad (3.7)$$

where the complications involved in the integration over resonance structure, as indicated by Eq. (3.5), are separated from the calculation of the effective multigroup constants for a specific mixture/composition. Tables of f-factors are pre-computed for the elastic, fission, capture, total, and transport cross sections and for arbitrary sets of T and σ_0 values. The f-factors for any given T and σ_0 can then be obtained by interpolating in these tables. Having obtained the f-factor we can then multiply it by the proper infinite-dilution cross section to get the required effective cross section, $\sigma_{xg}(T,\sigma_0)$, represented by Eqs. (3.5) and (3.7). The success of the above approach relies heavily on the availability of accurate schemes for both temperature and σ_0 interpolation of the self-shielding factor, $f_{xg}(T,\sigma_0)$. One expression for the self-shielding factor as a function of σ_0 at a fixed temperature T, which is used as a fitting function, is:

$$f_{cg}(\sigma_0) = A\tanh B(\ell n\sigma_0+C)+D \qquad (3.8)$$

where A, B, C, and D are constants determined by four values of f_{cg} at given σ_0 values.

An alternative expression is:

$$f_{cg}(\sigma_0) = \left(\frac{\sigma_{pf}+\sigma_0}{\eta_{tf}+\sigma_{pf}+\sigma_0}\right)^{\frac{1}{2}} \qquad (3.9)$$

where η_{tf} is the total cross section at the resonance peak, and σ_{pf} and σ_0 are as previously defined.

Equation (3.9) is an accurate representation of the self-shielding factor provided the group contains more than a few resonances - i.e. is applicable to coarse groups (S7). With a little algebra, Eq. (3.9) can be transformed into a more useful form, as follows:

$$\frac{1}{1 - f_{cg}^2(\sigma_0)} = A\sigma_0 + B \qquad (3.10)$$

where A, B are constants determined by two values of f_{cg} at given σ_0 values.

Note that the parameters η_{tf} and σ_{pf} appearing in Eq. (3.9) are contained in the constants A and B of Eq. (3.10), which are easily determined from the f-factor tables. Expression (3.8) is an empirical relation suggested by Kidman (K4); while Eq. (3.9) is an analytical expression obtained by Segev (S7). As for temperature interpolation at a fixed σ_0, a Lagrange-three-point interpolation scheme predicts, very accurately, the shielding factors for any current temperature, T.

Finally, let us very briefly discuss one last important item - namely the σ_0-ambiguity. As already defined, σ_0 is given by:

$$\sigma_{0i}^{g} = \frac{1}{N_i} \sum_{i \neq j} N_j \left(f_{cj}^{g} \, {}^{g}\sigma_{cj}^{\infty} + f_{fj}^{g} \, {}^{g}\sigma_{fj}^{\infty} + f_{ej}^{g} \, {}^{g}\sigma_{ej}^{\infty} + f_{in,j}^{g} \, {}^{g}\sigma_{in,j}^{\infty} \right) \qquad (3.11)$$

where c ≡ capture; f ≡ fission; e ≡ elastic-scattering; in ≡ inelastic-scattering. If at least one of the other elements - i.e. an element other than isotope i, in the mixture has a resonant cross section, then σ_0 will be ambiguous. A common remedy for this ambiguity is an iteration scheme, as follows:

$$ {}^{(0)}f_{x,i}^{g} = 1$$

$$ {}^{(n)}\sigma_{0i}^{g} = \frac{1}{N_i} \sum_{i \neq j} N_j \, {}^{(n-1)}f_{x,j}^{g} \, {}^{g}\sigma_{xj}^{\infty} \qquad (n=1,2,\ldots) \qquad (3.12)$$

where the superscript n denotes the order of iteration and x refers to the various processes, as explicitly defined in Eq. (3.11).

It suffices to say that the above iteration scheme converges; however, the question as to whether or not it converges to the correct value remains open. Since in the present work we are treating the case of a single dominant resonant isotope, the question of σ_0-ambiguity will not be crucial to our work. Interested readers may refer to Refs. (S6,S7) for a thorough investigation of the above problem.

This concludes the discussion of homogeneous self-shielding, hopefully adequate to lay the groundwork for the introduction of heterogeneous self-shielding factors. For more complete expositions on the subject of homogeneous self-shielding the following references are recommended: B3,G1,K1,K4,K6,S6,S7. Appendix D contains a more detailed discussion of the interpolation schemes introduced in this section, and the method of their application.

3.3 HETEROGENEOUS SELF-SHIELDING

Concentrating the fuel in a region separate from that of the moderator leads to a number of advantages, and a few disadvantages, from the reactor physics viewpoint. The benefits of having a heterogeneous system, however, generally outweigh the principal disadvantage, namely, the reduction in thermal utilization. The most important advantage associated with heterogeneity is the decrease of the resonance region absorption of neutrons undergoing slowing down, due to the self-shielding effect in the fuel lumps, see Fig. 3.1, i.e., the neutron flux is enhanced in the moderator and depressed in the fuel, which increases the resonance escape probability. The heterogeneous arrangement also results in an increase in the fast effect. All of these phenomena have been recognized from the earliest days of reactor design.

In what follows only the resonance self-shielding is to be analyzed.

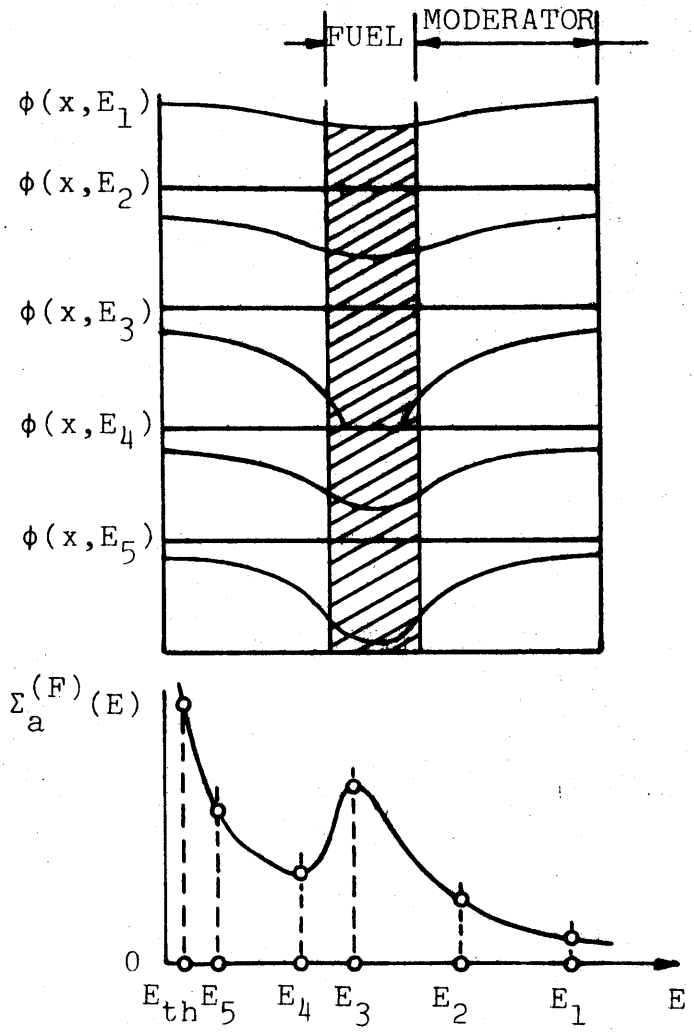

FIG. 3.1 FLUX DEPRESSION AS FUNCTION OF NEUTRON ENERGY

3.3.1 Volume-Averaged Fuel Flux in the WR, NR, and IR Approximations

In this section an expression will be derived from the basic slowing down equations for the spatially-averaged fuel flux in terms of the moderator-to-fuel flux ratio "R" for a two-region unit cell. It is at this point that we depart from conventional methods, where both the fuel and the moderator fluxes (the two essential quantities needed for cell-homogenization purposes) are found in terms of escape probabilities; in the present work the corresponding two quantities are the fuel flux "$\overline{\phi}_f(E)$" and the flux ratio "R(E)", and no escape probabilities are directly involved in the final results.

Ideally one would seek an exact analytical solution to the slowing-down equations; unfortunately such is not available. As a result, the narrow-resonance (NR) and wide-resonance (WR) approximations were introduced as initial attempts to obtain approximate analytical solutions. Improvements in these first approximations were subsequently made by iteration on the basic integral equation (B2). However there are instances when a choice between the two limiting approximations, NR and WR, is difficult to make. To overcome this difficulty a third approximation, namely, the intermediate resonance (IR) approximation was introduced (refer to Secton 2.7.1) which is designed to characterize all intermediate situations, including the limiting NR and WR extremes.

The slowing-down equations, subject to the following conditions:

(a) $\vec{n}\cdot\vec{J}(\underline{r},E) = 0$ (no leakage)

(b) $\chi(E) = 0$ (no fission source in the slowing-down range)

(c) elastic scattering is isotropic in the center of mass system,

are:

$$\Sigma_{tm}(E)\bar{\phi}_m(E) = [1-P_m(E)] \int_E^{E/\alpha_m} \frac{\Sigma_{sm}(E')\bar{\phi}_m(E')}{(1-\alpha_m)} \frac{dE'}{E'} +$$

$$P_f(E)\frac{V_f}{V_m} \int_E^{E/\alpha_f} \frac{\Sigma_{sf}(E')\bar{\phi}_f(E')}{(1-\alpha_f)} \frac{dE'}{E'} \qquad (3.13)$$

$$\Sigma_{tf}(E)\bar{\phi}_f(E) = [1-P_f(E)] \int_E^{E/\alpha_f} \frac{\Sigma_{sf}(E')\bar{\phi}_f(E')}{(1-\alpha_f)} \frac{dE'}{E'} +$$

$$P_m(E)\frac{V_m}{V_f} \int_E^{E/\alpha_m} \frac{\Sigma_{sm}(E')\bar{\phi}_m(E')}{(1-\alpha_m)} \frac{dE'}{E'} \qquad (3.14)$$

where $P_f(E)$ is the probability that a neutron of energy E born in the fuel will escape from the lump without a collision

$P_m(E)$ is the probability that a neutron of energy E born in the moderator has its next collision in the fuel.

$P_f(E)$ and $P_m(E)$ are thus escape-probabilities for average neutrons in the fuel and moderator. Moreover, it is important to note that, in general, the sum of $P_f(E)$ and $P_m(E)$ is not unity; the two probabilities belong to different initial sources of neutrons.

Considering the general case, in which some moderator is admixed with the fuel, and utilizing the (IR) parameters as introduced in Section 2.7.1, one can then solve Eqs. (3.13) and (3.14) to obtain the following results:

$$[\Sigma_{am}(E)+\Sigma_{sm}(E)]\bar{\phi}_m(E) = [1-P_m(E)]\bar{\mu}\Sigma_{sm}(E)\frac{C}{E} +$$

$$[1-P_m(E)][1-\bar{\mu}]\Sigma_{sm}(E)\bar{\phi}_m(E) + P_f(E)\frac{V_f}{V_m}[\lambda\Sigma_{pf}+\nu\Sigma_{snf}(E)]\frac{C}{E} +$$

$$P_f(E)\frac{V_f}{V_m}[(1-\lambda)\Sigma_{sf}(E)+(1-\nu)\Sigma_{snf}(E)]\bar{\phi}_f(E) \qquad (3.15)$$

$$[\Sigma_{af}(E)+\Sigma_{sf}(E)+\Sigma_{anf}(E)+\Sigma_{snf}(E)]\bar{\phi}_f(E) = [1-P_f(E)][\lambda\Sigma_{pf}+\nu\Sigma_{snf}(E)]\frac{C}{E}$$

$$+ [1-P_f(E)][(1-\lambda)\Sigma_{sf}(E)+(1-\nu)\Sigma_{snf}(E)]\bar{\phi}_f(E) +$$

$$P_m(E)\frac{V_m}{V_f}\bar{\mu}\Sigma_{sm}(E)\frac{C}{E} + P_m(E)\frac{V_m}{V_f}(1-\bar{\mu})\Sigma_{sm}(E)\bar{\phi}_m(E) \qquad (3.16)$$

Parameter C is a normalization constant given by

$$C = \frac{q\, V_{cell}}{V_m \bar{\xi}_m \Sigma_{sm} + V_f \bar{\xi}_f \Sigma_{pf}} ,$$

where q is the slowing-down density. Strictly speaking, C is an energy-dependent quantity which should reflect the decrease in q when moving down the resonance ladder from one resonance to the next. However, if the group width is such that it contains just a few resonances, then assuming a single mean value for q, and hence for C, leads to very little error.

Upon adding Eqs. (3.15) and (3.16), the terms multiplying the escape probabilities cancel out, and the following simpler expression remains:

$$V_m[\Sigma_{am}(E)+\Sigma_{sm}(E)]\bar{\phi}_m(E)+V_f[\Sigma_{af}(E)+\Sigma_{sf}(E)+\Sigma_{anf}(E)+\Sigma_{snf}(E)]\bar{\phi}_f(E)$$

$$= V_m\bar{\mu}\Sigma_{sm}(E)\frac{C}{E} + V_m(1-\bar{\mu})\Sigma_{sm}(E)\bar{\phi}_m(E) + V_f[\lambda\Sigma_{pf}+\nu\Sigma_{snf}(E)]\frac{C}{E}$$

$$+ V_f[(1-\lambda)\Sigma_{sf}(E)+(1-\nu)\Sigma_{snf}(E)]\bar{\phi}_f(E) \qquad (3.17)$$

which is further reduced to:

$$V_m[\Sigma_{am}(E)+\bar{\mu}\Sigma_{sm}(E)]\bar{\phi}_m(E) + V_f[\Sigma_{af}(E)+\lambda\Sigma_{sf}(E)+\Sigma_{anf}(E)+$$

$$\nu\Sigma_{snf}(E)]\bar{\phi}_f(E) = V_m\bar{\mu}\Sigma_{sm}(E)\frac{C}{E} + V_f[\lambda\Sigma_{pf}+\nu\Sigma_{snf}(E)]\frac{C}{E}$$

(3.18)

Equation (3.18) can now be used to obtain the spatially-averaged fuel flux in terms of the flux ratio $R(E) \equiv \frac{\bar{\phi}_m(E)}{\bar{\phi}_f(E)}$ as follows:

$$\bar{\phi}_f(E) = \frac{V_m\bar{\mu}\Sigma_{sm}(E)+V_f\lambda\Sigma_{pf}+V_f\nu\Sigma_{snf}(E)}{V_f[\Sigma_{af}(E)+\lambda\Sigma_{sf}(E)+\Sigma_{anf}(E)+\nu\Sigma_{snf}(E)]+V_m[\Sigma_{am}(E)+\bar{\mu}\Sigma_{sm}(E)]R(E)} \frac{C}{E} \tag{3.19}$$

As it stands, Eq. (3.19) is a quite general expression for the spatially-averaged fuel flux in terms of the flux ratio R(E); and it could thus serve as a weighting function. There are, however, a number of simplifying assumptions that can be introduced into Eq. (3.19) at this stage without significant loss of generality, and which greatly simplify some of the subsequent analysis: these assumptions are the following:

(a) $\Sigma_{sm}(E)$, $\Sigma_{am}(E)$, $\Sigma_{snf}(E)$, and $\Sigma_{anf}(E)$ are all weakly dependent on energy, especially within a given energy group; hence they will be replaced by group-averaged parameters.

(b) All moderator elements will be treated as NR scatterers. The error of the NR approximation as applied to the moderator is of the order of $\frac{\frac{1}{2}\Gamma_p}{E_r(1-\alpha_m)}$, where $\frac{1}{2}\Gamma_p \equiv$ practical half-width of the resonance, $E_r(1-\alpha_m) \equiv$ maximum energy loss in a moderator collision. For light moderators $E_r(1-\alpha_m)$ is usually much greater than Γ_p, (G4).

(c) Setting the normalization constant, C, arbitrarily equal to 1.0; this will lead to $\phi(E) = \frac{1}{E}$ as the off-resonance reference value for the flux per unit energy.

(d) $\Sigma_{am} << \Sigma_{sm}$ and $\Sigma_{anf} << \Sigma_{snf}$.

Introducing the above assumptions into Eq. (3.19) the following simpler expression is obtained:

$$\overline{\phi}_f(E) = \frac{V_m \Sigma_{sm} + V_f \Sigma_{snf} + V_f \lambda \Sigma_{pf}}{V_f[\Sigma_{af}(E) + \lambda \Sigma_{sf}(E) + \Sigma_{tnf}] + V_m \Sigma_{tm} R(E)} \cdot \frac{1}{E} \qquad (3.20)$$

Equation (3.20) reduces to the WR limit when $\lambda=0$, and to the NR limit when $\lambda=1$.

3.3.2 Effective Group Capture Cross-Section for a Resonance Absorber

We are now at a stage where almost all the groundwork necessary for generating "equivalent" group parameters , ($\overline{\nu\Sigma}_{fg}$, Σ_{cg}, $\Sigma_{gg'}$,... etc.), which are constant over the entire volume occupied by any given cell in a reactor, has been developed. The group constants generated should, when used in a group-diffusion-theory calculation for the whole reactor, reproduce the same average reaction rates over a given cell as would be determined if an exact energy dependent transport calculation was performed for a heterogeneous reactor with all the geometrical characteristics of the unit cells treated explicitly.

To start with a rigorously accurate definition of equivalent homogenized cross-section, recall the explanation given in Section 2.1 and especially the constraint set by Eq. (2.1) - namely:

$$\vec{n}\cdot\vec{J}(\underline{r},E) = 0 \tag{3.21}$$

Then, the definition of an equivalent homogenized capture cross-section specialized to a two-region unit cell will be:

$$\sum_{cg}^{j} = \frac{\int_{V_{cell}} dV \int_{\Delta Eg} dE \; \sum_{c}^{j}(\underline{r},E,T)\phi(\underline{r},E)}{\int_{V_{cell}} dV \int_{\Delta Eg} dE \;\; \phi(\underline{r},E)} \tag{3.22}$$

Further assume that the resonance absorber, j, is present only in the fuel region; then Eq. (3.22) can be expanded to yield the following form:

$$\sum_{cg} = \frac{\int_{\Delta Eg} dE \left| \Sigma_{cf}(E,T) \int_{V_f} \phi(\underline{r},E)dV \right|}{\int_{\Delta Eg} dE \left| \int_{V_f} \phi(r,E)dV + \int_{V_m} \phi(\underline{r},E)dv \right|} \tag{3.23}$$

Define the spatially averaged fluxes as:

$$\bar{\phi}_m(E) = \frac{1}{V_m} \int_{V_m} \phi(\underline{r},E)dV; \tag{3.24}$$

$$\bar{\phi}_f(E) = \frac{1}{V_f} \int_{V_f} \phi(\underline{r},E)dV; \tag{3.25}$$

Using Eq. (3.24) and (3.25) in Eq. (3.23) we get:

$$\Sigma_{cg} = \frac{\int_{\Delta Eg} \Sigma_{cf}(E,T) V_f \bar{\phi}_f(E) dE}{\int_{\Delta Eg} [V_f \bar{\phi}_f(E) + V_m \bar{\phi}_m(E)] dE} \tag{3.26}$$

or

$$\Sigma_{cg} = \frac{\int_{\Delta Eg} \Sigma_{cf}(E,T) \bar{\phi}_f(E) dE}{\int_{\Delta Eg} [1 + \frac{V_m}{V_f} R(E)] \bar{\phi}_f(E) dE} \tag{3.27}$$

Our next step is to solve Eq. (3.27), knowing R(E) and $\bar{\phi}_f(E)$ from Eqs. (2.81) and (3.20) respectively. As it stands the problem is essentially intractable unless plausible simplifications are introduced into Eq. (2.81): the following are to be implemented:

(a) Linearization of the expression for R(E), by using group-averaged values for the values of τ appearing in α_f, α_m, β, ρ. Numerical studies confirm that this is an acceptable device: in the present application one could even use the weak absorption asymptote without introducing significant error (see Appendix B). The numerator of Eq. (2.81) becomes $[1+\bar{\gamma}_f \delta_f(E)]$, with $\bar{\gamma}_f \equiv \alpha_f \beta \rho Q_m$ evaluated at group-averaged values for the τ involved. In like manner the denominator of Eq. (2.81) will take the similar form $[1+\bar{\gamma}_m \delta_m(E)]$.

(b) $\Sigma_{tm}(E)$ and $\Sigma_{tnf}(E)$ are very weakly dependent on energy, especially within the range of energy covered by a typical group width. Hence, we can treat $\delta_m(E)$ as constant over ΔEg. This last assumption in conjunction with the one made in part (a) immediately implies that the denominator of Eq. (2.81) can be taken as constant, and it shall henceforth be denoted by θ.

Based on assumptions (a) and (b) Eq. (2.81) can now be written in a more manageable form:

$$R(E,T) = \frac{1}{\theta}[1 + \bar{\gamma}_f \delta_f(E,T)] \tag{3.28}$$

where θ and $\bar{\gamma}_f$ are as previously defined.

Substituting Eqs. (3.20) and (3.28) into Eq. (3.27), the following is obtained:

$$\Sigma_{cg} = \frac{\int_{\Delta Eg} \frac{(V_m\Sigma_{sm}+V_f\Sigma_{snf}+V_f\lambda\Sigma_{pf})\cdot\Sigma_{cf}(E,T)}{V_f\Sigma_{af}(E,T)+V_f\lambda\Sigma_{sf}(E,T)+V_f\Sigma_{tnf}+V_m\Sigma_{tm}\frac{1}{\theta}[1+\bar{\gamma}_f\delta_f(E,T)]} \frac{dE}{E}}{\int_{\Delta Eg} \frac{(V_m\Sigma_{sm}+V_f\Sigma_{snf}+V_f\lambda\Sigma_{pf})\cdot\{1+\frac{V_m}{V_f}\frac{1}{\theta}[1+\bar{\gamma}_f\delta_f(E,T)]\}}{V_f\Sigma_{af}(E,T)+V_f\lambda\Sigma_{sf}(E,T)+V_f\Sigma_{tnf}+V_m\Sigma_{tm}\frac{1}{\theta}[1+\bar{\gamma}_f\delta_f(E,T)]} \frac{dE}{E}} \tag{3.29}$$

or more simply:

$$\Sigma_{cg} = \frac{\int_{\Delta Eg} \frac{\Sigma_{cf}(E,T)}{\sigma_{af}(E,T)+\lambda\sigma_{sf}(E,T)+\frac{\Sigma_{tnf}}{N_f}+\frac{V_m}{V_f}\frac{\Sigma_{tm}}{N_f}\frac{1}{\theta}[1+\bar{\gamma}_f\delta_f(E,T)]}\frac{dE}{E}}{\int_{\Delta Eg} \frac{1+\frac{V_m}{V_f}\frac{1}{\theta}[1+\bar{\gamma}_f\delta_f(E,T)]}{\sigma_{af}(E,T)+\lambda\sigma_{sf}(E,T)+\frac{\Sigma_{tnf}}{N_f}+\frac{V_m}{V_f}\frac{\Sigma_{tm}}{N_f}\frac{1}{\theta}[1+\bar{\gamma}_f\delta_f(E,T)]}\frac{dE}{E}} \quad (3.30)$$

where $(V_m\Sigma_{sm}+V_f\Sigma_{snf}+V_f\lambda\Sigma_{pf})$ has been cancelled-out, because it it treated as essentially constant over the energy range covered by ΔEg.

Using the explicit form of $\delta_f(E,T)$, given by Eq. (2.76) with $\nu=1$, in Eq. (3.30) we get:

$$\Sigma_{cg} = \frac{\int_{\Delta Eg} \frac{\Sigma_{cf}(E,T)}{\sigma_{af}+\lambda\sigma_{sf}+\frac{\Sigma_{tnf}}{N_f}+\frac{V_m}{V_f}\frac{\Sigma_{tm}}{N_f}\frac{1}{\theta}[1+\bar{\gamma}_f(\tau_{af}+\lambda\tau_{sf}+\tau_{tnf})]}\frac{dE}{E}}{\int_{\Delta Eg} \frac{1+\frac{V_m}{V_f}\frac{1}{\theta}[1+\bar{\gamma}_f(\tau_{af}+\lambda\tau_{sf}+\tau_{tnf})]}{\sigma_{af}+\lambda\sigma_{sf}+\frac{\Sigma_{tnf}}{N_f}+\frac{V_m}{V_f}\frac{\Sigma_{tm}}{N_f}\frac{1}{\theta}[1+\bar{\gamma}_f(\tau_{af}+\lambda\tau_{sf}+\tau_{tnf})]}\frac{dE}{E}} \quad (3.31)$$

Recalling the definition of optical thickness given in Section 2.2 and that $\sigma_{af} = \sigma_{\text{capture of the fuel}}+\sigma_{\text{fission of the fuel}} \equiv \sigma_{cf}+\sigma_{ff}$, the terms containing optical thicknesses can be written in terms of the basic microscopic cross sections. This facilitates collecting common terms - that is, taking the denominator of both the top and bottom part of Eq. (3.31) one gets:

$$\sigma_{cf}+\sigma_{ff}+\lambda\sigma_{sf}+\frac{\Sigma_{tnf}}{N_f}+\frac{V_m}{V_f}\,\frac{\Sigma_{tm}}{N_f}\,\frac{1}{\theta}[1+\bar{\gamma}_f N_f \ell_f(\sigma_{cf}+\sigma_{ff}+\lambda\sigma_{ff}+\frac{\Sigma_{tnf}}{N_f})], \quad (3.32)$$

which upon grouping the common terms becomes:

$$(1+\frac{\Omega}{\theta})[\sigma_{cf}+\sigma_{ff}+\lambda\sigma_{sf}]+(1+\frac{\Omega}{\theta})\frac{\Sigma_{tnf}}{N_f} + \frac{V_m}{V_f}\,\frac{1}{\theta}\,\frac{\Sigma_{tm}}{N_f} \quad (3.33)$$

where $$\Omega \equiv \bar{\gamma}_f N_f \frac{\Sigma_{tm}}{N_f}\,\ell_f\,\frac{V_m}{V_f} = \bar{\gamma}_f\,\Sigma_{tm}\ell_m = \bar{\gamma}_f \cdot \tau_{tm} \quad (3.34)$$

Based on the assumed constancy of $\bar{\gamma}_f$, θ, and τ_{tm} over the energy range ΔEg, it follows that the term $(1+\frac{\Omega}{\theta})$ is also constant over the same energy range and hence can be factored out of the integrands of both the numerator and denominator of Eq. (3.31). After factoring out the term $(1+\frac{\Omega}{\theta})$ from expression (3.33), one has:

$$(1+\frac{\Omega}{\theta})[\sigma_{af}+\lambda\sigma_{sf}+\frac{\Sigma_{tnf}}{N_f} + \frac{1}{\theta+\Omega}\cdot\frac{V_m}{V_f}\cdot\frac{\Sigma_{tm}}{N_f}] \quad (3.35)$$

If we volume-homogenize $(\Sigma_{tnf})/(N_f)$ and $(\Sigma_{tm})/(N_f)$ and note that their sum is the total background cross section per resonance absorber, then, based on the definitions given in Sections 3.2.2 and 3.2.3, the above sum is denoted by σ_0'. The prime is introduced to indicate the modification made on the second term - i.e. $(\Sigma_{tm})/(N_f)$, by the multiplicative factor $\frac{1}{\theta+\Omega}$. To put it quantitatively:

$$\sigma_0' = \frac{\frac{V_f}{V_{cell}}\Sigma_{tnf}}{\frac{V_f}{V_{cell}}N_f} + \frac{1}{\theta+\Omega}\frac{\frac{V_m}{V_{cell}}\Sigma_{tm}}{\frac{V_f}{V_{cell}}N_f} \equiv \frac{\bar{\Sigma}_{tnf}}{\bar{N}_f} + \frac{1}{\theta+\Omega}\frac{\bar{\Sigma}_{tm}}{\bar{N}_f} \qquad (3.36)$$

where the bars over Σ_{tnf}, Σ_{tm}, and N_f denote volume-weighted-homogenization.

Substituting expression (3.36) into expression (3.35), there results:

$$(1+\frac{\Omega}{\theta})(\sigma_{af}+\lambda\sigma_{sf}+\sigma_0') \qquad (3.37)$$

This factor can now be used as the denominator of both the top and bottom parts of Eq. (3.31), to give:

$$\frac{V_f}{V_{cell}}\cdot\sigma_{cg} = \frac{\int_{\Delta Eg}\frac{\sigma_{cf}}{\sigma_{af}+\lambda\sigma_{sf}+\sigma_0'}\frac{dE}{E}}{\int_{\Delta Eg}\frac{1+\frac{V_m}{V_f}\left[\frac{1}{\theta}+\varepsilon'''\sigma_{cf}+\varepsilon'''\sigma_{ff}+\varepsilon'''\lambda\sigma_{sf}+\varepsilon'''\frac{\Sigma_{tnf}}{N_f}\right]}{\sigma_{af}+\lambda\sigma_{sf}+\sigma_0'}\frac{dE}{E}} \qquad (3.38)$$

where

$$\varepsilon''' = \frac{1}{\theta}\bar{\gamma}_f N_f \frac{V_m}{V_f}\ell_f$$

Also note that the constant term $(1+\frac{\Omega}{\theta})$ has been cancelled out. Upon inversion, Eq. (3.38) becomes:

$$\frac{1}{\frac{V_f}{V_{cell}}\cdot\sigma_{cg}} = \frac{\int_{\Delta Eg}\frac{1}{\sigma_{af}+\lambda\sigma_{sf}+\sigma_0'}\frac{dE}{E}}{\int_{\Delta Eg}\frac{\sigma_{cf}}{\sigma_{af}+\lambda\sigma_{sf}+\sigma_0'}\frac{dE}{E}} + \frac{\frac{V_m}{V_f}\frac{1}{\theta}\int_{\Delta Eg}\frac{1}{\sigma_{af}+\lambda\sigma_{sf}+\sigma_0'}\frac{dE}{E}}{\int_{\Delta Eg}\frac{\sigma_{cf}}{\sigma_{af}+\lambda\sigma_{sf}+\sigma_0'}\frac{dE}{E}}$$

$$+ \frac{\varepsilon'''\int_{\Delta Eg}\frac{\sigma_{cf}}{\sigma_{af}+\lambda\sigma_{sf}+\sigma_0'}\frac{dE}{E}}{\int_{\Delta Eg}\frac{\sigma_{cf}}{\sigma_{af}+\lambda\sigma_{sf}+\sigma_0'}\frac{dE}{E}} + \frac{\varepsilon'''\int_{\Delta Eg}\frac{\sigma_{ff}}{\sigma_{af}+\lambda\sigma_{sf}+\sigma_0'}\frac{dE}{E}}{\int_{\Delta Eg}\frac{\sigma_{cf}}{\sigma_{af}+\lambda\sigma_{sf}+\sigma_0'}\frac{dE}{E}}$$

$$+ \frac{\varepsilon'''\int_{\Delta Eg}\frac{\lambda\sigma_{sf}}{\sigma_{af}+\lambda\sigma_{sf}+\sigma_0'}\frac{dE}{E}}{\int_{\Delta Eg}\frac{\sigma_{cf}}{\sigma_{af}+\lambda\sigma_{sf}+\sigma_0'}\frac{dE}{E}} + \frac{\varepsilon'''\frac{\Sigma_{tnf}}{N_f}\int_{\Delta Eg}\frac{1}{\sigma_{af}+\lambda\sigma_{sf}+\sigma_0'}\frac{dE}{E}}{\int_{\Delta Eg}\frac{\sigma_{cg}}{\sigma_{af}+\lambda\sigma_{sf}+\sigma_0'}\frac{dE}{E}} \qquad (3.39)$$

Upon comparing each of the different parts of Eq. (3.39) with Eq. (3.6) the following rigorous result is achieved,

$$\frac{1}{\sigma_{cg}^{het}} = \frac{V_f/V_{cell}}{\sigma_{cg}^{hom}} + \frac{V_m}{V_{cell}}\frac{1}{\theta}\frac{1}{\sigma_{cg}^{hom}} + \varepsilon'' + \varepsilon''\frac{\sigma_{fg}^{hom}}{\sigma_{cg}^{hom}} +$$

$$\varepsilon''\frac{\sigma_{sg}^{hom}}{\sigma_{cg}^{hom}} + \varepsilon''\frac{\Sigma_{tng}}{N_f}\frac{1}{\sigma_{cg}^{hom}} \qquad (3.40)$$

where

σ_{cg}^{hom} = group-averaged homogeneous capture cross-section

σ_{fg}^{hom} = group-averaged homogeneous fission cross-section

σ_{sg}^{hom} = group-averaged homogeneous elastic scattering cross-section

σ_{cg}^{het} = group-averaged "homogenized" capture cross-section

Σ_{tng} = total non-resonance cross section in the fuel region for group g.

$\varepsilon'' = (V_f/V_{cell})\varepsilon''' =$

$$\frac{V_f}{V_{cell}} \frac{\bar{\gamma}_f}{\theta} N_f \frac{V_m}{V_f} \ell_f = \frac{\bar{\gamma}_f}{\theta} \frac{V_m}{V_{cell}} N_f \ell_f$$

With a bit of straightforward algebra Eq. (3.40) can be further reduced to obtain the following simple form:

$$\sigma_{cg}^{het}(T,\sigma_0) = \frac{\sigma_{cg}^{hom}(T,\sigma_0')}{\eta + \varepsilon''\sigma_{cg}^{hom}(T,\sigma_0')} \tag{3.41}$$

where

$$\eta = \frac{V_f}{V_{cell}} + \frac{1}{\theta} \frac{V_m}{V_{cell}} + \varepsilon''\sigma_{fg}^{hom}(T,\sigma_0') + \varepsilon''\sigma_{sg}^{hom}(T,\sigma_0') + \frac{\bar{\gamma}_f}{\theta} \frac{V_m}{V_{cell}} \tau_{tng}$$

$$\varepsilon'' = \frac{\bar{\gamma}_f}{\theta} \frac{V_m}{V_{cell}} N_f \ell_f$$

It is important to note, as evident from the method of derivation, that Eq. (3.41) predicts the correct homogenized cross-section under any condition so long as the homogeneous part (i.e. $\sigma_{cg}^{hom}(T,\sigma_0')$) is treated, under those same conditions, correctly elsewhere in the literature.

3.3.3 The Heterogeneous Self-Shielding Factor and a New Equivalence Theorem

The present aim, as mentioned before, is to devise a method by which one can obtain accurate heterogeneous self-shielding factors embodying all the characteristics and properties of the well-established Bondarenko f-factor formalism, previously developed for homogeneous systems.

Recalling Eq. (3.7) for the definition of the self-shielding factor, and applying it to Eq. (3.41), leads to the following important expression:

$$f_{cg}^{het}(T,\sigma_0) = \frac{f_{cg}^{hom}(T,\sigma_0')}{\eta + \varepsilon' f_{cg}^{hom}(T,\sigma_0')} \tag{3.42}$$

where

$$\eta = \frac{V_f}{V_{cell}} + \frac{1}{\theta}\frac{V_m}{V_{cell}} + \varepsilon'' f_{fg}^{hom}(T,\sigma_0')\cdot\sigma_{fg}^{\infty} + \varepsilon'' f_{sg}^{hom}(T,\sigma_0')\cdot\sigma_{sg}^{\infty} + \frac{\bar{\gamma}_f}{\theta}\frac{V_m}{V_{cell}}\tau_{tng}$$

$$\varepsilon' = \varepsilon''\cdot\sigma_{cg}^{\infty}$$

or

$$f_{cg}^{het}(T,\sigma_0) = \frac{1}{\eta + \varepsilon} \; f_{cg}^{hom}(T,\sigma_0') \qquad (3.43)$$

where $\varepsilon = \varepsilon' f^{hom}(T, \sigma_0')$

which is in the form of a New Equivalence Relationship, whereby the corresponding f-factor for the heterogeneous cell is expressed in terms of the f-factor for a homogeneous cell evaluated at a modified value of the constant background cross-section - namely σ_0'. Equation (3.42) was derived assuming a single resonance is embedded in the energy group of width ΔEg. However, as it stands, the applicability of the equation can easily be extended to coarse groups by simply referring all the parameters appearing in Eq. (3.42) to their corresponding coarse group values.

Finally, it is worthwhile to present a brief review of what we will call the "conventional" methods used hitherto and compare their results with those of the present method - i.e. Eq. (3.43) and all of its implications. Conventionally, one uses the second equivalence theorem to make the heterogeneity correction. The statement of the theorem is as follows (H1,L4): a heterogeneous system will have the same resonance integral as a homogeneous system evaluated at:

$$\sigma_0' = \frac{\overline{\Sigma}_{tnf}}{\overline{N}_f} + \frac{1-c}{N_f \ell_f} \frac{a}{1+(a-1)c} = \frac{\overline{\Sigma}_{tnf}}{\overline{N}_f} + \frac{1}{1+\frac{1}{a}\tau_{tm}} \frac{\overline{\Sigma}_{tm}}{\overline{N}_f} \qquad (3.44)$$

where c is the Dancoff-Ginsberg factor given by:

$$1-c = \frac{\tau_{tm}}{1+\frac{1}{a}\tau_{tm}} \quad , \text{ in Bell's approximation (B1)} \qquad (3.45)$$

with "a" known as the Levine correction factor (L2), which typically takes on values lying between $1/a \simeq 0.63$ and $1/a \simeq 0.84$. It has been found, however - refer to (H2,L2) - that a value of $1/a \simeq 0.79$ yields accurate results over the entire range of practical lump sizes.

Although the theorem is strictly valid for resonance integrals, it is also utilized to predict group cross sections via the following equations - consult Refs. (F4,H4,K6):

$$\sigma_{cg} = \frac{RI_{cg}}{F\Delta U} \qquad (3.46)$$

where RI_{cg} = capture resonance integral for group g

ΔU = lethargy width for group g, obtained by assuming a 1/E flux shape

F = flux shape correction factor (corrects for both the non-1/E shape of the flux envelope, and for resonance-induced flux dips)

Applying the preceding theorem to either (or both) Eqs. (3.46) and (3.6) yields the following conventional result in terms of the f-factors:

$$r_{cg}^{het}(T,\sigma_0) = r_{cg}^{hom}(T,\sigma_0') \qquad (3.47)$$

Upon comparing Eqs. (3.43) and (3.47) we immediately note that the factor $\frac{1}{\eta + \varepsilon}$ has been set equal to 1.0 in the conventional method. This factor, as will be seen in Section 3.5, would induce some difference into the heterogeneous cross-sections obtained conventionally and those obtained using the new method. This discrepancy raises questions as to the validity of the second equivalence theorem as applied to cross-sections but not to resonance integrals. The difficulty stems from the fact that the true integrated heterogeneous flux, as given by the denominator of Eqs. (3.26) and (3.27), has in the conventional approach been replaced by a homogeneous flux evaluated at σ_0' in the denominator of Eqs. (3.6) and (3.45), thus leading to the present disparity.

As for the first equivalence theorem, it states: heterogeneous systems with the same σ_0' (refer to Eq. (3.44)) have equal resonance integrals. It can easily be shown that the statement of the theorem is in accordance with the predictions of Eq. (3.43).

The above conclusions, in conjunction with the result of Eq. (3.43), constitute the present New Equivalence Theorem.

3.4 A COMPARISON BETWEEN THE CONVENTIONAL AND THE PRESENT DANCOFF FACTOR AND ESCAPE PROBABILITY EXPRESSIONS

In this section we will obtain expressions for the Dancoff factor and the fuel escape probability by comparing the various results of the present method with the corresponding conventional results. Before getting into the algebra, some simplifying assumptions are introduced, which are not to be taken as limiting approximations, however:

(a) Impose the NR approximation. Therefore, strictly speaking, all results obtained in this section are for the NR case. Results for the WR and IR cases are obtainable by exactly the same methods.

(b) Consider only thermal reactors, where the slowing down source is in the moderator, hence $Q_f=0$ and $\theta=1$.

Using the above assumptions and comparing Eqs. (3.36) and (3.44) we get:

$$\frac{1}{1+\Omega} \equiv \frac{1}{1+\bar{\gamma}_f\tau_{tm}} \Leftrightarrow \frac{1}{1+\frac{1}{a}\tau_{tm}}, \tag{3.48}$$

which says that $\bar{\gamma}_f \Leftrightarrow \frac{1}{a}$, thus leading to a similar expression for the Dancoff factor: given by Eq. (3.44) with the only change being the replacement of $\frac{1}{a}$ by $\bar{\gamma}_f$.

$$1 - c = \frac{\tau_{tm}}{1+\bar{\gamma}_f\tau_{tm}} \qquad \text{present method} \tag{3.49}$$

The next task is to find a corresponding expression for the escape probability, $P_f(E)$. Utilizing Eqs. (3.15) and (3.16) in conjunction with the above assumptions, and going through some simple algebra the following result is obtained:

$$R(E) = \frac{1 + (\frac{\tau_{sf}(E)}{\tau_{tf}(E)} - 1)\frac{\tau_{tf}(E)}{\tau_{tm}(E)} P_f(E)}{1 + (\frac{\tau_{sf}(E)}{\tau_{tf}(E)} - 1)(1 - \frac{\tau_{tm}(E)}{\tau_{tf}(E)})P_m(E)} \tag{3.50}$$

(I) in the asymptotic region $\tau_{sf}(E) \simeq \tau_{pf} \simeq \tau_{tf}(E)$, which when substituted in Eq. (3.50) results in $R(E) \simeq 1$, as to be expected.

(II) in the resonance region where $\tau_{tf} >> \tau_{sf}$ (black fuel) one obtains:

$$R(E) = \frac{1}{P_f(E)} - \frac{\tau_{tf}(E)}{\tau_{tm}(E)} \tag{3.51}$$

Conventionally, the fully rational approximation for $P_f(E)$ is:

$$P_f(E) = \frac{1}{1 + \frac{1+\frac{1}{a}\tau_{tm}}{\tau_{tm}} \tau_{tf}(E)} \tag{3.52}$$

Substituting Eq. (3.52) into Eq. (3.51) gives:

$$R(E) = 1 + \frac{1}{a} \tau_{tf}(E) \tag{3.53}$$

which has exactly the same form as predicted by our results - namely:

$$R(E) = 1 + \bar{\gamma}_f \tau_{tf}(E) \tag{3.54}$$

Upon comparing Eqs. (3.53) and (3.54) we note:

$$\frac{1}{a} \Leftrightarrow \bar{\gamma}_f \tag{3.55}$$

Using the equivalence relation given by Eq. (3.55), and working backward, we obtain the following expression for $P_f(E)$:

$$P_f(E) = \frac{1}{1 + \frac{1+\bar{\gamma}_f \tau_{tm}}{\tau_{tm}} \tau_{tf}(E)} \tag{3.56}$$

Equation (3.56) is the analog of Eq. (3.52).

The above encouraging results strengthen our confidence in the present method. We will see in Section 3.4 that the range of values for $\bar{\gamma}_f^*$ for cylindrical unit cells is:

$$0.47 \lesssim \bar{\gamma}_f \lesssim 0.64 \tag{3.57}$$

which can be compared to the variation of 1/a reported earlier to be:

$$0.63 \lesssim \frac{1}{a} \lesssim 0.84 \tag{3.58}$$

Figure 3.2 shows a plot of the Dancoff correction obtained in Ref. (L3) using the MOCUP Monte Carlo program. The Monte

*Also note that $\bar{\gamma}_f$ approaches the asymptotic limit of 1.0 as the moderator optical thickness (τ_{tm}) gets large, see the footnote on page 96.

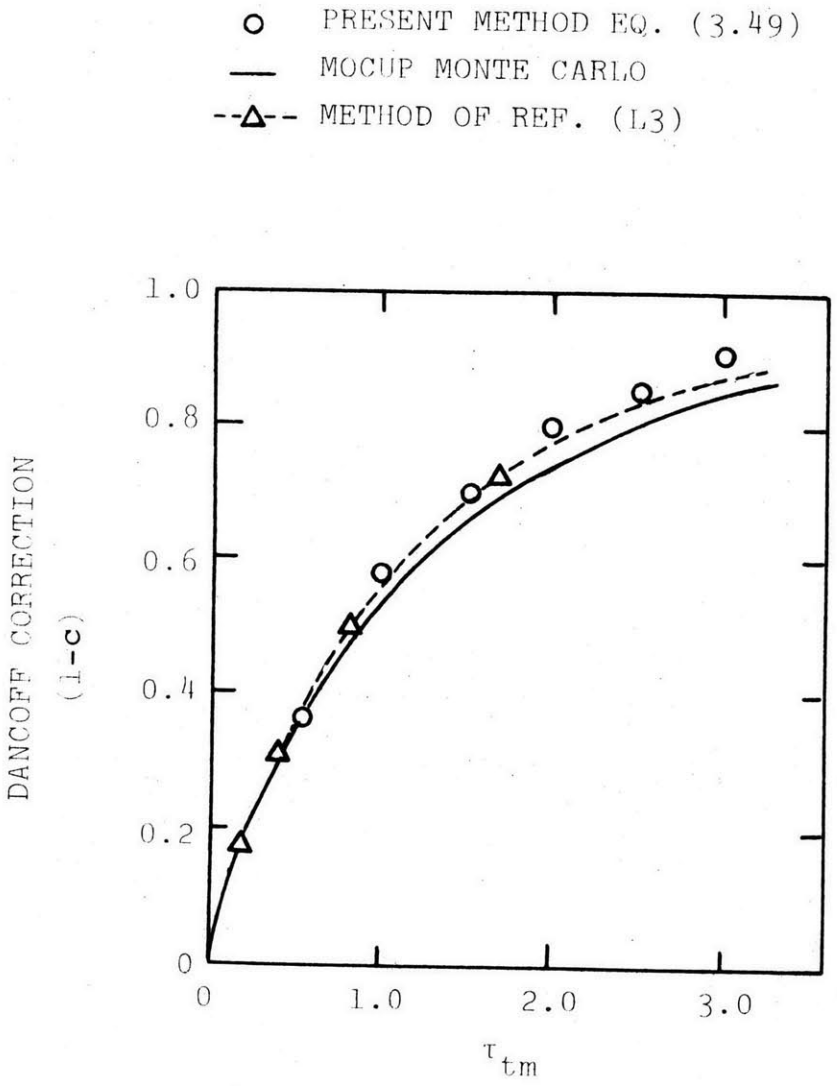

FIG. 3.2 VARIATION OF THE DANCOFF CORRECTION WITH MODERATOR OPTICAL THICKNESS FOR A SQUARE PIN CELL WITH $V_F/V_M = 1.$

Carlo program computation was performed on a two-region "square pin cell" of high fuel cross-section* and with $V_m/V_f=1$. As can be seen, the present analytical results are in as good agreement with the Monte Carlo computations as are the results of the analytical model proposed in Ref. (L3); with the exception that the present model is considerably simpler than the model proposed in the reference. Both models, however, are obtained assuming unit cell cylindricalization; as a result, they do not distinguish between square and hexagonal cells. Finally, the results of the two models are about 3% higher than the corresponding Monte Carlo computations.

3.5 COMPARISON OF MODEL RESULTS WITH LEOPARD CALCULATIONS

In the present section homogeneous-to-heterogeneous corrections are calculated with the new equivalence theorem, and the results compared to equivalent output from the LEOPARD Code (L5), a state-of-the-art LWR unit cell program. The base-case unit cell data used in both calculations is representative of current commercial PWR reactors (specifically, Maine Yankee); Table 3.7 summarizes pertinent dimensions and compositions.

---

* $\bar{\gamma}_f$ in the limit of high fuel optical thickness is, (refer to Chapter 2):

$$\bar{\gamma}_f = \frac{\frac{2}{3} + 0.24\tau_{tm}^{1/2}}{1 + 0.24\tau_{tm}^{1/2}}$$

The EPRI version of LEOPARD was employed, together with its ENDF/B IV derived cross-section library. For the self-shielding-factor method cross-sections, and f-factors as a function of σ_0, were taken from the LIB-IV fast-reactor cross-section set developed by LASL (also derived from the ENDF/B IV library)(K6).

3.5.1 Energy (Group) Dependence of Essential Parameters

Table 3.1 gives the group* values for Q_m, $\bar{\nu}_f$, θ, η, ε, σ_0, and σ_0' calculated for the base case PWR unit cell. Appendix E contains a step-by-step procedure for calculating one of the table values; moreover, a brief discussion of some aspects of LEOPARD, pertinent to the present problem, will be given in Appendix C.

There are several important observations to be made in the above table. First, we note that the value of Q_m (fraction of the neutron source originating in the moderator) is approximately 1.0; hence, justifying the widely used assumption, in thermal reactors, of considering the epithermal slowing down density to be zero within the fuel. Another effect of the above observation would be to make $\theta \simeq 1.0$, as indeed is the case upon referring to the foregoing table; this validates assumption (b) made in Section 3.4; furthermore, the indicated slow variation of $\bar{\nu}_f$ over the groups helps to partially justify assumption (a) of Section 3.3.2.

---

* Group structures are given in Table 3.8.

Table 3.1

Group Values of Q_m, $\bar{\gamma}_f$, θ, η, ε, σ_0, and σ_0' for the Base-Case PWR Unit Cell

Group No.*	Q_m	$\bar{\gamma}_f$	θ	η	ε	σ_0 barns	σ_0' barns
26	0.987	0.473	1.008	1.138	0.006	100	61
27		0.482		1.162	0.006	105	63
28		0.481		1.141	0.007	106	64
29		0.478		1.148	0.007	100	60
30	0.988	0.483		1.148	0.008	100	60
31		0.477		1.130	0.007	102	61
32		0.481		1.139	0.009	100	60
33		0.478		1.126	0.011	100	60
34		0.481		1.132	0.012	102	61
35		0.474		1.118	0.011	101	61
36		0.471		1.117	0.010	101	61
37		0.489		1.130	0.010	107	63
38		0.525		1.159	0.013	101	62
39		0.536		1.159	0.020	102	62
40		0.511		1.119	0.022	102	63
41		0.473	1.007	1.139	0.007	103	66
42	0.979	0.632	1.019	1.327	0.030	103	59
43	0.988	0.588	1.010	1.134	0.057	103	61
44		0.467	1.007	1.114	0.004	105	68
45		0.607	1.011	1.142	0.160	103	60

* See Table 3.8 for group structure.

In Table 3.2 the analytic and the LEOPARD results for the ratio of heterogeneous-to-homogeneous self-shielding factors, evaluated at the same σ_0, are compared. There are two group number entries in the table, one for LIB-IV and another for LEOPARD; their energy groups are matched using the corresponding group structures given in Table 3.8. Note that only the resonance part of the LEOPARD results for the absorption cross section is considered - i.e., the smooth or "$\frac{1}{V}$" term, which is of small effect, has been omitted. Hence, the dashed lines shown in the table imply that there are no resonance contributions in the corresponding groups. Use of the LIB-IV cross section set did not permit separation of resonance and smooth effects in the present model. The important point to note in this table, however, is the near constancy of the LEOPARD results for the ratio $f^{het}(\sigma_0)/f^{hom}(\sigma_0)$ over groups 26-45. This would suggest that weak resonances undergo as much self-shielding as strong resonances, counter to both intuitive and analytical expectations. Our results, on the other hand, indicate less self-shielding for weak resonances and greater self-shielding for strong resonances.

3.5.2 Dependence of the Ratio $f^{het}(\sigma_0)/f^{hom}(\sigma_0)$ on Moderator Optical Thickness

Figure 3.3 is a plot of homogeneous broad group capture cross-section (σ_c^{hom}) as a function of moderator optical thickness (τ_{tm}), with the fuel diameter kept constant. The broad group cross section is defined by a 1/E weighted group collapse:

Table 3.2

Group Values for the Ratio of Heterogeneous-to-Homogeneous Self-Shielding Factor

LIB-IV Group No.*	LEOPARD Group No.*	This Model $\left\|\frac{f^{het}(\sigma_0)}{f^{hom}(\sigma_0)}\right\|$ (resonance + smooth)	LEOPARD $\left\|\frac{f^{het}(\sigma_0)}{f^{hom}(\sigma_0)}\right\|$ (resonance)
26 & 27	26	0.836	0.596
28 & 29	27	0.822	0.598
30 & 31	28	0.799	0.601
32 & 33	29	0.776	0.601
34 & 35	30	0.749	0.593
36 & 37	31	0.741	0.586
38	32	0.652	0.610
39	33 & 34	0.661	0.611
40	35 & 36	0.679	0.613
41	37 & 38	0.768	--
42	39 & 40	0.556	0.630
43	41 & 42	0.631	0.644
44	43 & 44	0.892	--
45	45 & 46	0.592	0.660
46	47 & 48	0.900	--
47	49 & 50	↓	--
48	51 & 52	↓	--
49	53 & 54	↓	--

* See Table 3.8 for group structure.

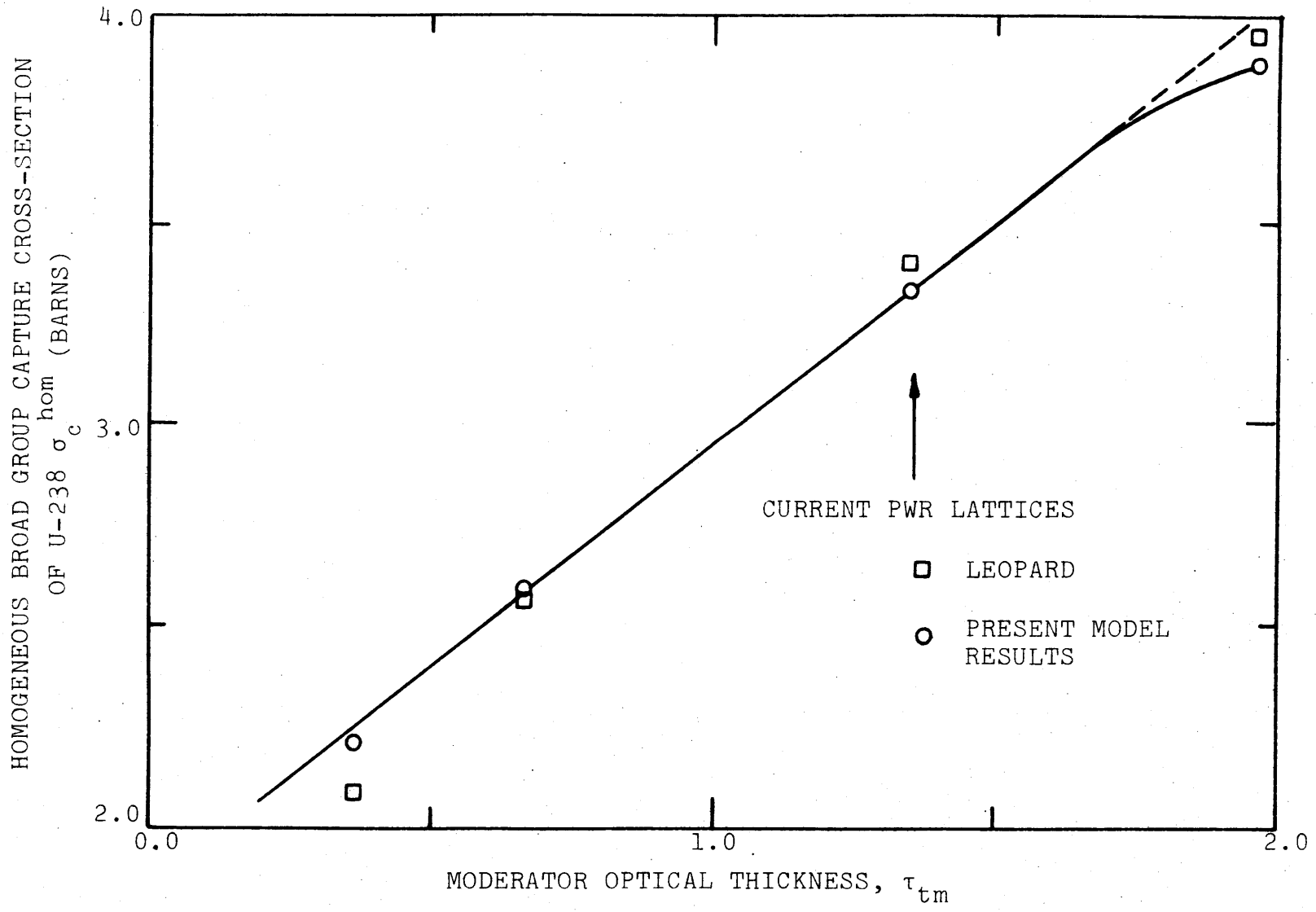

FIG. 3.3 HOMOGENEOUS BROAD GROUP CAPTURE CROSS-SECTION OF U-238 AS A FUNCTION OF MODERATOR OPTICAL THICKNESS

Table 3.3

Tabulated Results Applicable to Fig. 3.3

oderator Optical Thickness	σ_c^{hom} (barns) analytical, using f-factor formalism	σ_c^{hom} (barns) LEOPARD	Δ% percent difference
0.361	2.218	2.088	+6.2
0.663	2.591	2.565	+1.0
1.354	3.336	3.410	-2.2
1.965	3.883	3.962	-2.0

$$\sigma_c^{hom} = \sum_{GP26}^{GP49} \sigma_i \Delta u_i / \sum_{26}^{49} \Delta u_i$$

As is evident from the figure the capture cross sections obtained using self-shielding factors are in good agreement with the corresponding parameters generated using LEOPARD. Depending on one's point of view this either validates the f-factor formalism, LEOPARD, or both. Table 3.3 contains the tabulated results of Fig. 3.3 including percentage differences.

In Fig. 3.4 the analytic and the LEOPARD results for the ratio of heterogeneous-to-homogeneous self-shielding factors ($f^{het}(\sigma_0)/f^{hom}(\sigma_0)$) as a function of moderator optical thickness (at constant fuel pin diameter) are shown. The agreement shown between the two results is good (particularly for $\tau_{tm} \underline{\sim}$ that of current PWR designs); also note that the results fall very nearly on a straight line. This observation can be explained as follows. Considering Eq. (4.22) (to be derived in Chapter 4) one gets:

$$\frac{f^{het}(\sigma_0)}{f^{hom}(\sigma_0)} \simeq 1 - \frac{1}{2} \frac{\bar{\gamma}_f \tau_{tm}}{1+\bar{\gamma}_f \tau_{tm}} \{1 - [f^{hom}(\sigma_0)]^2\} \qquad (3.59)$$

or in a more condensed form:

$$\frac{f^{het}(\sigma_0)}{f^{hom}(\sigma_0)} \simeq 1 - \psi \cdot \tau_{tm} \qquad (3.60)$$

where

$$\psi = \frac{\frac{1}{2}\bar{\gamma}_f(1-f^2)}{1+\bar{\gamma}_f \tau_{tm}}$$

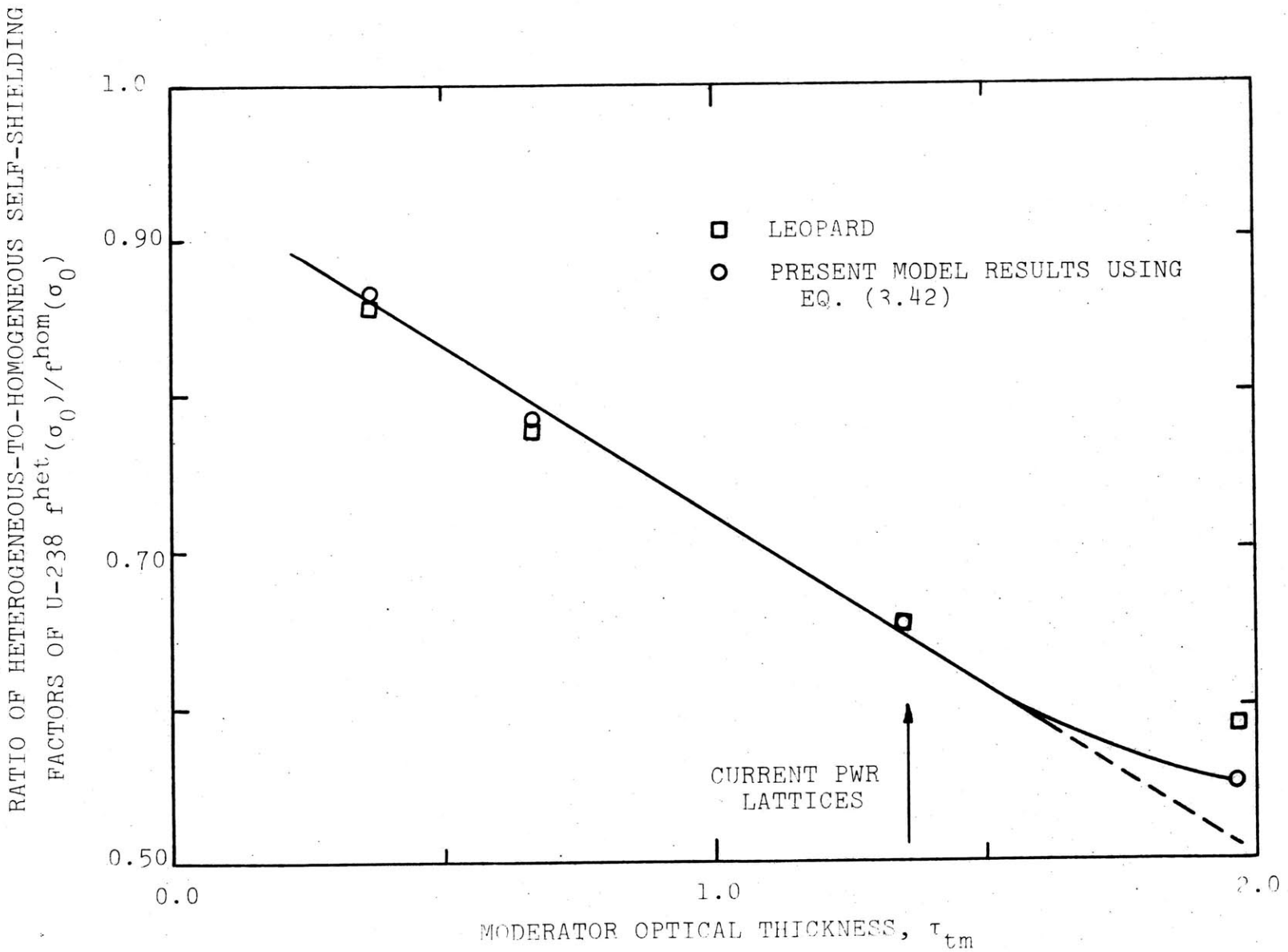
RATIO OF HETEROGENEOUS-TO-HOMOGENEOUS SELF-SHIELDING FACTORS OF U-238 $f^{het}(\sigma_0)/f^{hom}(\sigma_0)$
1.0
0.90
0.70
0.50
0.0
1.0
2.0
MODERATOR OPTICAL THICKNESS, τ_{tm}
LEOPARD
PRESENT MODEL RESULTS USING EQ. (3.42)
CURRENT PWR LATTICES

Table 3.4

Tabulated Results Applicable to Fig. 3.4

Moderator Optical Thickness	$\frac{f_c^{het}(\sigma_0)}{f_c^{hom}(\sigma_0)}$ present model Eq. (3.42)	$\frac{f_c^{het}(\sigma_0)}{f_c^{hom}(\sigma_0)}$ LEOPARD	$\Delta\%$ percent difference
0.361	0.865	0.857	+0.9
0.663	0.784	0.782	+0.3
1.354	0.653	0.653	0.0
1.965	0.551	0.587	-6.5

Note that as the pitch shrinks, σ_0 decreases and the parameters (f^2, $\bar{\gamma}_f \tau_{tm}$, $\bar{\gamma}_f$) approach the following limiting values quite rapidly.

$$f^2(\sigma_0) << 1 \tag{3.61}$$

$$\bar{\gamma}_f \tau_{tm} << 1 \tag{3.62}$$

$$\bar{\gamma}_f \rightarrow \text{constant} \tag{3.63}$$

Hence, ψ will approach a constant value; and, in accordance with Eq. (3.60) $f^{het}(\sigma_0)/f^{hom}(\sigma_0)$ versus τ_{tm} is indeed a linear function with negative slope. The plotted data of Fig. 3.4 are given in Table 3.4 with the percentage differences included: the agreement between the present model and LEOPARD is excellent for all but the thickest moderator case.

3.5.3 Dependence of the Ratio $f^{het}(\sigma_0)/f^{hom}(\sigma_0)$ on Cell Shrinkage Factor

Figure 3.5 shows the ratio $f^{het}(\sigma_0)/f^{hom}(\sigma_0)$ as a function of cell shrinkage factor, which is defined as the factor by which all radial dimensions in the unit cell are multiplied, to shrink or dilate the cell in a manner such that the volume fraction of all constituents is unchanged. The results agree within $\pm$8% (see Table 3.5): however agreement is exact for the base-case PWR cell typical of current commercial lattice designs.

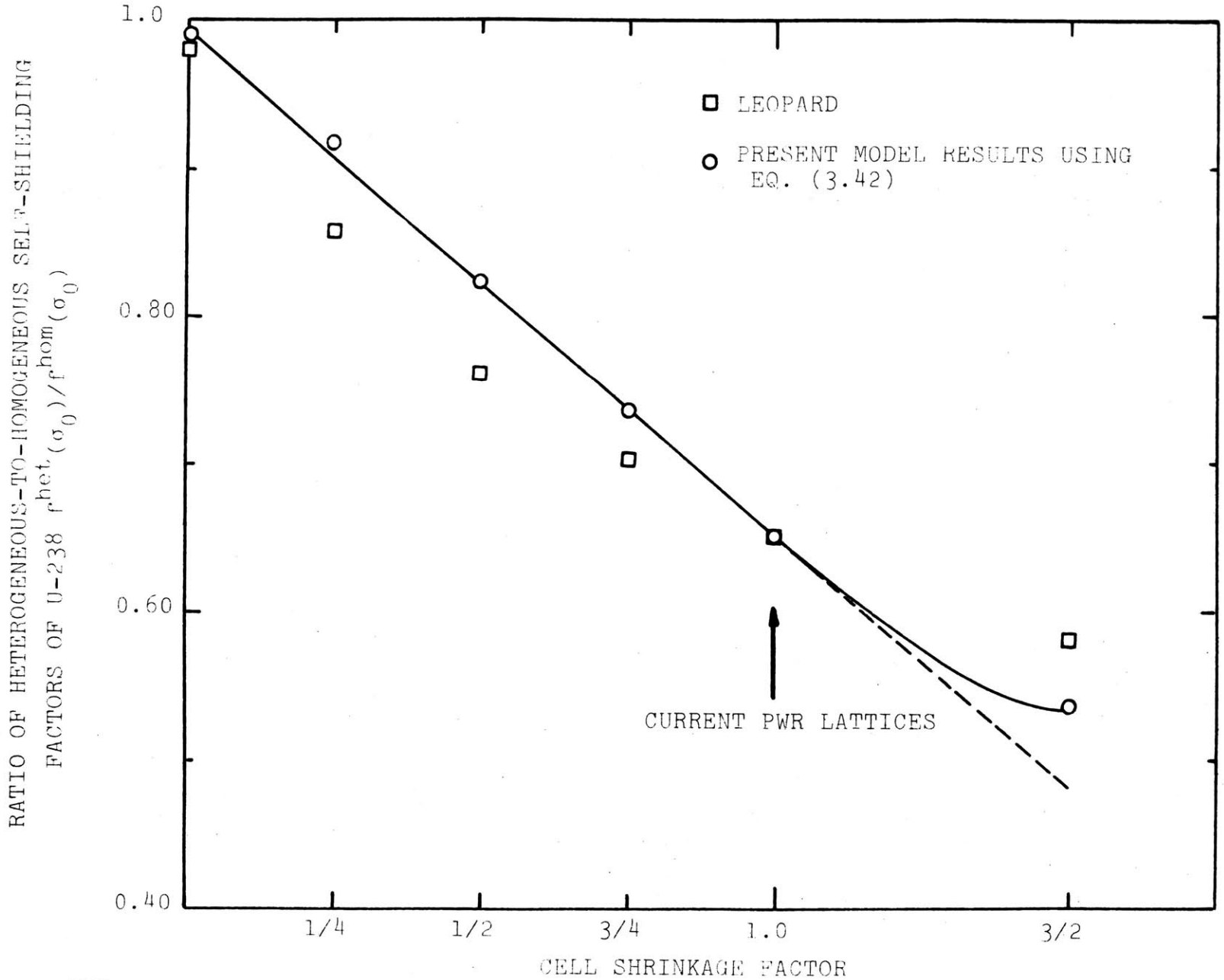

FIG. 3.5 RATIO OF THE BROAD GROUP HETEROGENEOUS-TO-HOMOGENEOUS CAPTURE SELF-SHIELDING FACTORS OF U-238 AS A FUNCTION OF CELL SHRINKAGE FACTOR

Table 3.5

Tabulated Results Applicable to Fig. 3.5

Cell Shrinkage Factor	$\frac{f_c^{het}(\sigma_0)}{f_c^{hom}(\sigma_0)}$ present model Eq. (3.42)	$\frac{f_c^{het}(\sigma_0)}{f_c^{hom}(\sigma_0)}$ LEOPARD	Δ%
Base-Case PWR Unit Cell Dimensions	0.653	0.653	0.0
10^{-3} x the above unit cell dimension	0.999	0.981	+2.0
1/4 x the above unit cell dimension	0.917	0.856	+7.1
1/2 x the above unit cell dimension	0.824	0.762	+8.1
3/4 x the above unit cell dimension	0.735	0.702	+4.7
3/2 x the above unit cell dimension	0.538	0.581	-8.0

3.5.4 Heterogeneous Cross-Section as a Function of Moderator Optical Thickness

Table 3.6 contains the data for the U-238 broad group "heterogeneous" capture cross-sections evaluated at various moderator optical thicknesses and at a fixed fuel pin diameter. As seen from the table, the two central points agree within 2%, and the end points within 8%; these data are plotted in Fig. 3.6. The important point to note here is the approach of the curve to an asymptotic limit as the moderator thickness increases, the reason being that as the moderator optical thickness increases, the results approach the isolated-lump limit.

3.6 DISCUSSION AND CONCLUSIONS

A new approach for obtaining equivalent homogenized cross-sections has been developed. It has been shown to validate most prior (conventional) results, with the exception, on theoretical grounds, of the second equivalence theorem used for generating homogenized cross-sections. However, heterogeneity corrections calculated using the present method were generally in good agreement with the same corrections obtained using LEOPARD; agreement is particularly good for unit cells typical of current commercial PWR lattices.

Although the present and the conventional equivalence relations differ by the factor $\frac{1}{\eta+\varepsilon}$ (see Section 3.3.3), actual numerical results agree reasonably well. Let us recall some of the previous expressions:

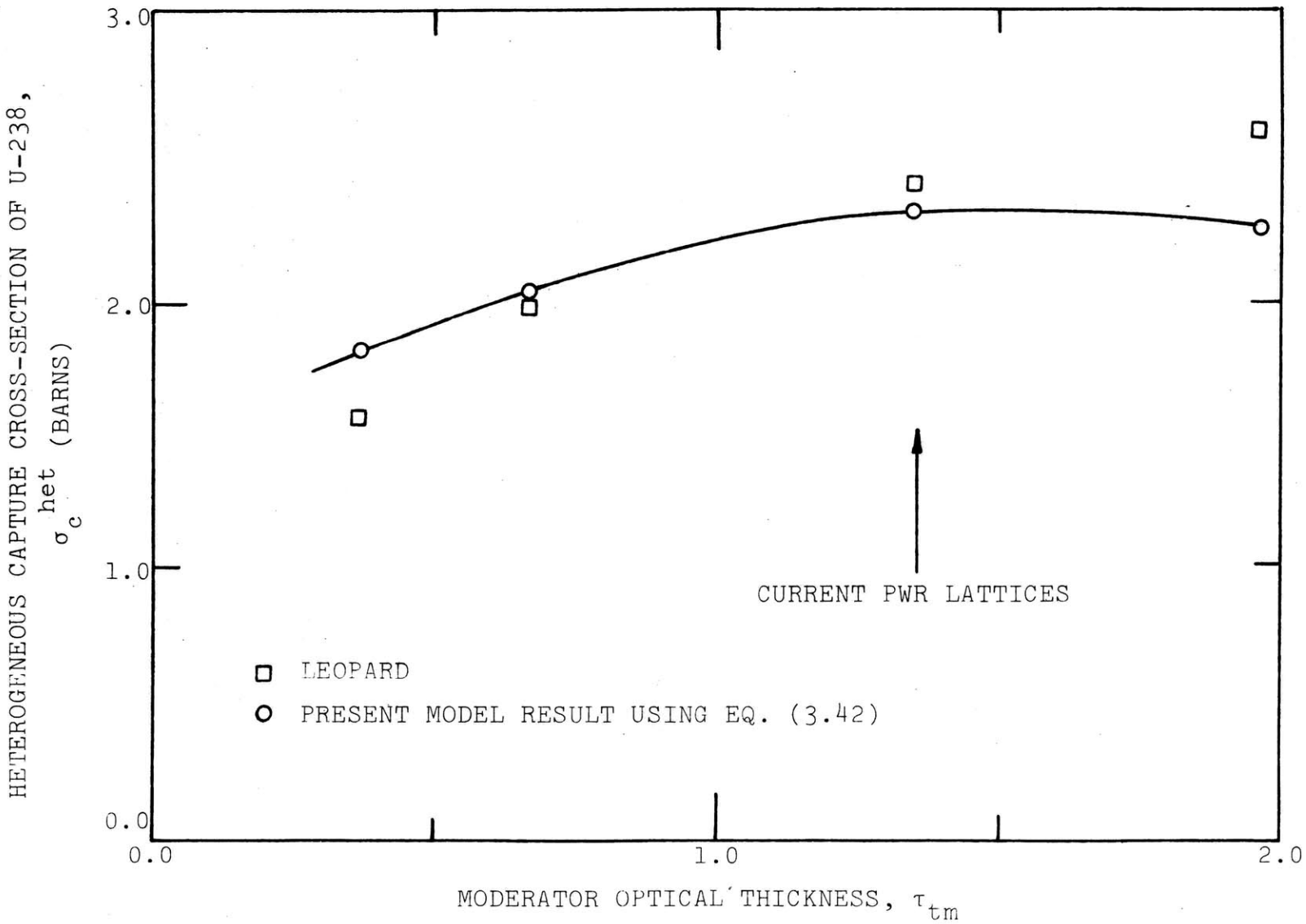

FIG. 3.6 HETEROGENEOUS BROAD GROUP CAPTURE CROSS-SECTION OF U-238 AS A FUNCTION OF MODERATOR OPTICAL THICKNESS

Table 3.6

Tabulated Results Applicable to Fig. 3.6

Moderator Optical Thickness	σ_c^{het} (barns) present model Eq. (3.24)	σ_c^{het} (barns) LEOPARD	Δ% percent difference
0.361	1.919	1.790	+7.2
0.663	2.032	2.005	+1.3
1.354	2.180	2.228	-2.2
1.965	2.141	2.326	-8.6

Table 3.7

Base-Case PWR Unit Cell Data

Homogenized Atom Densities	
Element	Number Density (nuclei/barn cm)
Hydrogen	2.6960×10^{-2}
Oxygen	2.7625×10^{-2}
Zircaloy-2	5.1680×10^{-3}
Carbon	4.3687×10^{-8}
Iron	1.5179×10^{-5}
Nickel	3.1127×10^{-5}
Aluminum	1.9762×10^{-7}
Chromium	1.01414×10^{-5}
Manganese	1.7398×10^{-7}
Uranium-235	2.0767×10^{-4}
Uranium-238	6.8656×10^{-3}

Cell Dimensions

$r_{fuel} = 0.186$ in ; $r_{gap} = 0.189$ in; $r_{clad} = 0.220$ in; pitch = 0.580 in

Temperature

$T_{pellet} = 1209.50$ °F; $T_{clad\ and\ void} = 614.80$ °F; $T_{moderator} = 562.50$ °F

Table 3.8

Energy Group Structure of Cross Section Libraries

LIB IV ENERGY GROUPS			LEOPARD ENERGY GROUPS		
No.	$E_{\text{Lower Boundary}}$	ΔU_i	No.	$E_{\text{Lower Boundary}}$	ΔU_i
upper boundary	5.530 Kev		upper boundary	5.530 Kev	
26	4.31	0.25	26	3.35	0.50
27	3.35	↓	27	2.03	↓
28	2.61		28	1.23	
29	2.03		29	750 ev	
30	1.58		30	454	
31	1.23		31	275	
32	961 ev		32	167	↓
33	749		33	130	0.25
34	583		34	101	↓
35	454		35	78.7	
36	354		36	61.3	
37	275		37	47.8	
38	167	↓	38	37.2	
39	101	0.50	39	29.0	
40	61.4	↓	40	22.6	
41	37.3		41	17.6	
42	22.6		42	13.7	
43	13.7		43	10.7	
44	8.32		44	8.32	
45	5.04		45	6.50	
46	3.06		46	5.10	
47	1.86		47	3.97	
48	1.13		48	3.06	
49	0.6826	↓	49	2.38	
50	1×10^{-5}		50	1.855	↓
			51	1.440	0.2538
			52	1.1250	0.2462
			53	0.8350	0.3000
			54	0.6250	0.2884

$$f_{cg}^{het}(\sigma_0) = \frac{1}{\eta+\varepsilon} f_c^{hom}(\sigma_0') \quad \text{new equivalence relation} \tag{3.64}$$

with

$$\sigma_0 = \frac{\bar{\Sigma}_{tnf}}{\bar{N}_f} + \frac{\bar{\Sigma}_{tm}}{\bar{N}_f} \tag{3.65}$$

$$\sigma_0' = \frac{\bar{\Sigma}_{tnf}}{\bar{N}_f} + \frac{1}{1+\bar{\gamma}_f \tau_{tm}} \frac{\bar{\Sigma}_{tm}}{\bar{N}_f} \tag{3.66}$$

and

$$f_{cg}^{het}(\sigma_0) = f_{cg}^{hom}(\sigma_0') \quad \text{conventional equivalence relation} \tag{3.67}$$

with

$$\sigma_0 = \frac{\bar{\Sigma}_{tnf}}{\bar{N}_f} + \frac{\bar{\Sigma}_{tm}}{\bar{N}_f} \tag{3.68}$$

$$\sigma_0' = \frac{\bar{\Sigma}_{tnf}}{\bar{N}_f} + \frac{1}{1+\frac{1}{a}\tau_{tm}} \frac{\bar{\Sigma}_{tm}}{\bar{N}_f} \tag{3.69}$$

If for the moment we assume that the σ_0' values given by Eqs. (3.66) and (3.69) are equal to each other (note that the σ_0 values are always equal), then the resulting f factors (hence capture cross sections) predicted by the new equivalence relation would be 12 to 25 percent less than the results obtained using the conventional method due to the presence of the factor $\frac{1}{\eta+\varepsilon}$: see Table 3.1 for typical magnitudes of η and ε. The reason, however, that the observed agreement is better, is that the σ_0' given by Eq. (3.69) is considerably lower than the σ_0' given by Eq. (3.66), because the Levine factor 1/a taken here as 1/a=0.79 (see Section 3.3.3) is considerably higher than

the corresponding parameter $\bar{\gamma}_f$, which has an average value of 0.50 (see Table 3.1). Hence, the lower σ_0' used in the present model provides an offsetting correction.

One major advantage in the new approach comes from the fact that the flux ratio R(E) appears both in the numerator and the denominator of Eq. (3.29), which leads to results which are only weakly dependent on the accuracy of R(E) (see Appendix B for numerical justification of this observation). This being the case, it is important to note that the only place at which the flat-flux assumption was introduced is in Section 2.5 in conjunction with the source used in the flux ratio R. In this regard it is shown by Gregory (G1), that for a general parabolic source ($S(r)=1+\alpha^2 r^2$) distribution the mean escape chord length for a transparent cylindrical rod is:

$$\ell_e = \frac{4}{3} r_1 \left(1 - \frac{\alpha^2 r_1^2}{66}\right) \tag{3.70}$$

Assuming that the distribution of scattering sources is given by (G1):

$$\Sigma_s \phi_{FF} = \Sigma_s \cdot \frac{\pi}{2} r_1^2 \left[1 - \frac{1}{4}\left(\frac{r}{r_1}\right)^2 + \ldots.\right] \tag{3.71}$$

where

ϕ_{FF} = first flight flux due to a uniform source. The source of Eq. (3.71) is a parabolic source with $\alpha^2 = -1/4r_1^2$. Substituting this α^2 in Eq. (3.70) we get:

$$\ell_e = \frac{4}{3} r_1 \left(1 + \frac{1}{264}\right) \tag{3.72}$$

which differs by less than 0.4% from the mean escape chord length introduced earlier in Section 2.6, derived under the assumption of a spatially uniform collision source distribution - i.e., flat-flux. Thus, we conclude that the flat-flux assumption is not a significant weakness in our methodology, since it apparently cannot introduce any significant error into the final results. This assertion is also put forth by Kirby and Karam (K2) with regard to the flat-flux assumption as utilized in the conventional methodology. Note also that the flux ratio model was force-fit to transport program calculations in which collision sources were proportional to flux shape. Hence while its analytic form stems from a flat-flux model, its numerical validity is not so constrained.

A final point to note is that we have not merely validated the older conventional approaches to this problem. While the present results include the earlier work as limiting cases, several distinctions must be made:

(a) even in the limiting cases the present work leads to more accurate approximations to "exact" results;

(b) the most general form of the present results handles cases not easily dealt with conventionally - e.g. when fuel moderation is not negligible compared to that of the coolant;

(c) the present result more clearly identifies the nature of the approximations involved, facilitating error analysis;

(d) the present results are a better vehicle for unifying fast and thermal reactor methodology.

The numerical results already given in the past sections and those to be given in the next chapter help underscore the above assertions.

Chapter 4

THE EFFECTS OF HETEROGENEITY IN FAST REACTORS

4.1 INTRODUCTION

The effects of heterogeneity in fast reactors are far less prominent than the corresponding effects in thermal reactors. Fast reactors are so nearly homogeneous because fast neutron mean free paths are for the most part an order of magnitude larger than any dimensions over which physical properties change. This being the case, we can, by using Eqs. (3.9) and (3.43), derive a very simple and practical expression for the ratio $f^{het}(\sigma_0)/f^{hom}(\sigma_0)$, which will predict the heterogeneity corrections to within reasonable accuracy.

For detailed discussions of the effects of heterogeneity in FBR blankets refer to (F2, G1, K1, L1): the blanket is of particular interest here because the diameter of radial blanket fuel pins may be as much as twice that of the core fuel pins, and the ambient neutron spectrum is softer than that of the core - both of which circumstances accentuate the effects of heterogeneity.

4.2 AN APPROXIMATE EXPRESSION FOR $f^{het}(\sigma_0)/f^{hom}(\sigma_0)$ APPLICABLE TO FAST REACTORS

By referring to Table 4.1 which shows groupwise parameters for the metal-fueled blanket mockup described later in this chapter, we observe that:

$$n \simeq 1.0 \quad \text{and} \quad \varepsilon \simeq 0.0 \tag{4.1}$$

Table 4.1

Group Values for Q_f, $\bar{\nu}_f$, η, ε, σ_0, and σ_0' for a Metal-Fueled* Blanket Mockup Unit Cell

G	Q_f	$\bar{\nu}_f$	θ	η	ε	σ_0 barns	σ_0' barns
26	0.032	0.400	1.013	1.014	0.001	59	52
27	0.022	0.440	1.009	1.022	0.002	66	53
28	0.006	0.747	1.003	1.037	0.003	58	20
29	0.021	0.450	1.009	1.023	0.002	107	91
30	0.037	0.397	1.015	1.013	↓	71	64
31	0.042	0.382	1.017	1.007	↓	71	65
32	0.044	0.392	1.018	1.009	↓	76	68
33	0.045	0.384	1.018	1.004	↓	31	28
34	0.044	0.388	1.018	1.006	↓	↓	↓
35	0.042	0.383	1.017	1.004	↓	↓	↓
36	↓	0.380	1.017	1.005	↓	↓	↓
37	↓	0.393	1.017	1.006	0.001	↓	↓
38	↓	0.439	1.020	1.009	0.003	↓	29
39	↓	0.459	1.022	1.009	0.003	↓	↓
40	↓	0.428	1.020	1.002	0.004	↓	↓
41	↓	0.380	1.017	1.010	0.001	32	30
42	↓	0.588	1.030	1.002	0.006	↓	↓
43	↓	0.533	1.028	1.000	0.010	↓	↓
44	↓	0.373	1.016	1.007	0.001	↓	↓
45	↓	0.561	1.032	1.000	0.032	↓	↓

* For oxide fuel only group 45, which contains the largest (and hence most heavily shielded) U-238 resonance is reported:

45	0.444	0.304	1.311	0.916	0.034	24	19

See Table 3.8 for LIB-IV group structure.

which, when substituted into Eq. (3.43), will yield:

$$f_{cg}^{het}(T,\sigma_0) = f_{cg}^{hom}(T,\sigma_0') \tag{4.2}$$

or

$$\frac{f_{cg}^{het}(\sigma_0)}{f_{cg}^{hom}(\sigma_0)} = \frac{f_{cg}^{hom}(\sigma_0')}{f_{cg}^{hom}(\sigma_0)} \tag{4.3}$$

where the explicit "T" dependence has been suppressed for convenience.

Equation (4.3) is a simple and accurate expression for most fast reactor applications, with the proviso that the conditions of Eq. (4.1) are satisfied.

Equation (4.2) is similar to the expression obtained using the second equivalence theorem - namely Eq. (3.47).

Additional simplifications are possible, and while not needed in order to apply the method, will prove useful for the purpose of justifying the linear functional dependence shown in Figs. 3.4 and 3.5. Recalling Eq. (3.9) and casting it in terms of σ_0' gives:

$$f_{cg}^{hom}(\sigma_0') = \left(\frac{\sigma_{pf} + \sigma_0'}{\eta_{tf} + \sigma_{pf} + \sigma_0'}\right)^{1/2} \tag{4.3}$$

Let us define the following quantity:

$$\Delta\sigma_0 = \sigma_0 - \sigma_0' \tag{4.4}$$

or:

$$\sigma_0' = \sigma_0 - \Delta\sigma_0 \tag{4.5}$$

Substituting Eq. (4.5) into Eq. (4.3) yields:

$$f_{cg}^{hom}(\sigma_0') = \left(\frac{\sigma_{pf} + \sigma_0 - \Delta\sigma_0}{\eta_{tf} + \sigma_{pf} + \sigma_0 - \Delta\sigma_0}\right)^{1/2} \tag{4.6}$$

or

$$f^2(\sigma_0') = \frac{\sigma_{pf} + \sigma_0}{\eta_{tf} + \sigma_{pf} + \sigma_0 - \Delta\sigma_0} - \frac{\Delta\sigma_0}{\eta_{tf} + \sigma_{pf} + \sigma_0 - \Delta\sigma_0} \tag{4.7}$$

hence

$$f^2(\sigma_0') = \left[\frac{\eta_{tf}+\sigma_{pf}+\sigma_0}{\sigma_{pf}+\sigma_0} - \frac{\Delta\sigma_0}{\sigma_{pf}+\sigma_0}\right]^{-1} - \left[\frac{\eta_{tf}+\sigma_{pf}+\sigma_0}{\Delta\sigma_0} - \frac{\Delta\sigma_0}{\Delta\sigma_0}\right]^{-1} \tag{4.8}$$

and finally:

$$f^2(\sigma_0') = \left[\frac{1}{f^2(\sigma_0)} - \frac{\Delta\sigma_0}{\sigma_{pf}+\sigma_0}\right]^{-1} - \left[\frac{1}{f^2(\sigma_0)}\,\frac{\sigma_{pf}+\sigma_0}{\Delta\sigma_0} - 1\right]^{-1} \tag{4.9}$$

With a bit of straightforward algebra Eq. (4.9) can be further reduced to obtain the following form:

$$f^{hom}(\sigma_0') = f^{hom}(\sigma_0)\left[\frac{\sigma_{pf}+\sigma_0-\Delta\sigma_0}{\sigma_{pf}+\sigma_0-f^2(\sigma_0)\Delta\sigma_0}\right]^{1/2} \tag{4.10}$$

or

$$f^{hom}(\sigma_0') = f^{hom}(\sigma_0)\left(1+\frac{\sigma_{pf}}{\sigma_0} - \frac{\Delta\sigma_0}{\sigma_0}\right)^{1/2}\left(1+\frac{\sigma_{pf}}{\sigma_0} - f^2(\sigma_0)\frac{\Delta\sigma_0}{\sigma_0}\right)^{-1/2} \tag{4.11}$$

Next we have to expand the square root factors in Eq. (4.11) using the following expansions:

$$(1+x)^{1/2} = 1 + \frac{1}{2}x - \frac{1}{8}x^2 + \ldots \qquad x < 1 \tag{4.12}$$

$$(1+x)^{-1/2} = 1 - \frac{1}{2}x + \frac{3}{8}x^2 + \ldots. \qquad x < 1 \tag{4.13}$$

Retaining only the first order quantities we obtain:

$$f^{hom}(\sigma_0') = f^{hom}(\sigma_0)[1+\frac{1}{2}(\frac{\sigma_{pf}}{\sigma_0} - \frac{\Delta\sigma_0}{\sigma_0}) - \frac{1}{2}(\frac{\sigma_{pf}}{\sigma_0} - f^2(\sigma_0)\frac{\Delta\sigma_0}{\sigma_0})+\ldots] \tag{4.14}$$

or

$$f^{hom}(\sigma_0') \simeq f^{hom}(\sigma_0)[1 - \frac{1}{2}\frac{\Delta\sigma_0}{\sigma_0}(1 - f^2(\sigma_0))] \tag{4.15}$$

Substituting Eq. (4.15) into Eq. (4.3) leads to the following simple formula:

$$\frac{f^{het}(\sigma_0)}{f^{hom}(\sigma_0)} = 1 - \frac{1}{2}\frac{\Delta\sigma_0}{\sigma_0}\{1 - [f^{hom}(\sigma_0)]^2\} , \tag{4.16}$$

which upon using Eq. (4.4), can be written:

$$\frac{f^{het}(\sigma_0)}{f^{hom}(\sigma_0)} = 1 - \frac{1}{2}(1 - \frac{\sigma_0'}{\sigma_0})(1 - f^2(\sigma_0)) \tag{4.17}$$

Substituting the definitions of σ_0 and σ_0' from Chapter 3 into Eq. (4.17) yields:

$$\frac{f^{het}(\sigma_0)}{f^{hom}(\sigma_0)} = 1 - \frac{1}{2}\cdot\frac{\theta+\Omega-1}{\theta+\Omega}\ \frac{1}{1+\frac{\tau_{tnf}}{\tau_{tm}}}\cdot(1 - f^2(\sigma_0)) \tag{4.18}$$

Recall that our intention is to derive a simple approximate expression serving the following purposes:

(1) justifying the linear functional dependence shown in Figs. 3.4 and 3.5;

(2) obtaining a simple and explicit function dependence for the effect of moderation in the fuel (Q_f);

(3) obtaining an expression for $f^{het}(\sigma_0)/f^{hom}(\sigma_0)$ identical to the one derived by Kadiroglu (K1) through different arguments.

To fulfill the above we need to introduce several additional approximations, such as:

(a) assume that the optical thickness of the moderator admixed with fuel is much less than that of the coolant optical thickness: $\tau_{tnf} << \tau_{tm}$, a reasonable assumption;

(b) assume that $\theta \simeq 1.0$: this is not always true especially when Q_f is appreciable, nevertheless it is frequently close to 1.0 - see Table 4.1, for example;

(c) assume the weak-absorption asymptotic limit, in the sense of both low fuel and low coolant/moderator optical thicknesses, hence $\bar{\gamma}_f \simeq \frac{1}{3}Q_m = \frac{1}{3}(1-Q_f)$: see Section 3.3.2 and Table 4.1.

Using assumptions (a) and (b) Eq. (4.18) becomes:

$$\frac{f^{het}(\sigma_0)}{f^{hom}(\sigma_0)} = 1 - \frac{1}{2}\frac{\Omega}{1+\Omega}\left(1 - f^2(\sigma_0)\right) \tag{4.19}$$

or

$$\frac{f^{het}(\sigma_0)}{f^{hom}(\sigma_0)} = 1 - \frac{1}{2}\frac{\bar{\gamma}_f \tau_{tm}}{1+\bar{\gamma}_f \tau_{tm}}\left(1-f^2(\sigma_0)\right) \tag{4.20}$$

which is the expression used in Section 3.5.2. Finally, upon applying assumption (c) to Eq. (4.20) one gets:

$$\frac{f^{het}(\sigma_0)}{f^{hom}(\sigma_0)} = 1 - \frac{1}{6}\frac{\tau_{tm} Q_m}{1+\frac{1}{3}\tau_{tm} Q_m}\left(1 - f^2(\sigma_0)\right) \tag{4.21}$$

or

$$\frac{f^{het}(\sigma_0)}{f^{hom}(\sigma_0)} = 1 - \frac{1}{6}\frac{\tau_{tm}(1-Q_f)}{1+\frac{1}{3}\tau_{tm}(1-Q_f)}\left(1 - f^2(\sigma_0)\right) \tag{4.22}$$

Equation (4.21) is identical to the expression derived by Kadiroglu (K1) via basically different arguments. The strong dependence on Q_f is evident, as is the linear variation with τ_{tm} for small τ_{tm}. The absolute accuracy of Eq. (4.22) is not especially good (it predicts ratios of 0.980 (metal) and 0.988 (oxide) for group 45, compared to the "exact" values of 0.941 and 0.989 in Table **4.4**), however this is not a significant flaw because heterogeneity is of such small consequence.

4.3 SELF-SHIELDING FOR U-METAL-FUELED AND UO_2-FUELED BLANKET UNIT CELLS

As already noted, heterogeneity effects in an LMFBR are expected to be most noticeable in the radial blanket, and of particular importance with regard to the spatial dependence of U-238 capture reaction rates. In order to obtain quantitative data on these and other blanket related phenomena, a facility - the Blanket Test Facility (BTF) - was constructed at M.I.T. to irradiate mock-ups of LMFBR blankets. This facility employs a converter assembly to transform the highly thermalized neutrons from the reactor's thermal column into a spectrum typical of LMFBR core leakage neutrons (F2, L1).

Two types of pin-cell assemblies have been studied in the M.I.T. facility: metal-fueled square lattices, and a single triangular-pitch UO_2-fueled sodium-cooled assembly which is a very realistic simulation of a real LMFBR radial blanket assembly. Thus heterogeneity calculations are of interest for both metal and oxide-fueled unit cells. The geometrical details of the assemblies and the means employed to match their homogenized nuclide compositions with those of a realistic blanket are discussed in Refs. (F2, L1). Data pertinent to the present work are summarized in Tables 4.2 and 4.3.

Table 4.4 gives the calculated values of $f^{het}(\sigma_0)/f^{hom}(\sigma_0)$, obtained using Eq. (3.43), for various groups. As seen from the magnitude of the results, the heterogeneity effects for

Table 4.2

Data Pertinent to U-Metal-Fueled Blanket Mockup Unit Cell

Homogenized Atom Densities*	
Element	Atom Densities (nuclei/barn-cm)
Uranium-28	8.108×10^{-3}
Uranium-25	8.8×10^{-5}
Oxygen	1.6293×10^{-2}
Sodium	8.128×10^{-3}
Chromium	4.064×10^{-3}
Iron	1.375×10^{-2}
Hydrogen	7.3×10^{-5}
Carbon	9.6×10^{-5}

Cell Dimensions

r_f= 0.318 (cm); r_g= 0.351 (cm); r_{clad}= 0.397 (cm); $r_{coolant}$=0.732 (cm)

Temperature

T=300°K

* atom densities are averaged over entire assembly.

Table 4.3

Data Pertinent to Oxide-Fueled Blanket Unit Cell

Homogenized Atom Densities*	
Element	Atom Densities (nuclei/barn-cm)
Uranium-28	0.007043
Uranium-25	0.000078
Oxygen	0.014242
Sodium	0.010740
Chromium	0.001746
Iron	0.014639
Nickel	0.000696
Manganese	0.000228
Silicon	0.000180
Carbon	0.000095

Cell Dimensions

r_f=0.546(cm); r_g=0.564(cm); r_{clad}=0.635(cm); $r_{coolant}$=0.814(cm)

Temperature

T=300°K

* atom densities are averaged over entire assembly.

Table 4.4

Group Values* for $f^{het}(\sigma_0)/f^{hom}(\sigma_0)$, σ_c^{hom}, and σ_c^{het}: Metal Fueled Blanket Mockup

G	$\frac{f^{het}(\sigma_0)}{f^{hom}(\sigma_0)}$ (present model) (Eq.3.43)	$\frac{f^{het}(\sigma_0)}{f^{hom}(\sigma_0)}$ (present model) (Eq.4.22)	σ_c^{hom}(U-238) (barns)	σ^{het}(U-238) (barns)
26	0.972	0.985	0.821	0.798
27	0.948	0.969	0.850	0.806
28	0.876	0.961	1.103	0.967
29	0.951	0.975	1.102	1.048
30	0.965	0.977	1.078	1.040
31	0.975	0.980	1.052	1.025
32	0.964	0.974	1.274	1.228
33	0.967	0.973	1.081	1.046
34	0.964	0.970	1.125	1.084
35	0.963	0.970	1.006	0.968
36	0.963	0.972	0.951	0.915
37	0.952	0.968	0.664	0.632
38	0.971	0.982	1.377	1.337
39	0.962	0.982	1.735	1.700
40	0.975	0.982	2.120	2.067
41	0.973	0.986	0.823	0.801
42	0.965	0.981	2.679	2.584
43	0.958	0.981	4.923	4.718
44	0.991	0.999	0.589	0.584
45	0.941	0.980	14.118	13.284

*For the oxide fuel only group 45, which contains the largest (and hence most heavily shielded)U-238 resonance is reported:

45	0.989	0.988	12.887	12.742

See Table B.1 for LIB-IV group structure.

both the metal-fueled and the oxide-fueled cells are very small indeed: less than the 10% uncertainty currently assigned to U-238 capture cross-section values in this energy range. For the oxide fuel only group 45, which contains the largest (and hence most heavily shielded) U-238 resonance is reported. As seen in the table, the heterogeneity correction for this group (G=45) is only about 1.2% for the oxide case and about 6% for the metal case; this, coupled with the fact that only about 0.015% of the blanket-averaged total neutron flux is in this group, result in very small heterogeneity effects in this assembly in particular and in fast reactors in general.

Since the metal and oxide fuel pins were selected to have comparable optical thicknesses for U-238 capture, the difference between their calculated heterogeneity effects (see Table 4.4) can be attributed to the presence of an appreciable slowing down source in the UO_2 (for which Q_f=0.444), whereas the source in uranium metal is negligible. As can be seen in Eq. (4.22), as Q_f is increased $f^{het}(\sigma_0)/f^{hom}(\sigma_0)$ approaches 1.0.

4.4 DISCUSSION AND CONCLUSIONS

In this chapter heterogeneity effect for typical metal and oxide-fueled unit cells employed in LMFBR blanket mockups studied at M.I.T. were calculated using Eq. (3.43). The cells were part of two distinct assemblies, each with homogeneous nuclide compositions representative of a realistic LMFBR blanket, and also very close to one another. There are several important

observations which can be made based on the tabulated results:

(a) the approximate equivalence relation of Eq. (4.22) shows in an explicit way the effect of moderation in the fuel, through Q_f, which acts to decrease heterogeneous effects. This fact is easily overlooked if one uses thermal reactor treatments which often implicitly assume that the source is entirely in the coolant/moderator region.

(b) the effects of heterogeneity are shown to be small.

(c) the difference in the heterogeneity corrections for metal and oxide-fueled assemblies is apparent; however, it is shown in Ref. (K1) that this difference leads to no significant breeding gain.

Thus while it is conceptually more correct to use the methods developed in the present work to correct for heterogeneity in LMFBR's, the consequences of using even much cruder models are not harmful.

Chapter 5

SUMMARY, CONCLUSIONS AND RECOMMENDATIONS

This chapter is comprised of three parts as follows: first a summary of the subject research will be given; next conclusions pertinent to the work will be drawn; and finally, suggestions for further work will be presented.

5.1 SUMMARY

5.1.1 Introduction

The purpose of this work is to explore and evaluate a new approach to the problem of unit cell homogenization. Two major needs motivated this work:

(a) The results of applying the conventional approach based on equivalence theory to the problem of cell homogenization are still not satisfactory. State of the art LWR computer methods, such as LEOPARD, presently rely upon normalization to an experimental base (L5).

(b) The common failure to consider the slowing down source in the fuel in fast reactors is a demonstrably incorrect oversimplification.

The basis for a new approach has been laid down by the prior investigations of Gregory (G1) and Kadiroglu (K1) at M.I.T. The essential feature is the use of an analytic approximation for the ratio of spatially-averaged moderator to fuel

fluxes in the expression for the equivalent homogenized cross-section. A major contribution of the present work is the development of a generalized correlation for this flux ratio ($R = \overline{\phi}_m/\overline{\phi}_f$), by recourse to various methods such as integral transport and collision probability theory. The derived relationship is valid over a broad range of fuel and moderator optical thicknesses. The final prescription for the flux ratio has been checked against, and normalized to, numerical calculations using the ANISN program (A1).

A linearized form of the flux ratio prescription is developed and used in the expression for the equivalent homogenized cross-section to yield a new equivalence relation that casts heterogeneous cross sections (for any physical process of any isotope) at a given constant background cross-section, σ_0, in terms of the corresponding homogeneous cross-sections evaluated at a modified background cross-section σ_0'. The new equivalence relation, which is applicable to both fast and thermal reactors, is the major achievement of this work.

5.1.2 Flux Ratio Calculations for Unit Cells

As noted in the introduction, the key to the approach analyzed in the present work is the use of simple analytic expressions for the ratio of coolant/moderator to fuel fluxes which can accurately describe the region-average fluxes in a cell. The proposed flux ratio model has the following form:

$$\frac{\bar{\phi}_m(E)}{\bar{\phi}_f(E)} = \frac{1 + F(\tau_{af},\tau_{am},\tau_{sf},\tau_{sm})\cdot\tau_{af}\cdot Q_m}{1 + F(\tau_{am},\tau_{af},\tau_{sm},\tau_{sf})\cdot\tau_{am}\cdot Q_f} \qquad (5.1)$$

where

$\tau_{xi}(E) = \Sigma_x(E)\ell_i$, the optical thickness for process x in region i

ℓ_i = mean Dirac penetration chord length through region i

$\Sigma_x = \sum_j \Sigma_x^j$ macroscopic cross section summed over all j isotopes in the region i (fuel, f, or moderator, m)

Q_m = fraction of neutron source originating in the moderator

Q_f = fraction of neutron source originating in the fuel

The next task is to find an explicit functional form for F in terms of the parameters shown in Eq. (5.1). It has been shown (G1), through the use of collision probability methods, that, in the limit of weak scattering and low absorption optical thicknesses for both the fuel and the moderator, F (for cylindrical unit cells) has the asymptotic value of 1/3. Similarly, it has been found (K1), through track length arguments, that in the limit of strong fuel absorption and weak moderator absorption (with weak scattering in both fuel and moderator) F takes the asymptotic value of 2/3. In the present work it has been shown that for nearly black fuel and moderator regions (still in the limit of weak scattering in

both fuel and moderator) F takes the asymptotic value of 1.0. Finally, we have also shown that for appreciable scattering in both fuel and moderator, the functional dependence of F on scattering optical thickness is of the form:

$$F \propto (1 + \omega'\tau_{sm})(1 + \omega'\tau_{sf}) \tag{5.2}$$

where ω' is a fitting parameter chosen to force agreement with numerical results.

Using the foregoing results as guidelines, an analytical expression for F has been developed to cover the intermediate ranges of optical thicknesses. Numerous functions could be used to smoothly join the various asymptotic limits; we have chosen one that is both simple in form and which agrees quite well with numerical results. This function has the following general form:

$$F(\tau_{af},\tau_{am},\tau_{sm},\tau_{sf}) = \frac{\frac{1}{3}\left(1+\frac{\omega\tau_{af}^{\,n}}{1+\tau_{af}^{\,n}}\right) + \omega\tau_{am}^{\,n'}}{1 + \omega\tau_{am}^{\,n'}} (1+\omega'\tau_{sm})(1+\omega'\tau_{sf}) \tag{5.3}$$

Noting the symmetry between the numerator and denominator of Eq. (5.1) (the necessity of symmetry can be shown quite rigorously by use of integral transport theory and/or the governing slowing down equations) the final form of the flux ratio model will thus be:

$$\frac{\bar{\phi}_m}{\bar{\phi}_f} = \frac{1+\dfrac{\frac{1}{3}\left(1+\dfrac{\omega\tau_{af}}{1+\omega\tau_{af}}\right)^{n}+\omega\tau_{am}}{1+\omega\tau_{am}}^{n'}\cdot(1+\omega'\tau_{sf})(1+\omega'\tau_{sm})\cdot\tau_{af}\cdot Q_m}{1+\dfrac{\frac{1}{3}\left(1+\dfrac{\omega\tau_{am}}{1+\omega\tau_{af}}\right)^{n}+\omega\tau_{af}}{1+\omega\tau_{af}}^{n'}\cdot(1+\omega'\tau_{sm})(1+\omega'\tau_{sf})\cdot\tau_{am}\cdot Q_f} \qquad (5.4)$$

where ω and ω' are fitting parameters

n and n' are positive powers to which τ_{af} and τ_{am} are raised, respectively.

So far no mention has been made of resonance cross sections, and the way in which the associated WR, IR, and NR approximations are to be incorporated into the flux ratio model. Here, we will only discuss, very briefly, the intermediate resonance approximation (IR) since it incorporates the wide resonance (WR) and narrow resonance (NR) limits. The basis for the IR approximation (B2, G3, G4, G5, H3, L4, S3, S4) is that it neither completely denies nor totally admits the role of scattering for removing neutrons: absorption plus a fraction of the scattering events remove neutrons from under a resonance. The IR approximation is implemented through the introduction of three new parameters λ, ν, $\bar{\mu}$. For a resonance absorber with no admixed moderator the removal cross section, $\sigma_r(E)$ becomes:

$$\sigma_r(E) \equiv \sigma_f(E) = \sigma_{af} + \lambda\sigma_{sf} \qquad (5.5)$$

where λ determines the fraction of scattering events contributing to removal.

Note that for $\lambda = 1$:

$$\sigma_f(E) = \sigma_{af}(E) + \sigma_{sf}(E) = \sigma_{tf}(E) \tag{5.6a}$$

which is the NR case; and for $\lambda = 0$:

$$\sigma_f(E) = \sigma_{af}(E) \tag{5.6b}$$

which is the WR case.

Similar arguments hold for moderator admixed with fuel and for moderator/coolant in the moderator/coolant region.

To implement the above ideas in conjunction with the flux ratio model, it is convenient to introduce the following parameters, which greatly simplify the subsequent notation:

$$\delta_f(E) = \tau_{af}(E) + \lambda\tau_{sf}(E) + \tau_{anf}(E) + \nu\tau_{snf}(E) \tag{5.7}$$

$$\delta_m(E) = \tau_{am}(E) + \bar{\mu}\tau_{sm} \tag{5.8}$$

$$\beta(E) = 1 + \omega'[(1-\lambda)\tau_{sf}(E) + (1-\nu)\tau_{snf}(E)] \tag{5.9}$$

$$\rho(E) = 1 + \omega'(1-\bar{\mu})\tau_{sm}(E) \tag{5.10}$$

$$\alpha_f(E) = \frac{\frac{1}{3}\left[1 + \frac{\omega\delta_f{}^n(E)}{1+\omega\delta_f{}^n(E)}\right] + \omega\delta_m{}^{n'}(E)}{1 + \omega\delta_m{}^{n'}(E)} \tag{5.11}$$

$$\alpha_m(E) = \frac{\frac{1}{3}\left[1 + \frac{\omega\delta_m{}^n(E)}{1+\omega\delta_m{}^n(E)}\right] + \omega\delta_f{}^{n'}(E)}{1 + \omega\delta_f{}^{n'}(E)} \tag{5.12}$$

where

τ_{anf} and τ_{snf} are the absorption and scattering optical thicknesses of the non-resonance material in the fuel.

The rest of the parameters are as previously defined.

Substituting Eqs. (5.7) - (5.12) in Eq. (5.4) there results:

$$\frac{\bar{\phi}_m(E)}{\bar{\phi}_f(E)} \equiv R(E) = \frac{1 + \alpha_f(E)\beta(E)\rho(E)Q_m(E)}{1 + \alpha_m(E)\beta(E)\rho(E)Q_f(E)} \tag{5.13}$$

which is the generalized form for the flux ratio taking into account the (IR) parameters. Note that Eq. (5.13) is a continuous function of energy; its discretization into energy groups by defining group-averaged parameters is straightforward:

$$\left|\frac{\bar{\phi}_m}{\bar{\phi}_f}\right|_g \equiv R_g = \frac{1 + \alpha_{fg}\beta_{gg}\rho_{gg}\delta_{fg}Q_{mg}}{1 + \alpha_{mg}\beta_{gg}\rho_{gg}\delta_{mg}Q_{fg}} \tag{5.14}$$

Cylindrical and spherical unit cells share similar functional forms for the flux ratio model: only the values of (n,n') and (ω,ω') are changed. The planar case, however, required inclusion of an extra term $(1+\omega'\ell n\,\frac{1}{\delta_m})$ multiplying β_{gg} in Eq. (5.14), introduced here without proof (see Ref.(Z1)).

Lastly, parameters (n,n') and (ω,ω') are found to have the following values for the three unit cell configurations:

(1) cylindrical:

$n = 1.0$; $n' = 0.5$

$\omega = 0.24$; $\omega' = 0.06$

(2) spherical:

$n = 0.5$; $n' = 0.5$

$\omega = 0.27$; $\omega' = 0.09$

(3) planar:

$n = 1.0$; $n' = 0.5$

$\omega = 0.15$; $\omega' = 0.03$

5.1.3 Numerical Verification of the Unit Cell Model

In what follows we will be discussing numerical results developed using the ANISN code, primarily employed in the S_8P_1 option , comparing them with our predicted results. The calculations are done for two-region unit cells with a white boundary condition used for the outer region of the cylindrical and spherical unit cells to minimize the effects of specular reflections (N1).

The dependence of the flux ratio on the magnitude of the scattering and removal cross-sections in cylindrical unit cells are shown in samples from an extensive series of numerical computations, summarized in Tables 5.1 and 5.2. As seen, the results of the analytical model are within a maximum discrepancy

Table 5.1

Numerical and Calculated Flux Ratios as a Function of Fuel Optical Absorption Thickness

τ_{af}	τ_{am}	τ_{sm}	τ_{sf}	ω	ω'	R calc.	R ANISN
0.01181	0.00006	0.12992	0.60355	0.24	0.06	1.004	1.005
0.42251						1.161	1.176
0.84482						1.345	1.360
1.26713						1.545	1.551
1.68944						1.760	1.750
2.1117						1.985	1.954
2.53402						2.218	2.164
2.95619						2.459	2.380
3.37883						2.706	2.600
3.80095						2.958	2.825
4.22324						3.214	3.053
4.64556						3.474	3.286
5.06787						3.737	3.521
5.49017						4.003	3.760
5.91248						4.271	4.002
8.02775						5.641	5.247
8.87278						6.198	5.757
9.71781						6.758	6.271
10.56285						7.322	6.789
28.16759						19.367	17.825
45.71309						31.528	28.859
63.37708						43.805	39.969
218.29797						151.698	137.360
373.21802						259.641	234.779
528.14229						367.594	332.206
6.33771						4.543	4.248

$V_f/V_m = 0.30122$ $r_f = 0.3175$ $r_m = 0.6599$

Table 5.2

Numerical and Calculated Flux Ratios as a Function of Optical Scattering Thickness

τ_{af}	τ_{am}	τ_{sm}	τ_{sf}	ω	ω'	R calc.	R ANISN
1.00	1.8002	0.1000	0.1000	0.24	0.06	1.551	1.463
1.00	1.8002	0.5001	0.1000	↓	↓	1.564	1.473
1.00	1.8002	2.50028	0.100	↓	↓	1.630	1.527
1.00	1.8002	50.0057	0.100	↓	↓	3.191	2.855
1.00	1.8002	0.5001	0.800	↓	↓	1.588	1.523
1.00	1.8002	0.5001	5.000	↓	↓	1.729	1.818
1.00	1.8002	0.5001	50.000	↓	↓	3.244	3.711
1.00	1.8002	0.5001	99.9998	↓	↓	4.926	4.960

$r_f = 0.3175$ $r_m = 0.4490$ $V_f/V_m = 1$

Table 5.3

Numerical and Calculated Flux Ratios as a Function of Source Distribution

τ_{af}	τ_{am}	τ_{sm}	τ_{sf}	Q_m/Q_f	ω/ω'	R calc.	R ANISN
2.5	1.20709	1.20709	0.13970	1.0 0.0	0.24 0.06	2.545	2.390
				0.8 0.2		1.946	1.860
				0.6 0.4		1.484	1.445
				0.4 0.6		1.118	1.109
				0.2 0.8		0.820	0.832
				0.0 1.0		0.573	0.599

of 15%, and an average error of about 5%, of the ANISN results. As shown in Table 5.3 the flux ratio model correctly predicts the effects of source distribution; a property which is very important in fast reactor calculations.

As a final note, it is important to point out that the agreement between the predicted and the numerical results could be improved substantially, if desired, by a different choice of values for the fitting parameters (n,n') and (ω,ω') in the range of maximum interest for a specific application.

5.1.4 Homogeneous Self-Shielding Factors

The discussion which follows immediately is confined to homogeneous systems where the spatial and angular dependence of the flux are suppressed, and only the energy variable, E, is of concern. Homogeneous self-shielding is discussed first to introduce the basic concepts necessary for the later extension of the methodology to heterogeneous media.

The fundamental and physically meaningful assumption made in most reactor physics calculations is conservation of total reaction rate. In fact, it is through the utilization of the above assumption that we shall define the group-averaged homogeneous cross-section as:

$$\int_{V_{cell}} \int_{\Delta Eg} \Sigma_x^j(E)\phi(E)dVdE = \Sigma_{xg}^j \cdot \int_{V_{cell}} \int_{\Delta Eg} \phi(E)dVdE \qquad (5.15)$$

where the quantity on the left of Eq. (5.15) is the true reaction rate, "$\Sigma_{xg}{}^{j}$" is the macroscopic group-averaged cross section for the particular process "x" of isotope "j", and the double integral multiplying "$\Sigma_{xg}{}^{j}$" is the true total flux of neutrons in the energy range ΔEg (ΔEg is to be interpreted as a fine-width group containing only one resonance). The appropriate weighting flux $\phi(E)$ in Eq. (5.15) can be found by solving the slowing down equation for a uniform mixture of infinite extent:

$$[\sigma_0+\sigma_{tf}(E,T)]\phi(E,T,\sigma_0) = \int_E^{E/\alpha_m} \frac{\sigma_0}{(1-\alpha_m)}\,\phi(E')\frac{dE'}{E'} + \int_E^{E/\alpha_f} \frac{\sigma_{sf}(E',T)}{(1-\alpha_f)}\,\phi(E')\frac{dE'}{E'} \qquad (5.16)$$

where

$\sigma_0 = \frac{\Sigma_{tm}}{N_f}$; Σ_{tm} = constant moderator cross section ($\Sigma_{am} << \Sigma_{sm}$)

N_0 = number of resonance absorber nuclei per unit volume

σ_{af}, σ_{rf}, σ_{pf} = resonance absorption, resonance scattering, and potential scattering cross-section, respectively, of the resonance absorber

$\sigma_{sf}(E,T) = \sigma_{rf}(E,T) + \sigma_{pf}$

$\sigma_{tf}(E,T) = \sigma_{af}(E,T) + \sigma_{sf}(E,T)$

$\alpha_j = \left(\frac{A_j-1}{A_j+1}\right)^2$; A_j being the ratio of the mass of isotope j to the mass of the neutron

Note that "moderator" in the above usage refers to all non-resonance-absorber nuclei present. Using the NR approximation for the moderator and the IR approximation for the absorber (G4), leads to:

$$\phi(E,T,\sigma_0) = \frac{\sigma_0 + \lambda\sigma_{pf}}{\sigma_{af}(E,T) + \lambda\sigma_{sf}(E,T) + \sigma_0} \frac{1}{E} \qquad (5.17)$$

where the source is normalized such that "$\phi = 1/E$" will be the off-resonance reference value for the flux per unit energy. Upon substituting Eq. (5.17) into Eq. (5.15), and specializing to the U-238 capture cross-section as an important example, one obtains:

$$\sigma_{cg}(T,\sigma_0) = \frac{\int_{\Delta Eg} \frac{\sigma_0 + \lambda\sigma_{pf}}{\sigma_{af}(E,T)+\lambda\sigma_{sf}(E,T)+\sigma_0} \sigma_c(E,T)\frac{dE}{E}}{\int_{\Delta Eg} \frac{\sigma_0 + \lambda\sigma_{pf}}{\sigma_{af}(E,T)+\lambda\sigma_{sf}(E,T)+\sigma_0} \frac{dE}{E}} \qquad (5.18)$$

Because σ_0 and σ_{pf} are essentially constant within ΔEg, they can be cancelled-out from the numerator and denominator of Eq. (5.18) to give:

$$\sigma_{cg}(T,\sigma_0) = \frac{\int_{\Delta Eg} \frac{\sigma_c(E,T)}{\sigma_{af}(E,T)+\lambda\sigma_s(E,T)+\sigma_0} \frac{dE}{E}}{\int_{\Delta Eg} \frac{1}{\sigma_{af}(E,T)+\lambda\sigma_s(E,T)+\sigma_0} \frac{dE}{E}} \qquad (5.19)$$

which is the effective capture cross-section at temperature T and constant background cross-section σ_0. If σ_0 in Eq. (5.19) approaches infinity, the following result will be obtained:

$$\sigma_{cg}^{\infty} = \frac{\int_{\Delta Eg} \sigma_c(E,T)\frac{dE}{E}}{\int_{\Delta Eg} \frac{dE}{E}} \tag{5.20}$$

which is the definition of the infinite dilution cross-section.

For convenience one can represent the effective cross-section given by Eq. (5.19), which is a function of both T and σ_0, by an infinite dilution cross-section and a set of modifying functions called self-shielding factors; or to put it quantitatively:

$$\sigma_{cg}(T,\sigma_0) = f_{cg}(T,\sigma_0)\cdot\sigma_{cg}^{\infty} \tag{5.21}$$

Thus the complications involved in the integration over resonance structure, as indicated by Eq. (5.19), are separated from the calculation of the effective multigroup constants for a specific material composition. Tables of f-factors are precomputed for the elastic, fission, capture, total, and transport cross sections and for arbitrary sets of T and σ_0 values (B3, K6). The f-factors for any given T and σ_0 can then be obtained by interpolating in these tables. The f-factor can then be multiplied by the proper infinite-dilution cross section to get the required effective cross section, $\sigma_{xg}(T,\sigma_0)$ as indicated by Eq. (5.21). The success of the above approach, however, relies heavily on the availability of accurate schemes for both

temperature and σ_0 interpolation of the self-shielding factor, $f_{xg}(T,\sigma_0)$. One expression used as a fitting function (K4) for the self-shielding factor as a function of σ_0, at a fixed temperature T, is:

$$f_{cg}(\sigma_0) = A \tanhB(\ell n\sigma_0 + C) + D \qquad (5.22)$$

where A, B, C, and D are constants determined by four values of f_{cg} at given σ_0 values. As for temperature interpolation at a fixed σ_0, a Lagrange-three-point interpolation scheme predicts, very accurately, the shielding factors for any current temperature, T.

Figures 5.1 and 5.2 (from Ref. (K4)) show the self-shielding factor for group 14 (86.5-111 Kev) of U-238 as a function of σ_0 and T, respectively. As seen, the results predicted by the aforementioned interpolation schemes (shown by the solid line) are in excellent agreement with the actual self-shielding represented by the dark circles. This concludes the discussion of homogeneous self-shielding, hopefully adequate to lay the groundwork for the introduction of heterogeneous self-shielding factors. For more complete expositions on the subject of homogeneous self-shielding the following references are recommended: B2, G1, K1, K4, K6, S6, S7.

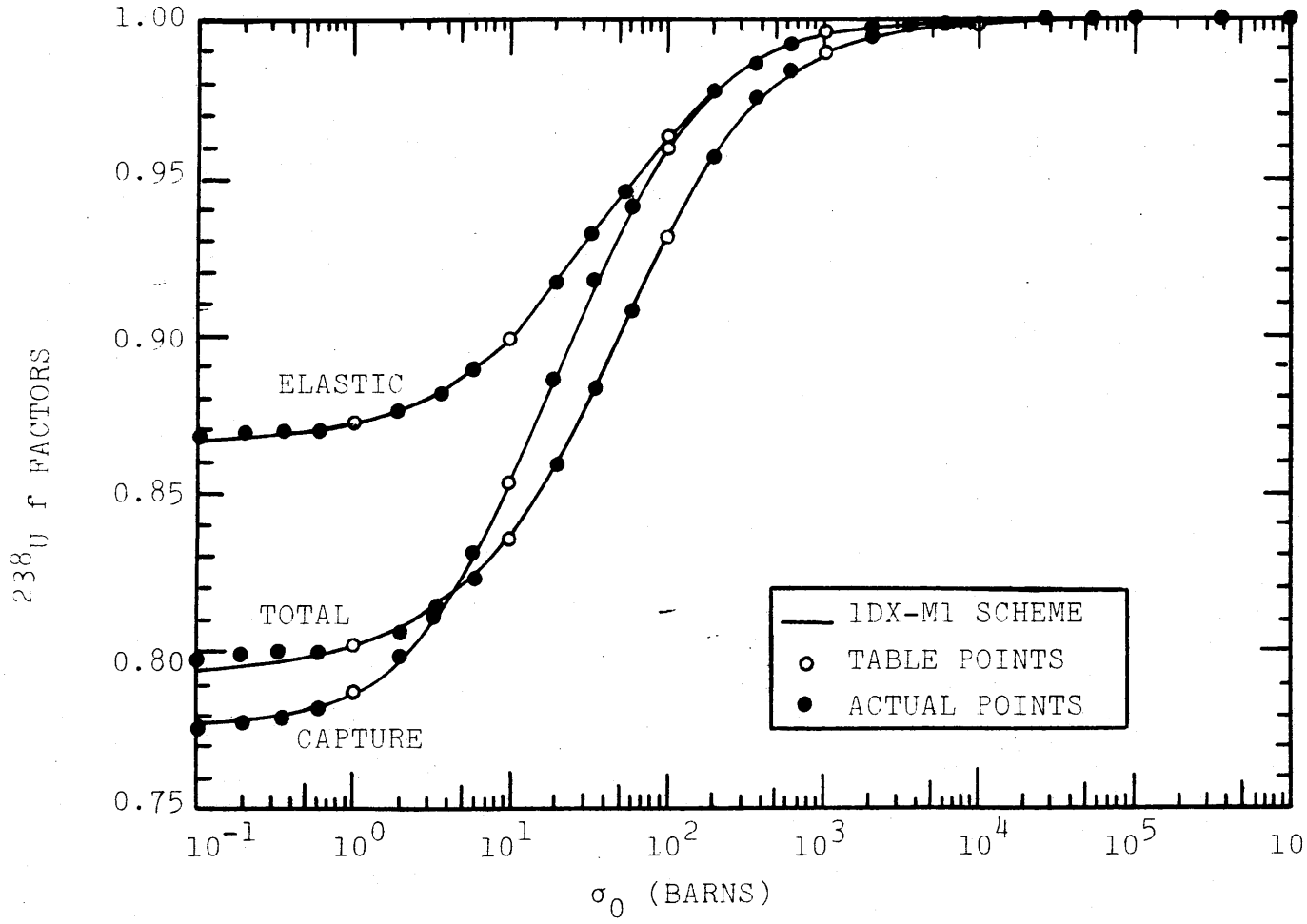

FIG. 5.1 A COMPARISON OF THE 1DX-M1 σ_0 INTERPOLATION WITH THE ACTUAL f FACTOR σ_0 BEHAVIOR (FOR GROUP 14 AND T=300°K)

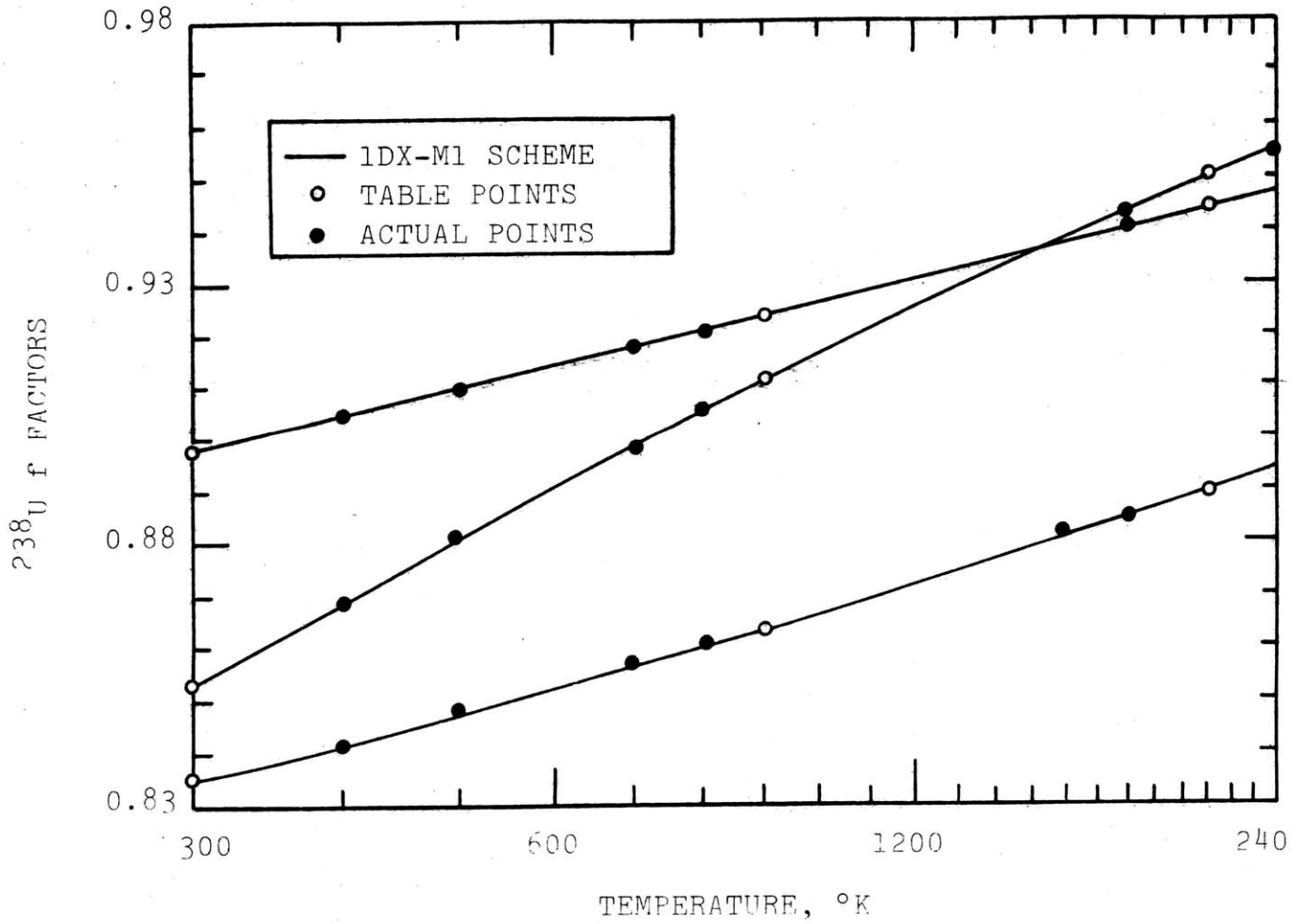

FIG. 5.2 A COMPARISON OF THE 1DX-M1 TEMPERATURE INTERPOLATION SCHEME WITH THE ACTUAL f FACTOR TEMPERATURE BEHAVIOR (FOR GROUP 14 AND σ_0 = 10 BARNS)

5.1.5 Heterogeneous Self-Shielding Factors

At this point almost all the groundwork necessary for generating "equivalent" group parameters, ($\overline{\nu\Sigma}_{fg}$, $\overline{\Sigma}_{cg}$, $\overline{\Sigma}_{gg'}$,... etc.), which are constant over the entire volume occupied by any given cell in a reactor, has been developed. The group constants generated should, when used in a group-diffusion-theory calculation for the whole reactor, reproduce the same average reaction rates over a given cell as would be determined if an exact energy dependent transport calculation was performed for a heterogeneous reactor with all geometrical characteristics of the unit cells treated explicitly.

An appropriate starting point is with the definition of an equivalent homogenized capture cross-section specialized to a two-region unit cell:

$$\Sigma_{cg}^{j} = \frac{\int_{V_{cell}} dV \int_{\Delta Eg} dE\ \Sigma_c^{j}(\underline{r},E,T)\phi(\underline{r},E)}{\int_{V_{cell}} dV \int_{\Delta Eg} dE\ \phi(\underline{r},E)} \tag{5.23}$$

If the resonance absorber, j, is present only in the fuel region; then Eq. (5.23) can be expanded to yield the following form:

$$\Sigma_{cg} = \frac{\int_{\Delta Eg} \Sigma_{cf}(E,T)\overline{\phi}_f(E)dE}{\int_{\Delta Eg} [1+\frac{V_m}{V_f} R(E)]\overline{\phi}_f(E)dE} \tag{5.24}$$

where

$$\bar{\phi}_m(E) = \frac{1}{V_m} \int_{V_m} \phi(\underline{r},E)dV \; ; \tag{5.25}$$

$$\bar{\phi}_f(E) = \frac{1}{V_f} \int_{V_f} \phi(\underline{r},E)dV \tag{5.26}$$

To be able to solve Eq. (5.24) both R(E) and $\bar{\phi}_f(E)$ must be known. An expression for the flux ratio R(E) has already been derived in Section 5.1.2; as for the spatially averaged fuel flux $\bar{\phi}_f(E)$, one can write down the equivalent of Eq. (5.16) for each region of the assumed two-region unit cell, and solve the pair of relations to find:

$$\bar{\phi}_f(E) = \frac{V_m\Sigma_{sm} + V_f\Sigma_{snf} + V_f\lambda\Sigma_{pf}}{V_f[\Sigma_{af}(E)+\lambda\Sigma_{sf}(E)+\Sigma_{tnf}(E)]+V_m\Sigma_{tm}(E)R(E)} \frac{1}{E} \tag{5.27}$$

Although expressions for R(E) and $\bar{\phi}_f(E)$ have been obtained, the problem is still intractable unless plausible simplifications are introduced into Eq. (5.13); the following are to be implemented:

(a) Linearization of the expression for R(E), by using group-averaged values for the values of τ appearing in α_f, α_m, β, ρ. Numerical studies confirm that this is an acceptable device. Thus the numerator of Eq. (5.13) becomes $[1+\bar{\gamma}_f\delta_f(E)]$, with $\bar{\gamma}_f=\alpha_f\beta\rho Q_m$ evaluated at group-averaged values for the τ involved. In like manner the denominator of Eq. (5.13) will

take the similar form $[1+\bar{\gamma}_m \delta_m(E)]$. As will shortly become clear, such linearization is apparently a sufficient and necessary condition for the existence of an equivalence theorem.

(b) $\Sigma_{tm}(E)$ and $\Sigma_{tnf}(E)$ are very weakly dependent on energy, especially within the range of energy covered by a typical group width. Hence we can treat $\delta_m(E)$ as constant over ΔEg. This last assumption in conjunction with the one made in part (a) immediately implies that the denominator of Eq. (5.13) can be taken as constant, and it shall henceforth be denoted by θ.

Based on assumptions (a) and (b), Eq. (5.13) can now be written in a more manageable form:

$$R(E,T) = \frac{1}{\theta}\left[1 + \bar{\gamma}_f \delta_f(E,T)\right] \tag{5.28}$$

where θ and $\bar{\gamma}_f$ are as previously defined.

Substituting Eqs. (5.27) and (5.28) into Eq. (5.24), the following is obtained:

$$\Sigma_{cg} = \frac{\displaystyle\int_{\Delta Eg} \frac{(V_m\Sigma_{sm}+V_f\Sigma_{snf}+V_f\lambda\Sigma_{pf})\cdot\Sigma_{cf}(E,T)}{V_f\Sigma_{af}(E,T)+V_f\lambda\Sigma_{sf}(E,T)+V_f\Sigma_{tnf}+V_m\Sigma_{tm}\frac{1}{\theta}[1+\bar{\gamma}_f\delta_f(E,T)]}\frac{dE}{E}}{\displaystyle\int_{\Delta Eg} \frac{(V_m\Sigma_{sm}+V_f\Sigma_{snf}+V_f\lambda\Sigma_{pf})\cdot\{1+\frac{V_m}{V_f}\frac{1}{\theta}[1+\bar{\gamma}_f\delta_f(E,T)]\}}{V_f\Sigma_{af}(E,T)+V_f\lambda\Sigma_{sf}(E,T)+V_f\Sigma_{tnf}+V_m\Sigma_{tm}\frac{1}{\theta}[1+\bar{\gamma}_f\delta_f(E,T)]}\frac{dE}{E}} \tag{5.29}$$

By performing some simple algebra on the above equation, it follows that:

$$\frac{V_f}{V_{cell}}\,\sigma_{cg} = \frac{\int_{\Delta Eg} \frac{\sigma_{cf}}{\sigma_{af} + \lambda\sigma_{sf} + \sigma_0'}\,\frac{dE}{E}}{\int_{\Delta Eg} \frac{1+\frac{V_m}{V_f}\,\frac{1}{\theta}+\varepsilon'''\sigma_{cf}+\varepsilon'''\sigma_{ff}+\varepsilon'''\lambda\sigma_{sf}+\varepsilon'''\frac{\Sigma_{tnf}}{N_f}}{\sigma_{af} + \lambda\sigma_{sf} + \sigma_0'}\,\frac{dE}{E}} \tag{5.30}$$

where

$$\sigma_0' = \frac{\overline{\Sigma}_{tnf}}{\overline{N}_f} + \frac{1}{\theta+\overline{\gamma}_f\delta_m}\,\frac{\overline{\Sigma}_{tm}}{\overline{N}_f} \tag{5.31}$$

with the bars denoting volume-weighted homogenization

$$\varepsilon''' = \frac{1}{\theta}\,\overline{\gamma}_f N_f\,\frac{V_m}{V_f}\,\ell_f$$

σ_{ff} = the resonance absorber fission cross-section

The rest of the parameters are as previously defined.

By inverting Eq. (5.30) and using the definition of the effective homogeneous cross-section, namely Eq. (5.19), one can show the following rigorous result:

$$\sigma_{cg}^{het}(T,\sigma_0) = \frac{\sigma_{cg}^{hom}(T,\sigma_0')}{\eta + \varepsilon''\sigma_{cg}^{hom}(T,\sigma_0')} \tag{5.32}$$

where

$$\eta = \frac{V_f}{V_{cell}} + \frac{1}{\theta}\frac{V_m}{V_{cell}} + \varepsilon''\sigma_{fg}^{hom}(T,\sigma_0') + \varepsilon''\sigma_{sg}^{hom}(T,\sigma_0') + \frac{\bar{\gamma}_f}{\theta}\frac{V_m}{V_{cell}}\tau_{tng}$$

$$\varepsilon'' = \frac{V_f}{V_{cell}}\varepsilon'''$$

σ_{cg}^{hom} = group-averaged homogeneous capture cross-section

σ_{fg}^{hom} = group-averaged homogeneous fission cross-section

σ_{sg}^{hom} = group-averaged homogeneous elastic scattering cross section

σ_{cg}^{het} = group-averaged "homogenized" capture cross-section

Σ_{tng} = total non-resonance cross-section in the fuel region for group g

It is important to note that Eq. (5.32) predicts the correct homogenized cross-section under any condition so long as the homogeneous part (i.e. $\sigma_{cg}^{hom}(T,\sigma_0')$) is treated correctly elsewhere in the literature.

Recalling Eq. (5.21) for the definition of the self-shielding factor, and applying it to Eq. (5.32), leads to the following important expression:

$$f_{cg}^{het}(T,\sigma_0) = \frac{1}{\eta + \varepsilon} f_{cg}^{hom}(T,\sigma_0') \qquad (5.33)$$

where $\varepsilon = \varepsilon' \; f^{hom}(T,\sigma_0')$.

Equation (5.33) and its accompanying prescriptions constitute a New Equivalence Relationship, whereby the corresponding f-factor for the heterogeneous cell is expressed in terms of the f-factor for a homogeneous cell evaluated at a modified value of the constant background cross-section - namely σ_0'.

Finally, it is worthwhile to present a brief review of what we will call the "conventional" methods used hitherto and compare their results with those of the present method - i.e. Eq. (5.33). Conventionally, one uses the second equivalence theorem to make the heterogeneity correction. The statement of the theorem is as follows (H1, L4): a heterogeneous system will have the same resonance integral as a homogeneous systems evaluated at:

$$\sigma_0' = \frac{\bar{\Sigma}_{tnf}}{\bar{N}_f} + \frac{1-c}{N_f \ell_f} \frac{a}{1+(a-1)c} = \frac{\bar{\Sigma}_{tnf}}{\bar{N}_f} + \frac{1}{1+\frac{1}{a}\tau_{tm}} \frac{\bar{\Sigma}_{tm}}{\bar{N}_f} \qquad (5.34)$$

where c is the Dancoff-Ginsberg factor given by:

$$1-c = \frac{\tau_{tm}}{1+\frac{1}{a}\tau_{tm}} \text{ , in Bell's approximation (B1)} \qquad (5.35)$$

The parameter "a" is known as the Levine correction factor (L2). It has been found that a value of $\frac{1}{a} \simeq 0.79$ yields accurate results over the entire range of practical lump sizes. Note that the σ_0' defined in Eq. (5.34) differs from that in Eq. (5.31).

Applying the theorem to Eq. (5.19) yields the following conventional result in terms of the f-factors:

$$f_{cg}^{het}(T,\sigma_0) = f^{hom}(T,\sigma_0') \tag{5.35}$$

Upon comparing Eqs. (5.33) and (5.36) we immediately note that the factor $\frac{1}{\eta + \varepsilon}$ has been set equal to 1.0 in the conventional method. This discrepancy raises questions as to the validity of the second equivalence theorem as applied to cross-sections but not to resonance integrals. The difficulty stems from the fact that the true integrated heterogeneous flux, as given by the denominator of Eq. (5.23), has in the conventional approach been replaced by a homogeneous flux evaluated at σ_0' in the denominator of Eq. (5.19), thus leading to the present disparity. The modified total background cross section, however, is smaller than σ_0' in Eq. (5.31), which helps cancel part of this discrepancy.

5.1.6 Numerical Verification of Self-Shielding Factors

In the present section homogeneous-to-heterogeneous corrections are calculated with the new equivalence theorem, and the results compared to equivalent output from the LEOPARD code (L5), a state-of-the-art LWR unit cell program. The base-case unit cell data used in both calculations is representative of current commercial PWR reactors (specifically, Maine Yankee). The EPRI version of LEOPARD was employed,

together with its ENDF/B IV derived cross-section library. For the self-shielding-factor method, cross-sections and f-factors as a function of σ_0 were taken from the LIB-IV fast reactor cross-section set developed by LASL (also derived from the ENDF/B IV library).

Figure 5.3 is a plot of homogeneous broad group capture cross-sections (σ_c^{hom}) for U-238 as a function of moderator optical thickness (τ_{tm}), with the fuel diameter kept constant. The broad group cross section is defined by a 1/E-weighted group collapse:

$$\sigma_c^{hom} = \sum_{GP26}^{GP49} \sigma_i \Delta u_i / \sum_{26}^{49} \Delta U_i \qquad (5.37)$$

where groups 26 through 49 span the energy range from 0.6826 ev to 5.53 Kev. As is evident from the figure the capture cross-sections obtained using self-shielding factors are in good agreement with the corresponding parameters generated using LEOPARD. Depending on one's point of view this either validates the f-factor formalism, LEOPARD, or both. Table 5.4 contains the tabulated results of Fig. 5.3, including percentage differences.

In Fig. 5.4 the analytic and the LEOPARD results for the ratio of heterogeneous-to-homogeneous self-shielding factors $[f^{het}(\sigma_0)/f^{hom}(\sigma_0)]$ as a function of moderator optical thickness (at constant fuel pin diameter) are shown. The agreement shown between the two results is tolerably good (particularly

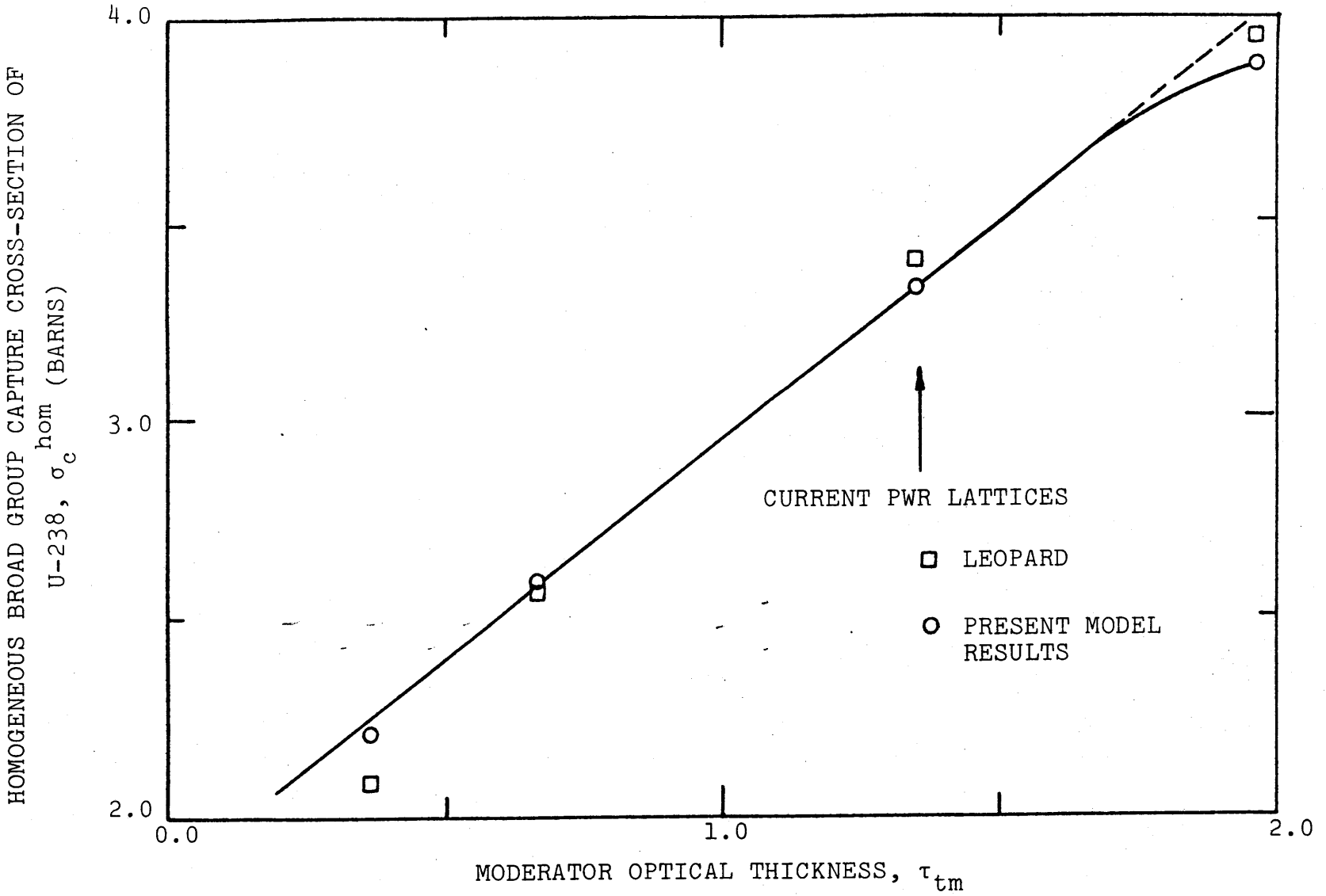

FIG. 5.3 HOMOGENEOUS BROAD GROUP CAPTURE CROSS-SECTION OF U-238 AS A FUNCTION OF MODERATOR OPTICAL THICKNESS

Table 5.4

Tabulated Results Applicable to Fig. 5.3

Moderator Optical Thickness	σ_c^{hom} (barns) analytical, using f-factor formalism	σ_c^{hom} (barns) LEOPARD	Δ% percent difference
0.361	2.218	2.088	+6.2
0.663	2.591	2.565	+1.0
1.354	3.336	3.410	-2.2
1.965	3.883	3.962	-2.0

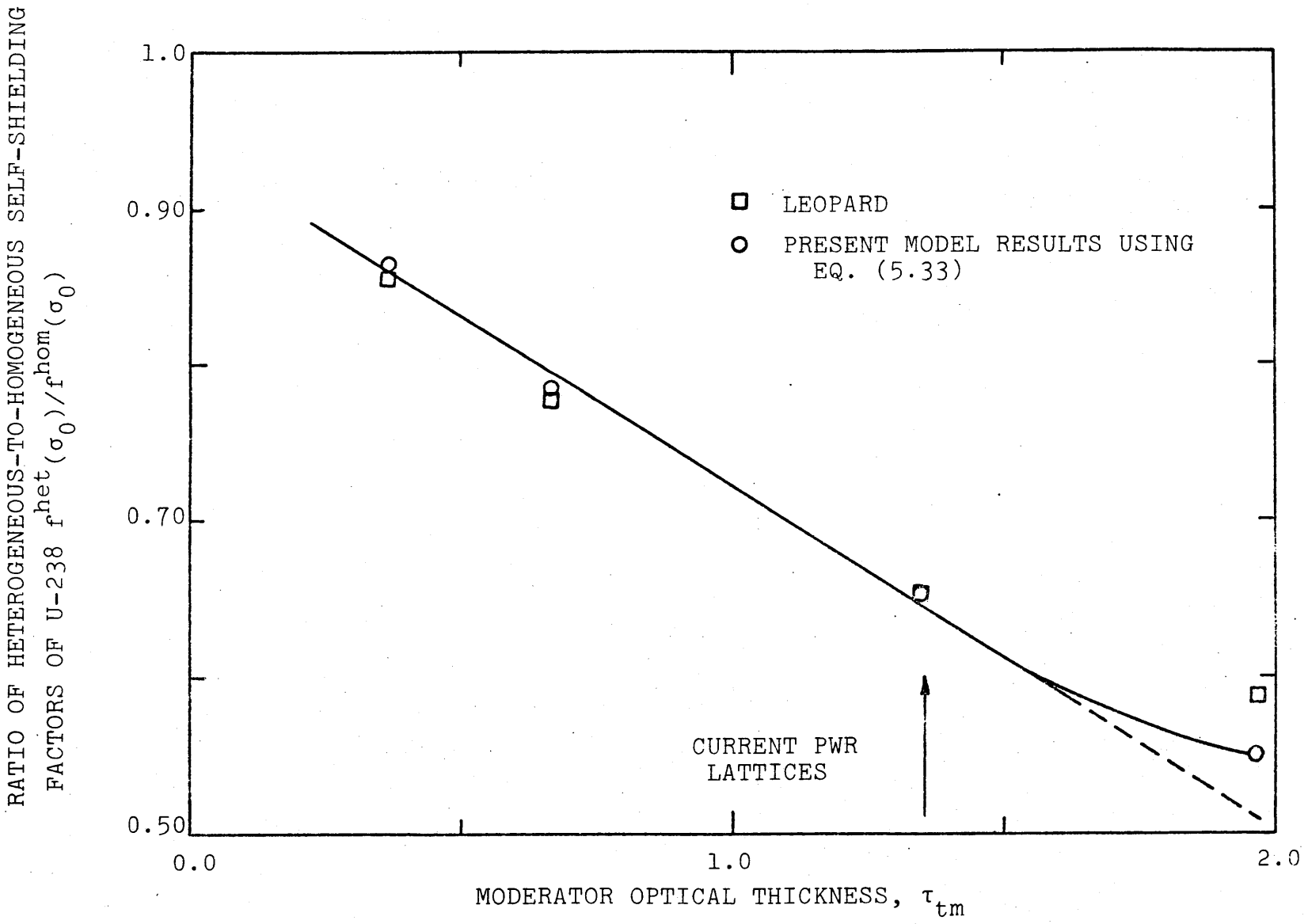

FIG. 5.4 RATIO OF THE BROAD GROUP HETEROGENEOUS-TO-HOMOGENEOUS CAPTURE SELF-SHIELDING FACTORS OF U-238 AS A FUNCTION OF MODERATOR OPTICAL THICKNESS

Table 5.5

Tabulated Results Applicable to Fig. 5.4

Moderator Optical Thickness	$\frac{f_c^{het}(\sigma_0)}{f_c^{hom}(\sigma_0)}$ present model (Eq. 5.33)	$\frac{f_c^{het}(\sigma_0)}{f_c^{hom}(\sigma_0)}$ LEOPARD	$\Delta\%$ percent difference
0.361	0.865	0.857	+0.9
0.663	0.784	0.782	+0.3
1.354	0.653	0.653	0.0
1.965	0.551	0.587	-6.5

for the point closest to current PWR designs); also note that the results fall very nearly on a straight line. This observation can be confirmed analytically by an appropriate simplification of Eq. (5.33). The data plotted in Fig. 5.4 are listed in Table 5.5, again with percentage differences shown: the agreement between the present model and LEOPARD is excellent for all but the thickest moderator case.

Table 5.6 contains the data for the U-238 broad group heterogeneous capture cross-sections evaluated at various moderator optical thicknesses and at a fixed fuel pin diameter. As seen from the table, the two central points agree within 2%, and the end points within 8%: these data are plotted in Fig. 5.5. The important point to note here is the approach of the curve to an asymptotic limit as the moderator thickness increases, the reason being that as the moderator optical thickness increases, the results approach the isolated lump limit.

Finally, Table 5.7 gives the calculated values for $[f^{het}(\sigma_0)/f^{hom}(\sigma_0)]$ for various groups of two typical fast reactor pin-cell assemblies (metal-fueled and oxide-fueled) that have been studied in the M.I.T. Blanket Test Facility (BTF). (The blanket is of particular interest here because the diameter of radial blanket fuel pins may be as much as twice that of the core fuel pins, and the ambient neutron spectrum is softer than that of the core - both of which circumstances accentuate the effects of heterogeneity). As seen from the

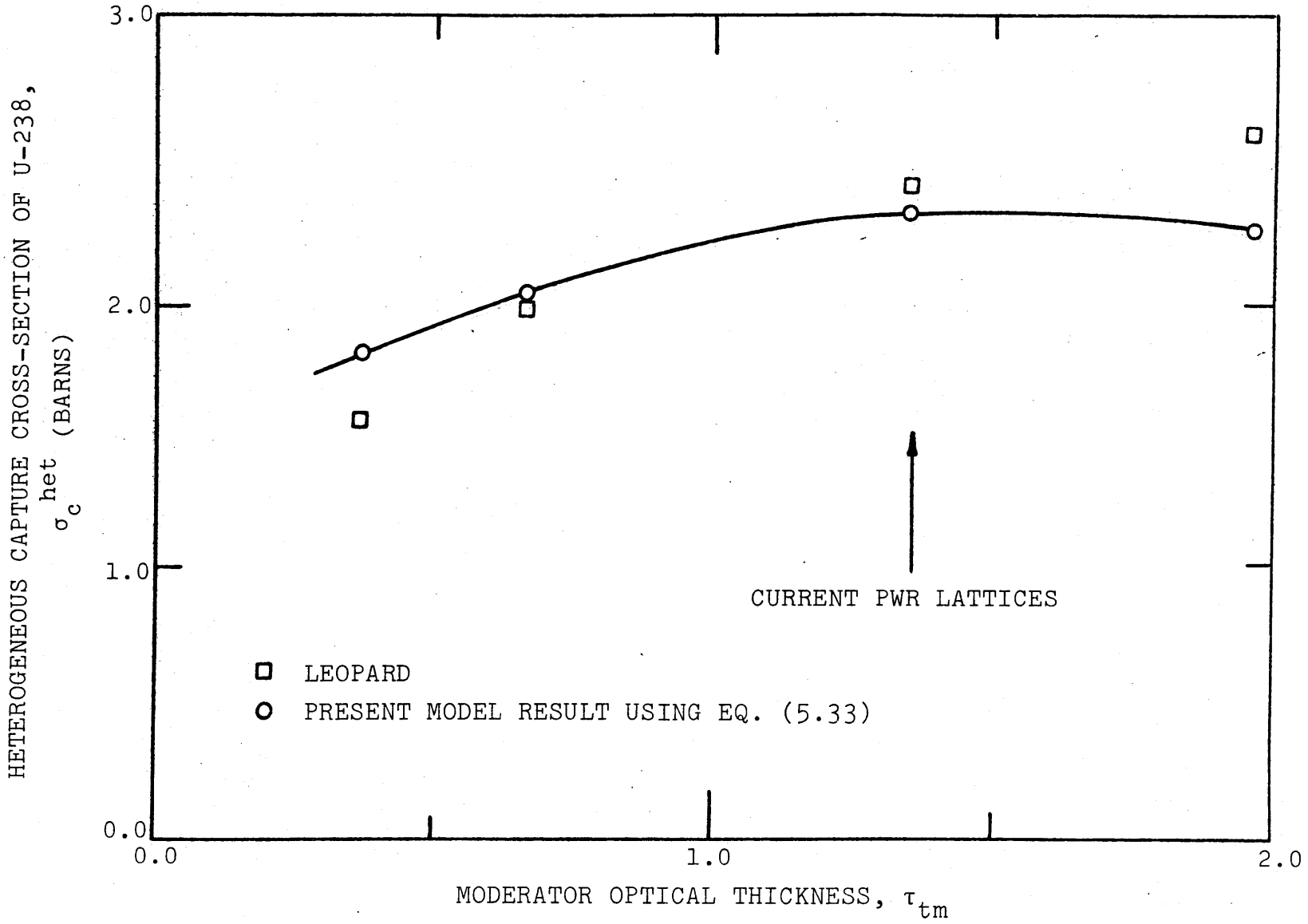

FIG. 5.5 HETEROGENEOUS BROAD GROUP CAPTURE CROSS-SECTION OF U-238 AS A FUNCTION OF MODERATOR OPTICAL THICKNESS

Table 5.6

Tabulated Results Applicable to Fig. 5.5

Moderator Optical Thickness	σ_c^{het} (barns) present model (Eq. 5.33)	σ_c^{het} (barns) LEOPARD	Δ% percent difference
0.361	1.919	1.790	+7.2
0.663	2.032	2.005	+1.3
1.354	2.180	2.228	-2.2
1.965	2.141	2.326	-8.6

Table 5.7

Group Values* for $f^{het}(\sigma_0)/f^{hom}(\sigma_0)$, $\sigma_c{}^{hom}$, and $\sigma_c{}^{het}$: Metal Fueled Blanket Mockup

G	$\frac{f^{het}(\sigma_0)}{f^{hom}(\sigma_0)}$ (present model) (Eq.5.33)	$\sigma_c{}^{hom}$(U-238) (barns)	$\sigma_c{}^{het}$(U-238) (barns)
26	0.972	0.821	0.798
29	0.951	1.102	1.048
32	0.964	1.274	1.228
35	0.963	1.006	0.968
38	0.971	1.377	1.337
40	0.975	2.120	2.067
43	0.958	4.923	4.718
45	0.941	14.118	13.284

* For the oxide fuel only group 45, which contains the largest (and hence most heavily shielded) U-238 resonance is reported:

45	0.989	12.887	12.742

See Table 3.8 for LIB-IV group structure.

magnitude of the results, the heterogeneity effects for both the metal-fueled and the oxide-fueled cells are very small indeed: less than the 10% uncertainty currently assigned to U-238 capture cross-section values in this energy range. Nevertheless the effect of internal moderation in the oxide fuel can be observed in the form of a self-shielding factor, f, which is much closer to 1.0.

In conclusion, although the present and the conventional equivalence relations differ by the factor $\frac{1}{\eta + \varepsilon}$, actual numerical results agree reasonably well. This is because, as previously noted, the σ_0' given by Eq. (5.34) is considerably lower than the σ_0' given by Eq. (5.31), because the Levine factor, 1/a, taken here as 1/a= 0.79 is considerably higher than the corresponding parameter $\bar{\gamma}_f$ in the present model, which has an average value of 0.50 for the base-case PWR unit cell studied in this report (note that θ, appearing in Eq. (5.31), is approximately 1.0 for the case of thermal reactors, hence it is not responsible for the discrepancy). The lower σ_0' used in the conventional model results in a smaller value of f, which helps to partly offset the omission of a $(\eta+\varepsilon)$ term.

5.1.7 A Comparison Between the Conventional and the Present Dancoff Factor and Escape Probability Expressions

In this section expressions for the Dancoff factor and the fuel escape probability obtained by comparing the various

results of the present method with the corresponding conventional results will be reviewed. Before getting into the algebra, some simplifying assumptions are introduced, which are not to be taken as limiting approximations, however:

(a) Impose the NR approximation. Therefore, strictly speaking, all the results obtained in this section are for the NR case. Results for the WR and IR cases are obtainable by exactly the same methods.

(b) Consider only thermal reactors, where the slowing down source is in the moderator, hence $Q_f=0$ and $\theta=1$.

Using the above assumptions and comparing (as before) Eqs. (5.31) and (5.34) we get:

$$\frac{1}{1 + \bar{\gamma}_f \tau_{tm}} \Leftrightarrow \frac{1}{1 + \frac{1}{a}\tau_{tm}} \tag{5.38}$$

which says that $\bar{\gamma}_f$ corresponds to $\frac{1}{a}$, thus leading to an expression for the Dancoff correction factor: given by Eq. (5.35) with the only change being the replacement of $\frac{1}{a}$ by $\bar{\gamma}_f$.

$$1-C = \frac{\tau_{tm}}{1 + \bar{\gamma}_f \tau_{tm}} \qquad \text{present method} \tag{5.39}$$

The next task is to find a corresponding expression for the escape probability, $P_f(E)$. It can be shown, using the slowing-down equations pertinent to a two-region unit cell that:

$$\frac{\bar{\phi}_m(E)}{\bar{\phi}_f(E)} = R(E) = \frac{1 + \left(\frac{\tau_{sf}(E)}{\tau_{tf}(E)} - 1\right)\frac{\tau_{tf}(E)}{\tau_{tm}(E)} P_f(E)}{1 + \left(\frac{\tau_{sf}(E)}{\tau_{tf}(E)} - 1\right)\left(1 - \frac{\tau_{tm}(E)}{\tau_{tf}(E)}\right) P_m(E)} \tag{5.40}$$

(I) in the asymptotic region $\tau_{sf}(E) \simeq \tau_{pf} \simeq \tau_{tf}(E)$, which when substituted in Eq. (5.40) results in $R(E) = 1$, as to be expected.

(II) in the resonance region where $\tau_{tf} >> \tau_{sf}$ (black fuel) one obtains:

$$R(E) = \frac{1}{P_f(E)} - \frac{\tau_{tf}(E)}{\tau_{tm}(E)} \tag{5.41}$$

Conventionally, the fully rational approximation for $P_f(E)$ is:

$$P_f(E) = \frac{1}{1 + \frac{1+\frac{1}{a}\tau_{tm}}{\tau_{tm}} \tau_{tf}} \tag{5.42}$$

Substituting Eq. (5.42) into Eq. (5.41) gives:

$$R(E) = 1 + \frac{1}{a} \tau_{tf}(E) \tag{5.43}$$

which has exactly the same form as predicted by our results - namely:

$$R(E) = 1 + \bar{\gamma}_f \tau_{tf}(E) \tag{5.44}$$

Upon comparing Eqs. (5.43) and (5.44) we note, once again:

$$\frac{1}{a} \Leftrightarrow \bar{\gamma}_f \tag{5.45}$$

Using the above relation (Eq. (5.45)), and working backward, the following expression for $P_f(E)$ is obtained:

$$P_f(E) = \frac{1}{1 + \frac{1+\bar{\gamma}_f \tau_{tm}}{\tau_{tm}} \tau_{tf}(E)} \qquad (5.46)$$

Equation (5.46) is the analog of Eq. (5.42). The above encouraging results encourage confidence in the present method.

Figure 5.6 shows a plot of the Dancoff correction obtained in Ref. (L3) using the MOCUP Monte Carlo program. The Monte Carlo program computation was performed on a two-region "square pin cell" of high fuel cross-section and with $V_m/V_f = 1$. As can be seen, the present analytical results are in as good agreement with the Monte Carlo computations as are the results of the analytical model proposed in Ref. (L3); with the exception that the present model is considerably simpler than the model proposed in the reference. Both models, however, are obtained assuming unit cell cylindricalization; as a result, they do not distinguish between square and hexagonal cells. Finally, the results of the two models are about 3% higher than the corresponding Monte Carlo computations.

One should not conclude from the above comparisons that the present work merely validates prior methodology: the results include previous work as limiting cases, but are more general.

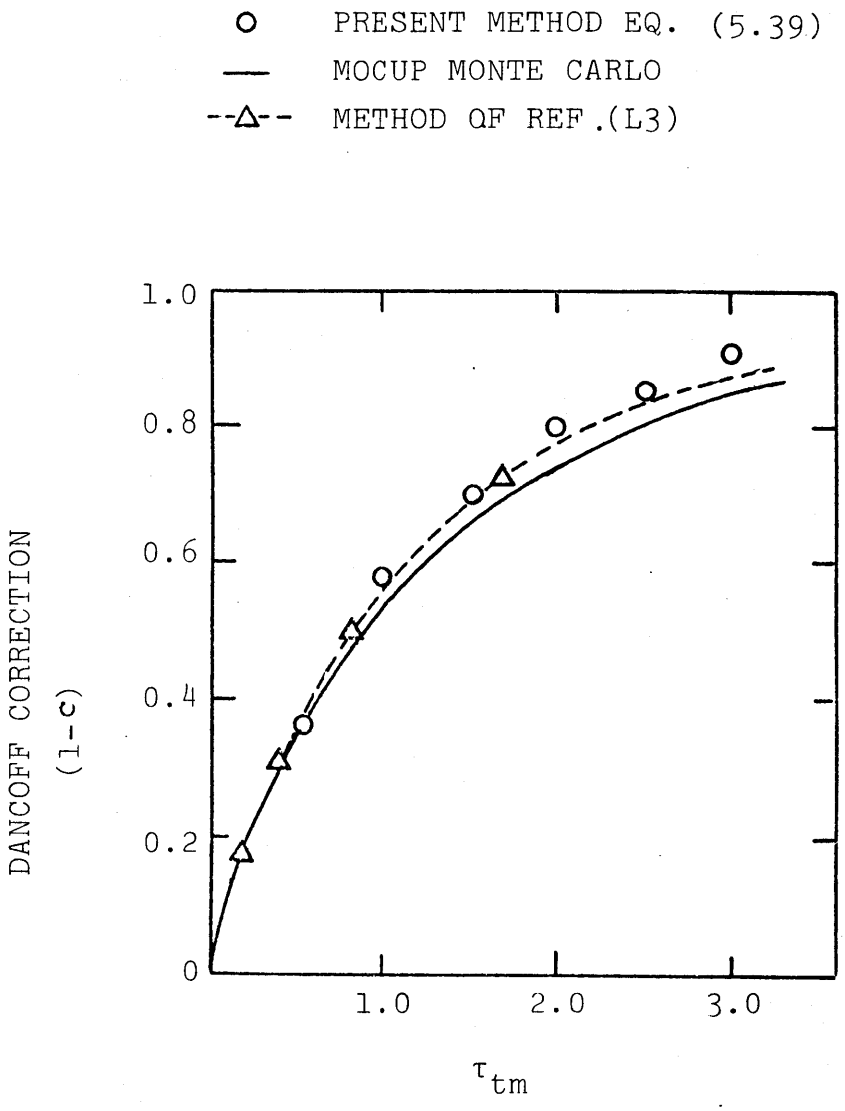

FIG. 5.6 VARIATION OF THE DANCOFF CORRECTION WITH MODERATOR OPTICAL THICKNESS FOR A SQUARE PIN CELL WITH V_M/V_F=1.

5.2 CONCLUSIONS

Based upon the work reported here the following conclusions are substantiated:

(1) A new and easily applied equivalence theorem, applicable to both fast and thermal reactors, has been developed.

(2) The present method handles cases not easily dealt with conventionally - e.g. when fuel moderation is not negligible compared to that of the coolant.

(3) The effects of heterogeneity in fast reactors are shown to be small: less than the uncertainty currently assigned to U-238 capture cross-section values.

5.3 RECOMMENDATIONS FOR FUTURE WORK

The following topics are envisioned as natural extensions of the present work:

(1) Treating mixtures containing more than one resonance absorber - i.e. accounting for the effects of resonance overlap (F4, S9).

(2) Dealing with cases in which cell leakage is permitted (perhaps by inclusion of a DB^2 term).

(3) Adapting the flux-ratio methodology to the thermal and fast energy region: for example as a flux group module in rapid versions of codes such as THERMOS (H5) or UNCOL and HEETR (W2).

(4) Utilizing the method to treat larger cells, such as (homogenized) core surrounding a control absorber or a reactivity sample in a critical facility.

In the above areas some additional theoretical developments are called for. However, it should be possible to adapt fast reactor processing codes to utilize the equivalence theorem proposed here without further ado, and to then use these codes for LWR calculations. This step is recommended as are further checks against LEOPARD, including eigenvalue and reaction rate comparisons, as well as comparisons with experimental benchmark data. All the above activities appear to be feasible extensions of what has been accomplished so far.

Appendix A

MEAN ESCAPE CHORD LENGTH CALCULATIONS

A.1 INTRODUCTION

To be able to solve for the fuel and the moderator fluxes of a particular unit cell, using either track length arguments or escape probability methods, one needs to know the appropriate escape chord lengths (to be distinguished from the familiar Dirac penetration chord, $\ell_p = 4V/S$). Therefore, in this appendix the escape chord lengths of the spherical and planar unit cells will be derived. Gregory has previously derived the cylindrical case (G1). The fundamental assumptions used in the calculation are:

(a) both the spherical and the planar cells are to be treated as transparent media;

(b) the internal source, in both cells, is taken to be uniform and isotropic.

A.2 SPHERICAL ESCAPE CHORD LENGTH

Figure A.1 pictures the situation for an isotropic source at point S inside the shell of a transparent sphere, emitting neutrons along the escape chord length ℓ described by the angle of inclination θ. Averaging all possible escape paths originating at point S over all solid angles gives the mean "local" escape chord length; integrating over all radii gives the mean escape chord for the entire population of neutrons.

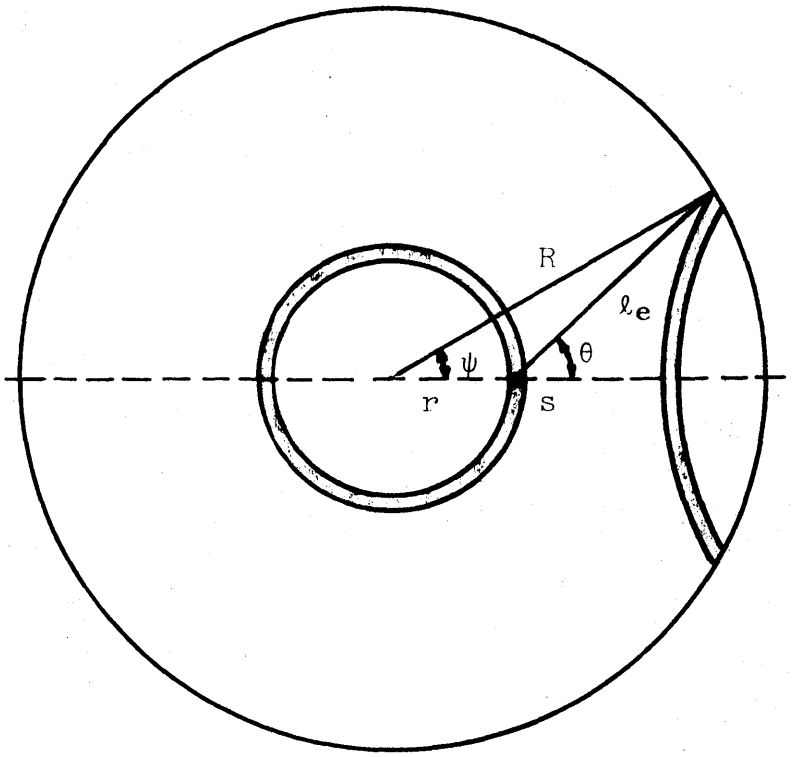

FIG. A.1 ESCAPE CHORD LENGTH FROM TRANSPARENT SPHERE

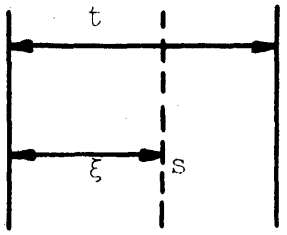

FIG. A.2 ESCAPE CHORD LENGTH FROM TRANSPARENT SLAB

From the law of cosines:

$$\ell_e = (r^2\cos^2\theta + R^2 - r^2)^{1/2} - r\cos\theta \qquad (A.1)$$

The mean chord length is defined as:

$$\bar{\ell}_e = \frac{\int\int \ell_e(r,\Omega)S(r)dr d\Omega}{\int\int S(r)dr d\Omega} \qquad (A.2)$$

or for the case of uniform source distribution:

$$\bar{\ell}_e = \int_{\theta=\pi}^{\theta=0} \int_{r=0}^{R} \ell_e \cdot 3(\frac{r}{R})^2 d(\frac{r}{R}) \frac{d\cos\theta}{2} \qquad (A.3)$$

where

$3(\frac{r}{R})^2 d(\frac{r}{R})$ = (normalized) source strength at r

and

$\frac{d\cos\theta}{2}$ = solid angle

Substituting $x \equiv \frac{r}{R}$ and $\mu \equiv \cos\theta$ in Eq. (A.3) we get:

$$\bar{\ell}_e = \frac{3}{2}R \int_{-1}^{+1} \int_{x=0}^{1} [(x^2\mu^2+1 - x^2)^{1/2} - x\mu]x^2 dx d\mu \qquad (A.4)$$

Integrating Eq. (A.4) over μ yields:

$$\bar{\ell}_e = \frac{3}{4}R \int_{x=0}^{1} [\frac{2}{x} + \frac{1-x^2}{x^2} \ell n(\frac{1+x}{1-x})]x^3 dx \qquad (A.5)$$

Next integrating over x gives:

$$\bar{\ell}_e = \frac{3}{4}R\{\frac{2}{3} + [\int_0^1 x\ell n(1+x)dx - \int_0^1 x^3\ell n(1+x)dx - \int_0^1 x\ell n(1-x)dx + \int_0^1 x^3\ell n(1-x)dx]\} \quad (A.6)$$

By using tables of integrals,* one can easily show that:

$$\bar{\ell}_e = \frac{3}{4}R \quad (A.7)$$

A.3 PLANAR ESCAPE CHORD LENGTH

Figure A.2 pictures the situation for an isotropic source at point S inside a transparent slab. Recognizing that half of the neutrons go to the right and half to the left and that each neutron penetrates the slab on its right or left, the planar escape chord length is just the weighted sum of penetration chord lengths for escape to the left and to the right:

$$\bar{\ell}_e = \frac{1}{2}\,2\xi + \frac{1}{2}\,2(t-\xi) = \xi + t - \xi = t \quad (A.8)$$

---

* I.S. Gradshteyn, I.M. Ryzhik, Tables of Integrals, Series, and Products, Academic Press, New York (1965).

Appendix B

TABULATED RESULTS, SUBSIDIARY DERIVIATIONS, DISCUSSIONS, AND NUMERICAL EXAMPLES

B.1 INTRODUCTION

This appendix is comprised of three main parts: the first includes extensive tabulated numerical results used to validate the flux ratio model, for the three different types of (two-region) unit cells - namely, cylindrical, slab, and spherical. Note that all calculations, except where noted, apply to cases in which all of the neutron source is in the moderator region - i.e., $Q_f=0$ and $\theta=1$. Next a simple prescription for $\bar{\phi}_{clad}/\bar{\phi}_{fuel}$ is derived and checked against numerical calculations. Finally, a brief discussion concerning the observed discrepancy between the results obtained from LEOPARD and those obtained with the present method is given.

B.2 VARIOUS TABULATED RESULTS

Tables B.1 through B.25 summarize the calculated results used to test the flux ratio model for slab, cylindrical and spherical unit cells. The results are reproduced in their entirety here as they may prove useful for others who may be motivated to improve upon the functions chosen to represent R in the present work, or to adjust parameters to obtain better agreement over a more limited range.

In the following tables:

(a) $Q_f = 0$ except where noted;

(b) "Numerical" results are calculated using the ANISN program in the S_8P_1 option and white outer boundary conditions;

(c) "Calculated" results refer to Eq.(2.90)of Chapter 2;

(d) The fuel and moderator optical thickness are varied as shown: the nomenclature of Section 2.7.1 of Chapter 2 applies.

B.3 CLAD (INTERFACE) FLUX RATIO PRESCRIPTION

In the present work it was quite acceptable to homogenize the clad with the coolant. In other applications this may not be so. We summarize here an approximate method for treating the clad explicitly (as an infinitesimally thin region between fuel and coolant).

In this section an approximate expression is derived for the ratio of the spatially-averaged flux in the clad to that in the fuel. Note that most of the arguments used in this section are exactly the same as those used in Chapter 2, hence the development can be abbreviated.

Consider a three-region cylindrical unit cell with the clad as the middle region; then if we assume that $\tau_{af} \to \infty$ we have:

$$\bar{\phi}_{clad} = \frac{\bar{L}_{clad}}{V_{clad}} \simeq \frac{\bar{L}_{clad}}{2\pi r_f \cdot t} \qquad (B.1)$$

Table B.1

Flux Ratios for a Two-Region Cylindrical Unit Cell

τ_{af}	τ_{am}	τ_{sm}	τ_{sf}	ω	ω'	R calc.	R ANISN
0.00356	0.00019	0.43132	0.1818	0.24	0.06	1.001	1.001
0.12727						1.046	1.053
0.25448						1.094	1.109
0.38168						1.144	1.168
0.50889						1.196	1.229
0.63609						1.250	1.292
0.7633						1.306	1.357
0.8905						1.364	1.425
1.01771						1.423	1.493
1.14492						1.483	1.493
1.27212						1.545	1.636
1.39933						1.605	1.710
1.52654						1.672	1.785
1.65374						1.737	1.862
1.78095						1.803	1.941
1.90904						1.871	2.020
2.16358						2.008	2.182
2.41811						2.147	2.349
2.67265						2.290	2.520
2.92719						2.435	2.695
3.18173						2.582	2.872
8.48462						5.913	6.854
13.76966						9.434	10.930
19.09039						13.042	15.044
65.75552						45.187	51.278
112.42040						77.469	87.165
159.08655						109.772	123.914

V_f/V_m = 0.30122 r_f = 0.3175 r_m = 0.6599

Table B.2

Flux Ratios for a Two-Region Cylindrical Unit Cell

τ_{af}	τ_{am}	τ_{sm}	τ_{sf}	ω	ω'	R calc.	R ANISN
0.00559	0.01181	0.60355	0.28569	0.24	0.03	1.002	1.009
0.19999	0.422521	↓	↓	↓	↓	1.092	1.231
0.39989	0.84483	↓	↓	↓	↓	1.201	1.372
1.39936	3.00132	↓	↓	↓	↓	1.868	1.958
1.59926	3.37865	↓	↓	↓	↓	2.014	2.083
1.79915	3.80096	↓	↓	↓	↓	2.165	2.213
1.99905	4.22327	↓	↓	↓	↓	2.319	2.348
29.99918	63.37738	↓	↓	↓	↓	28.556	29.116
103.33038	218.29901	↓	↓	↓	↓	101.612	100.889
176.66081	373.21979	↓	↓	↓	↓	175.931	172.210
249.99315	528.1448	↓	↓	↓	↓	250.786	244.553

V_f/V_m = 0.30122 r_f = 0.3175 r_m 0.6599

Table B.3

Flux Ratios for a Two-Region Cylindrical Unit Cell

τ_{af}	τ_{am}	τ_{sm}	τ_{sf}	ω	ω'	R calc.	R ANISN
0.08479	0.28569	0.60355	0.28569	0.24	0.06	1.037	1.002
0.19999	0.42252	↓	↓	↓	↓	1.092	1.089
0.39989	0.84483	↓	↓	↓	↓	1.201	1.187
0.59979	1.26713	↓	↓	↓	↓	1.321	1.293
0.79969	1.68944	↓	↓	↓	↓	1.449	1.405
0.99957	2.11171	↓	↓	↓	↓	1.583	1.524
1.79915	3.80096	↓	↓	↓	↓	2.165	2.059
1.99905	4.2236	↓	↓	↓	↓	2.319	2.206
2.19895	4.64558	↓	↓	↓	↓	2.475	2.357
2.39885	5.0679	↓	↓	↓	↓	2.634	2.513
2.59874	5.49019	↓	↓	↓	↓	2.795	2.673
2.79864	5.91251	↓	↓	↓	↓	2.957	2.673
2.99992	6.33774	↓	↓	↓	↓	3.123	3.004
4.99986	10.5629	↓	↓	↓	↓	4.834	4.796
13.3329	28.16772	↓	↓	↓	↓	12.502	12.847
21.63807	45.71331	↓	↓	↓	↓	20.439	20.950
29.99918	63.37738	↓	↓	↓	↓	28.556	29.115
103.33038	218.29901	↓	↓	↓	↓	101.612	101.385
176.66081	373.21979	↓	↓	↓	↓	175.931	172.710

Table B.4

Flux Ratios for a Two-Region Cylindrical Unit Cell

τ_{af}	τ_{am}	τ_{sm}	τ_{sf}	ω	ω'	R calc.	R ANISN
0.11214	0.03425	2.28766	0.15844	0.24	0.06	1.048	1.050
0.11214	0.07148	4.77467	0.15844	↓	↓	1.056	1.060
0.17493	0.02195	1.46645	0.24717	↓	↓	1.071	1.088
0.36511	0.02195	1.46645	0.51588	↓	↓	1.157	1.194
1.68204	0.02195	1.46645	2.37666	↓	↓	1.938	2.047
0.17621	0.08838	0.55984	0.24898	↓	↓	1.067	1.069
0.17621	0.01397	0.93309	0.24898	↓	↓	1.069	1.072
0.17621	0.04191	2.79959	0.24898	↓	↓	1.079	1.086
0.10571	0.01397	0.9332	0.14937	↓	↓	1.041	1.046
0.17619	0.01397	0.9332	0.24896	↓	↓	1.069	1.079
0.52864	0.01397	0.9332	0.74695	↓	↓	1.226	1.259
0.17621	0.02179	0.45579	0.24898	↓	↓	1.072	1.076
0.17621	0.04549	3.03843	0.24898	↓	↓	1.080	1.087
0.17621	0.20956	13.99794	0.24898	↓	↓	1.135	1.122
0.27489	0.01397	0.9332	0.38841	↓	↓	1.110	1.126
0.57374	0.01397	0.9332	0.81067	↓	↓	1.248	1.284
2.64320	0.01397	0.9332	0.39210	↓	↓	2.364	2.591

Table B.5

Flux Ratios for a Two-Region Cylindrical Unit Cell

τ_{af}	τ_{am}	τ_{sm}	τ_{sf}	ω	ω'	R calc.	R ANISN
0.2	0.015	1.5	0.500	0.24	0.06	1.082	1.095
0.2	0.015	1.5	0.005			1.080	1.087
0.2	0.015	1.5	0.7500			1.084	1.099
0.2	0.015	1.5	2.000			1.090	1.119
0.2	0.015	1.5	0.3000			1.081	1.091
0.2	0.0015	1.5	0.5000			1.080	1.095
0.2	0.600	1.5	0.5000			1.101	1.097
0.005	0.600	1.5	0.5000			1.002	1.002

$V_f/V_m = 0.3333$ $r_f = 0.5$ $r_m = 1$

Table B.6

Flux Ratios as a Function of Source Distribution for a Two-Region Cylindrical Unit Cell

τ_{af}	τ_{am}	τ_{sm}	τ_{sf}	Q_m/Q_f	ω/ω'	R calc.	R ANISN
0.35	1.20709	1.20709	0.13970	1.0 0.0	0.24 0.06	1.187	1.155
				0.8 0.2		1.021	1.015
				0.6 0.4		0.888	0.900
				0.4 0.6		0.780	0.804
				0.2 0.8		0.690	0.722
				0.0 1.0		0.614	0.652

V_f/V_m = 1.0001 r_f = 0.3175 r_m = 0.4490

Table B.7

Flux Ratios as a Function of Source Distribution for a Two-Region Cylindrical Unit Cell

τ_{af}	τ_{am}	τ_{sm}	τ_{sf}	Q_m/Q_f	ω/ω'	R calc.	R ANISN
0.50	1.20709	1.20709	0.13970	1.0 0.0	0.24 0.06	1.271	1.226
				0.8 0.2		1.078	1.065
				0.6 0.4		0.924	0.932
				0.4 0.6		0.799	0.821
				0.2 0.8		0.695	0.727
				0.0 1.0		0.608	0.647

Table B.8

Flux Ratios as a Function of Source Distribution for a Two-Region Cylindrical Unit Cell

τ_{af}	τ_{am}	τ_{sm}	τ_{sf}	Q_m/Q_f	ω/ω'	R calc.	R ANISN
49.99996	1.20709	1.20709	0.13970	1.0 0.0	0.24 0.06	39.711	38.805
				0.8 0.2		26.557	26.435
				0.6 0.4		17.211	17.356
				0.4 0.6		10.230	10.420
				0.2 0.8		4.816	4.949
				0.0 1.0		0.495	0.521

Table B.9

Flux Ratios for a Two-Region Planar Unit Cell

τ_{af}	τ_{am}	τ_{sm}	τ_{sf}	ω	ω'	R calc.	R ANISN
0.01118	0.00767	0.39212	0.57137	0.15	0.03	1.004	1.000
0.39999	0.2745			0.15	0.03	1.140	1.121
0.79978	0.54887			0.15	0.03	1.311	1.305
1.59937	1.0976			0.15	0.03	1.729	1.764
2.39893	1.64631			0.16	0.03	2.264	2.279
3.18582	2.19504			0.15	0.03	2.776	2.835
3.9981	2.74377			0.15	0.03	3.385	3.429
4.79769	3.29252			0.15	0.03	4.021	4.059
5.59227	3.84125			0.15	0.03	4.680	4.721
6.79981	4.66651			0.15	0.03	5.720	5.763
8.39977	5.76451			0.15	0.03	7.153	7.216
9.99973	6.86252			0.15	0.03	8.629	8.717
43.27614	29.69909			0.15	0.03	41.318	41.325
206.66075	14182482			0.15	0.03	198.647	201.931
499.9863	343.125899			0.19	0.03	488.521	490.321

$V_f/V_m = 0.92728$ $r_f = 0.3175$ $r_m = 0.6599$

Table B.10

Flux Ratios for a Two-Region Planar Unit Cell

τ_{af}	τ_{am}	τ_{sm}	τ_{sf}	ω	ω'	R calc.	R ANISN
0.37498	0.00008	0.9996	0.12500	0.12	0.03	1.143	1.146
0.99997	0.00008	2.00822	0.99997	0.15	0.03	1.543	1.546
3.5999	0.00008	4.00008	0.39999	0.13	0.03	3.435	3.464
3.5999	0.00008	20.00068	0.39999	0.13	0.03	6.767	6.884
0.99997	0.00008	10.00033	8.99975	0.11	0.02	2.365	2.309

$V_f/V_m = 0.9273$ $r_f = 0.3175$ $r_m = 0.6599$

Table B.11

Flux Ratios for a Two-Region Planar Unit Cell

τ_{af}	τ_{am}	τ_{sm}	τ_{sf}	ω	ω'	R calc.	R ANISN
0.62975	0.00008	0.17832	0.57137	0.15	0.03	1.245	1.231
1.19958	↓	↓	↓	0.15	0.03	1.494	1.408
1.59937				0.15	0.03	1.683	1.610
1.99913				0.15	0.03	1.880	1.831
2.39893				0.15	0.03	2.085	2.063
2.79872				0.15	0.03	2.297	2.306
3.19852				0.15	0.03	2.514	2.555
3.5983				0.15	0.03	2.738	2.809
3.9981				0.15	0.03	2.966	3.069
4.3979				0.15	0.03	3.433	3.332
4.79769				0.15	0.03	3.433	3.598
5.19749				0.15	0.03	3.673	3.867
5.59727				0.15	0.03	3.915	4.138
5.99984				0.20	0.03	4.432	4.413
6.79981				0.20	0.03	4.967	4.963
7.59979				0.20	0.03	5.510	5.517
8.39977				0.20	0.03	6.058	6.073
9.19974				0.20	0.03	6.612	6.632
9.99973				0.20	0.03	7.169	7.192
26.66581				0.15	0.03	18.162	18.762
43.27614				0.15	0.03	29.882	30.546
60.0049				0.15	0.03	41.765	42.292
206.66075				0.15	0.03	146.478	145.296
353.32162				0.15	0.03	251.328	248.346
499.9863	↓	↓	↓	0.15	0.03	356.198	351.40533

$V_f/V_m = 0.9273$ $r_f = 0.3175$ $r_m = 0.6599$

Table B.12

Flux Ratios for a Two-Region Planar Unit Cell

τ_{af}	τ_{am}	τ_{sm}	τ_{sf}	ω	ω'	R calc.	R ANISN
1.00	0.900	0.5	0.100	0.15	0.03	1.403	1.396
↓	↓	2.5	↓	0.15	0.03	1.515	1.553
↓	↓	49.99998	↓	0.12	0.03	3.468	3.545
↓	↓	0.5	0.8	0.15	0.03	1.444	1.455
↓	↓	↓	5.0	0.15	0.03	1.694	1.711
↓	↓	↓	50.00003	0.12	0.03	3.585	3.474

$V_f/V_m = 2.41445$ $r_f = 0.3175$ $r_m = 0.4490$

Table B.13

Flux Ratios for a Two-Region Planar Unit Cell

τ_{af}	τ_{am}	τ_{sm}	τ_{sf}	ω	ω'	R calc.	R ANISN
0.54887	0.00011	0.25984	0.39212	0.10	0.01	1.168	1.129
1.0976	↓	↓	↓	0.10	0.02	1.380	1.345
1.64631				0.15	0.03	1.691	1.616
2.19504				0.15	0.03	1.959	1.922
2.74377				0.15	0.03	2.241	2.249
3.29252				0.15	0.03	2.534	2.590
3.84125				0.15	0.03	2.837	2.942
4.66651				0.15	0.03	3.307	3.487
5.76451				0.20	0.03	4.197	4.228
6.86252				0.19	0.03	4.858	4.984

$V_f/V_m = 0.927$ $r_f = 0.3175$ $r_m = 0.6599$

Table B.14

Flux Ratios for a Two-Region Planar Unit Cell

τ_{af}	τ_{am}	τ_{sm}	τ_{sf}	ω	ω'	R calc.	R ANISN
0.43136	0.00007	0.16535	0.61618	0.15	0.03	1.165	1.115
1.29365	↓	↓	↓	0.15	0.03	1.542	1.476
2.15591	↓	↓	↓	0.15	0.03	1.966	1.945
3.01821	↓	↓	↓	0.15	0.03	2.426	2.467
3.8805	↓	↓	↓	0.15	0.03	2.912	3.018
4.74280	↓	↓	↓	0.15	0.03	3.419	3.588
5.6051	↓	↓	↓	0.15	0.03	3.942	4.172
6.47037	↓	↓	↓	0.15	0.03	4.479	4.766
8.19581	↓	↓	↓	0.20	0.03	5.961	5.965
9.92123	↓	↓	↓	0.20	0.03	7.167	7.174
28.75708	↓	↓	↓	0.15	0.03	19.768	20.433
64.70374	↓	↓	↓	0.15	0.03	45.437	45.758
381.03094	↓	↓	↓	0.15	0.03	273.144	268.787
539.19782	↓	↓	↓	0.15	0.03	387.080	380.331

$V_f/V_m = 0.927$ $r_f = 0.3175$ $r_m = 0.6599$

Table B. 15

Flux Ratios as a Function of Source Distribution for a Two-Region Planar Unit Cell

τ_{af}	τ_{am}	τ_{sm}	τ_{sf}	Q_m/Q_f	ω/ω'	R calc.	R ANISN
0.7	1.00	1.00	0.2794	0.623596 0.376410	0.15 0.03	1.028	1.023
				0.383198 0.616808	0.15 0.03	0.886	0.879
				0.216373 0.783633	0.15 0.03	0.800	0.792
				0.0938281 0.906175	0.15 0.03	0.743	0.735
				0.0 1.0	0.15 0.03	0.702	0.693
				1.0 0.0	0.15 0.03	1.309	1.310

V_f/V_m = 2.41445 r_f = 0.3175 r_m = 0.449

Table B.16

Flux Ratios as a Function of Source Distribution for a Two-Region Planar Unit Cell

τ_{af}	τ_{am}	τ_{sm}	τ_{sf}	Q_m/Q_f	ω/ω'	R calc.	R ANISN
1.00	1.00	1.00	0.2794	0.623596 0.376410	0.15 0.03	1.095	1.097
				0.383198 0.616808	0.15 0.03	0.918	0.916
				0.216373 0.783633	0.15 0.03	0.811	0.808
				0.0938281 0.906175	0.15 0.03	0.740	0.736
				0.0 1.0	0.15 0.03	0.689	0.684
				1.0 0.0	0.15 0.03	1.451	1.461

Table B.17

Flux Ratios as a Function of Source Distribution for a Two-Region Planar Unit Cell

τ_{af}	τ_{am}	τ_{sm}	τ_{sf}	Q_m/Q_f	ω/ω'	R calc.	R ANISN
5.00	1.00	1.00	0.27940	0.623596 0.376410	0.15 0.03	2.112	2.337
				0.383198 0.616808	0.15 0.03	1.422	1.567
				0.216373 0.783633	0.15 0.03	1.029	1.121
				0.0938281 0.906175	0.15 0.03	0.775	0.831
				0.0 1.0	0.15 0.03	0.598	0.626
				1.0 0.0	0.15 0.03	3.642	3.989

Table B.18

Flux Ratios as a Function of Source Distribution for a Two-Region Planar Unit Cell

τ_{af}	τ_{am}	τ_{sm}	τ_{sf}	Q_m/Q_f	ω/ω'	R calc.	R ANISN
99.99993	1.00	1.00	0.2794	0.623596 0.376410	0.15 0.03	30.787	37.299
				0.383198 0.616808	0.15 0.03	16.369	20.352
				0.216373 0.783633	0.15 0.03	8.631	10.859
				0.0938281 0.906175	0.15 0.03	3.803	4.788
				0.0 1.0	0.15 0.03	0.503	0.571
				1.0 0.0	0.15 0.03	66.096	76.104

Table B.19

Flux Ratios for a Two-Region Spherical Unit Cell

τ_{af}	τ_{am}	τ_{sm}	τ_{sf}	ω	ω'	R calc.	R ANISN
0.99999	0.9	0.1	0.1	0.27	0.09	1.484	1.503
		0.5	0.1			1.501	1.506
		2.5	0.1			1.588	1.527
		49.99983	0.1		0.06 0.09	2.913 3.638	2.861
		0.80000	0.79999			1.546	1.569
		0.80000	4.99995			1.739	1.905
		0.80000	49.99951			3.803	3.834

$V_f/V_m = 0.54699$ $r_f = 0.3175$ $r_m = 0.4490$

Table B.20

Flux Ratios for a Two-Region Spherical Unit Cell

τ_{af}	τ_{am}	τ_{sm}	τ_{sf}	ω	ω'	R calc.	R ANISN
0.00373	0.01891	0.9670	0.19046	0.27	0.09	1.001	1.001
0.13333	0.67695	↓	↓	↓	↓	1.064	1.067
0.26659	1.35356					1.141	1.137
0.39986	2.03018					1.226	1.211
0.53312	2.70679					1.315	1.288
0.66637	3.38335					1.408	1.368
0.79964	4.05997					1.504	1.452
0.9329	4.7366					1.602	1.539
1.06617	5.4132					1.703	1.629
1.19943	6.08983					1.805	1.722
1.33269	6.76642					1.909	1.818
1.46595	7.44305					2.015	1.916
1.59922	8.11968					2.121	2.017
1.73248	8.79627					2.229	2.120
1.86574	9.4729					2.338	2.225
1.99993	10.15419					2.449	2.333
2.26659	11.50809					2.672	2.552
2.53324	12.86169					2.898	2.778
2.7999	14.21585					3.217	3.010
3.06656	15.56975					3.359	3.252
3.33322	16.92365					3.593	3.492
8.88979	45.12974					8.757	8.826
14.42527	73.24092					14.173	14.230
19.99929	101.54191					19.755	19.676
68.88637	349.75413					70.564	67.650
117.77295	597.9649					122.498	118.988
166.66079	846.18261	↓	↓	↓	↓	174.861	163.76916

Table B.21

Flux Ratios for a Two-Region Spherical Unit Cell

τ_{af}	τ_{am}	τ_{sm}	τ_{sf}	ω	ω'	R calc.	R ANISN
0.02972	0.00002	0.05512	1.51957	0.27	0.09	1.010	1.014
2.12702	↓	↓	↓	↓	↓	1.878	2.027
4.25354						2.859	3.085
6.37996						3.886	4.175
8.50648						4.944	5.296
10.63296						6.025	6.442
12.75948						7.123	7.608
14.88596						8.235	8.791
18.18412						9.930	10.589
22.33921						12.219	13.007
24.46675						13.375	14.222
70.91782						39.663	40.855
159.56586						92.023	91.633
939.66024						572.886	538.421
1329.71553						816.932	761.860

V_f/V_m = 0.12535 r_f = 0.3175 r_m = 0.6599

Table B.22

Flux Ratios as a Function of Source Distribution for a Two-Region Spherical Unit Cell

τ_{af}	τ_{am}	τ_{sm}	τ_{sf}	Q_m/Q_f	ω/ω'	R calc.	R ANISN
0.23333	1.47135	1.47135	0.09313	1.00 0.00	0.27 0.09	1.129	1.107
				0.879703 0.12029		1.025	1.012
				0.732784 0.26721		0.919	0.914
				0.5493 0.45069		0.810	0.812
				0.313681 0.68632		0.698	0.707
				0.00 1.00		0.583	0.597

$V_f/V_m = 0.54699$ $r_f = 0.3175$ $r_m = 0.4490$

Table B.23

Flux Ratios as a Function of Source Distribution for a Two-Region Spherical Unit Cell

τ_{af}	τ_{am}	τ_{sm}	τ_{sf}	Q_m/Q_f	ω/ω'	R calc.	R ANISN
0.3333	1.47135	1.47135	0.09313	1.00 0.00	0.27 0.09	1.185	1.156
				0.879703 0.12029		1.068	1.050
				0.732784 0.26721		0.949	0.941
				0.5493 0.45069		0.827	0.829
				0.313681 0.68632		0.703	0.713
				0.00 1.00		0.576	0.593

Table B.24

Flux Ratios as a Function of Source Distribution for a Two-Region Spherical Unit Cell

τ_{af}	τ_{am}	τ_{sm}	τ_{sf}	Q_m/Q_f	ω/ω'	R calc.	R ANISN
1.6665	1.47135	1.47135	0.09313	1.00 0.00	0.27 0.09	1.977	1.935
				0.879703 0.12029		1.683	1.658
				0.732784 0.26721		1.392	1.381
				0.5493 0.45069		1.104	1.103
				0.313681 0.68632		0.817	0.826
				0.00 1.00		0.534	0.548

Table B.25

Flux Ratios as a Function of Source Distribution for a Two-Region Spherical Unit Cell

τ_{af}	τ_{am}	τ_{sm}	τ_{sf}	Q_m/Q_f	ω/ω'	R calc.	R ANISN
33.33305	1.47135	1.47135	0.09313	1.00 0.00	0.27 0.03	23.368	27.660
				0.879703 0.12029		17.967	21.422
				0.732784 0.26721		13.027	15.625
				0.5493 0.45069		8.489	10.225
				0.313681 0.68632		4.309	5.181
				0.00 1.00		0.444	0.458

where

$\bar{L}_{clad}$ = penetration chord length through the clad

$t \equiv (r_{clad}-r_f)$ = thickness of the (thin) clad region

r_f = radius of the fuel region

r_{clad} = outer radius of the clad.

Furthermore,

$$\bar{\phi}_f = \frac{\lambda_{af}}{V_f} = \frac{1}{\pi r_f^2 \Sigma_{af}} \tag{B.2}$$

Upon dividing Eq. (B.1) by Eq. (B.2) we get:

$$\frac{\bar{\phi}_{clad}}{\bar{\phi}_f} = \frac{\bar{L}_{clad}}{2\pi r_f t} \pi r_f^2 \Sigma_{af} \tag{B.3}$$

or

$$\frac{\bar{\phi}_{clad}}{\bar{\phi}_f} = \frac{\bar{L}_{clad}}{4t} \tau_{af} \tag{B.4}$$

It is possible to derive an analytical expression for the penetration chord length through an annular clad (M1) for isotropically incident neutrons:

$$\bar{L} = \frac{r_1}{r_2}\left[2\sin^{-1}\left(\frac{r_1}{r_2}\right) - \pi\left(\frac{r_1}{r_2}\right)^2 + 2\left(\frac{r_1}{r_2}\right)\left\{1-\left(\frac{r_1}{r_2}\right)^2\right\}^{1/2}\right] \tag{B.5}$$

where

$r_1 \equiv r_{fuel}$

$r_2 \equiv r_{clad}$

However, the above is a needlessly sophisticated expression for $\bar{L}$ for present purposes and we shall hence use the following approximate expression:

$$\bar{L} = 2(r_2 - r_1) \equiv 2t \tag{B.6}$$

which would be exact for a thin annulus resembling a slab.

Substituting Eq. (B.6) into Eq. (B.4) yields:

$$\frac{\bar{\phi}_{clad}}{\bar{\phi}_f} = \frac{1}{2}\,\tau_{af} \tag{B.7}$$

Recall that this was derived under the assumption of $\tau_{af} \to \infty$ (black fuel).

Next, it is shown by Gregory (G1) that in the limit of weak fuel absorption (small τ_{af}) one gets:

$$\frac{\bar{\phi}_{surface\ of\ the\ fuel}}{\bar{\phi}_f} \simeq \frac{\bar{\phi}_{clad}}{\bar{\phi}_f} \simeq 1 + \frac{1}{6}\,\tau_{af} \tag{B.8}$$

The function that best (or at least simply and conveniently) joins the two aysmptotic limits given by Eqs. (B.7) and (B.8) is found to be:

$$R_c \equiv \frac{\bar{\phi}_{clad}}{\bar{\phi}_f} = 1 + \left(\frac{1}{2} - \frac{1}{3}\,\frac{1}{1+\omega\tau_{af}}\right)\tau_{af} = 1 + \bar{\gamma}_f'\,\tau_{af} \tag{B.9}$$

where we have defined $\bar{\gamma}_f' = \frac{1}{2} - \frac{1}{3}\left(\frac{1}{1+\omega\tau_{af}}\right)$ (B.10)

and where ω is a fitting parameter which has a value of $\sim$0.12.

Equation (B.9) can be cast in terms of the flux ratio model developed in the body of this report, namely:

$$R(E) = \frac{1}{\theta}(1 + \bar{\gamma}_f \tau_{af}) \tag{B.11}$$

Using Eqs. (B.9) and (B.11), the following can be readily shown:

$$R_c(E) = \Lambda \cdot R(E) + \left(1 - \frac{\bar{\gamma}_f'}{\bar{\gamma}_f}\right) \quad \text{where } \Lambda = \frac{\gamma_f' \theta}{\bar{\gamma}_f} \tag{B.12}$$

In Eq. (B.12) $\bar{\gamma}_f$ and θ are obtained using Eq. (3.28) of Chapter 3 and $\bar{\gamma}_f'$ from Eq. (B.10).

Table B.26 gives numerical (ANISN) and calculated (Eq. (B.12)) results: the agreement is excellent.

B.4 FURTHER REMARKS ABOUT THE DISCREPANCY BETWEEN THE CALCULATED AND THE LEOPARD RESULTS

The LEOPARD self-shielding factor results presented in Chapter 3 are consistently lower than the calculated results using Eq. (3.42) for pitches smaller than the base-case PWR unit cell and higher for larger pitches. The reason for this behavior is that as we go to smaller pitches and smaller cells (in the sense of shrinking the cell) the factor $\frac{1}{\eta + \varepsilon}$ approaches "1.0" and $\bar{\gamma}_f$ approaches 0.40 (see Table B.27 But since in the conventional case Levine's factor $\frac{1}{a}$ (equivalent) to $\bar{\gamma}_f$ in our model) is taken as 0.79, the result will be that the σ_0' predicted by the conventional case will be much smaller

Table B.26

Numerical and Calculated Results for the Clad-to-Fuel Flux Ratio, with $Q_f=0$ and $\theta=1$

τ_{af}	τ_{am}	τ_{sm}	τ_{sf}	$\bar{\gamma}_f$	$\bar{\gamma}_f'$	R^{clad} calc.	R^{clad} ANISN
0.00356	0.00019	0.43132	0.1818	0.33	0.167	1.001	1.001
0.12727	↓	↓	↓	0.361	0.177	1.022	1.022
0.25448	↓	↓	↓	0.369	0.186	1.047	1.047
1.01771	↓	↓	↓	0.416	0.232	1.236	1.268
1.14492	↓	↓	↓	0.422	0.239	1.273	1.309
1.52654	↓	↓	↓	0.440	0.256	1.391	1.437
1.90904	↓	↓	↓	0.456	0.271	1.518	1.777
2.67265	↓	↓	↓	0.483	0.297	1.794	1.880
2.92719	↓	↓	↓	0.490	0.304	1.890	1.985
3.18173	↓	↓	↓	0.497	0.311	1.990	2.092
8.48462	↓	↓	↓	0.579	0.390	4.311	4.439
13.76966	↓	↓	↓	0.613	0.423	6.814	6.408
19.09039	↓	↓	↓	0.631	0.440	9.400	8.429
65.75552	↓	↓	↓	0.672	0.480	32.572	37.852
0.39989	0.84483	0.60355	0.28569	0.503	0.196	1.078	1.126
1.59926	3.37865	↓	↓	0.634	0.259	1.414	1.489
29.99918	63.37738	↓	↓	0.919	0.459	14.780	14.399

Table B.27

Group 45 Values of $\frac{1}{\eta + \varepsilon}$ and $\bar{\gamma}_f$ for Various Pitches and Cell Shrinkage Factors

Case	Pitch	$\frac{1}{\eta + \varepsilon}$	$\bar{\gamma}_f$
(1)	Base-Case PWR Unit Cell P = 0.580 in	0.768	0.607
(2)	$\frac{1}{4}$ x the above cell dimension	0.945	0.413
(3)	$\frac{3}{2}$ x the above cell dimension	0.668	0.715
(4)	P = 0.448 in	0.869	0.495
(5)	P = 0.649 in	0.718	0.681

Cases (1), (2), (3); fuel rod shrunk by same factor as pitch.

Cases (4), (5): fuel rod same as base case.

than the σ_0' predicted using the present method. Thus the self-shielding factor, which increases monotonically as σ_0 increases, will be smaller, and as a result the conventional results are predicted to be lower. On the other hand, when larger pitches are used $\frac{1}{\eta + \varepsilon}$ approaches approximately 0.70 and $\bar{\gamma}_f$ approaches 0.70. Thus while the $f(\sigma)$ values are nearly the same, the present result is reduced by the multiplicative factor $\frac{1}{\eta + \varepsilon}$, and it is easy to conclude that the present model's results should now be lower than the conventional results - as observed. Tables 3.5 through 3.6 illustrate this behavior of the relevant parameters. Since our results correspond to use of a variable Levine factor, they are potentially more accurate than the conventional approach.

It was pointed out in Chapter 2 that it is possible to replace a three-region unit cell by an equivalent two-region unit cell without introducing appreciable error into the calculated heterogeneous cross-sections. Table B.28 shows the values of the broad-group (i.e., collapsed over groups 26 to 54, see Table 3.8 for group structure) heterogeneous cross-sections obtained using LEOPARD for the two cases of the three-region and the equivalent two-region unit cells. As seen, the results are essentially the same: the percentage error is calculated to be about 0.3%. Data pertinent to the above unit cells are summarized in Table 3.7.

Table B.28

Heterogeneous Cross-Sections for Two and Three Region Unit Cells, Obtained Using LEOPARD

σ_c^{het} for a two-region cylindrical unit cell	σ_c^{het} for a three-region cylindrical unit cell	$\Delta\%$ percent difference
2.229119	2.235807	0.3

Furthermore, to be able to study the effect of the assumption of linearization introduced in Section 3.3.2 we have artifically introduced the following approximations. Recall Eq . (2.80) - namely:

$$\alpha_f = \frac{\frac{1}{3}[1 + \frac{0.24\delta_f}{1+0.24\delta_f}] + 0.24\delta_m^{1/2}}{1 + 0.24\delta_m^{1/2}} \qquad (2.80)$$

First we arbitrarily set the part

$$\frac{1}{3}[1 + \frac{0.24\delta_f}{1+0.24\delta_f}]$$

of the above equation to $\frac{1}{3}$; the resulting heterogeneous cross-section obtained this way was 2.282 (as opposed to 2.180 obtained without the above approximation). Next, the same part was put equal to $\frac{2}{3}$ and the resulting heterogeneous cross-section obtained was 1.925 (versus 2.180 obtained without

the above approximation). Table B.29 summarizes the results.

As seen from the results of the table an 11% difference in the average values of $\bar{\gamma}_f$ (corresponding to the exact and the $\frac{1}{3}$ limits) has introduced a 5% difference in the heterogeneous cross-section obtained using the "exact" and the "$\frac{1}{3}$" limits. Furthermore, a difference of 54% in the average values of the $\bar{\gamma}_f$ has been reflected as a 13% difference in the corresponding heterogeneous cross-sections. The preceding results justify the following statements:

(a) the assumption of linearization introduced in Section 3.3.2 is a valid assumption; since an artificial change in the value of $\bar{\gamma}_f$ ($\frac{1}{3}$ limit) did not reflect any significant difference in the calculated values of the heterogeneous cross-sections.

(b) heterogeneous cross-sections obtained using the present model are weakly sensitive to the accuracy of the flux ratio R.

(c) The $\frac{1}{3}$ limit yields better results (compared to the $\frac{2}{3}$ limit) because, as in the Doppler effect, the weakly absorbing wings of the resonance control the change in absorption.

As a final note, it is worth mentioning that the ad hoc assumption of linearization introduced in this work was absolutely essential in deriving the present equivalence

Table B.29

Heterogeneous Cross-Sections, Obtained by Introducing Arbitrary Changes into the Flux Ratio R

σ_c^{het} (barns) for the 1/3 limit	σ_c^{het} (barns) for the "exact" case	Δ% percent difference
2.282	2.180	-5.0

σ_c^{het} (barns) for the 2/3 limit	σ_c^{het} (barns) for the "exact" case	Δ% percent difference
1.925	2.180	+13.0

$\bar{\gamma}_f$ for the 1/3 limit averaged over the groups* (26-49)	$\bar{\gamma}_f$ for the "exact" case averaged over the groups* (26-49)	Δ% percent difference
0.48	0.52	+11.0

$\bar{\gamma}_f$ for the 2/3 limit averaged over the groups* (26-49)	$\bar{\gamma}_f$ for the "exact" case averaged over the groups* (26-49)	Δ% percent difference
0.80	0.52	-54.0

* Group structure is given in Table 3.8.

relation. The manner of implementing the assumption, however, through using infinite dilution cross-sections was quite arbitrary. As a result, further improvements in the implementation of the assumption, such as replacing the infinite dilution cross-section by an alternately defined averaged cross-section, are possible. A good starting-point for pursuing this idea would be the work of Amaldi (F5).

Appendix C

THE LEOPARD COMPUTER CODE

Normally LEOPARD, a state-of-the-art LWR unit cell program, prepares a one-group representation of the resonance cross-section in the entire epithermal region. The epithermal region spans the energy range from 0.625 ev to 5.53 Kev; and in terms of group numbers, this corresponds to G=26 to G=54 (in the EPRI version of LEOPARD using ENDF-IV cross-sections employed in the present work).*

Since we desired to obtain cross section output for a finer group structure, the following minor changes were made in the program:

(1) an additional named COMMON block was added in MAIN - namely the following three statements:

```
      COMMON/A/LIM1,LIM2
      READ(5,13),LIM1,LIM2
   13 FORMAT (2I5)
```

(2) a similar COMMON block was added to subroutine ED34, and a fortran statement was changed - namely:

```
      COMMON/A/LIM1,LIM2
```

and

```
      DO 40  N=26,54 was changed to
      DO 40  N=LIM1,LIM2
```

---

* The detailed group structure is given in Table 3.8.

LIM1 and LIM2 are the two group variables controlled by the user: by running successive problems varying LIM1 from 26 to 53, and with LIM2 = LIM1+1, it was possible to obtain a fine group breakdown of the LEOPARD-developed results in the epithermal region. Note that the above modifications apply only to the recovery of the fine group components of the resonance part of the absorption cross section, and not to its smooth part.* For a more detailed exposition on the structure of the code refer to the manual (L5). Furthermore, it is important to understand that when particular LIM1 and LIM2 are chosen, the resulting cross-section is to be interpreted as follows:

$$\text{e.g.} \qquad \sigma_g = \frac{\int_{G=LIM2}^{G=LIM1} \sigma(E)\phi(E)dE}{\int_{G=54}^{G=26} \phi(E)dE} \quad ;$$

note the limits of integration, especially in the denominator.

---

* the smooth part, while omitted from the fine group LEOPARD results, was included in all collapsed(26 to 54) results quoted in this work.

Appendix D

INTERPOLATION SCHEMES

D.1 TEMPERATURE INTERPOLATION AT A FIXED σ_0.

A Lagrange-three-point interpolation scheme predicts, very accurately, the shielding factors for any current temperature, T. The scheme is as follows:

self-shielding factor at three tabulated temperature points	f(T)	f(300)	f(900)	f(2100)
the natural log of the three tabulated temperature points	ℓn(T)	ℓn(300)	ℓn(900)	ℓn(2100)

Applying the interpolation scheme to the above table, there results:

$$f(T) = f(300)\frac{(\ell nT-\ell n900)(\ell nT-\ell n2100)}{(\ell n300-\ell n900)(\ell n300-\ell n2100)} + f(900)\frac{(\ell nT-\ell n300)(\ell nT-\ell n2100)}{(\ell n900-\ell n300)(\ell n900-\ell n2100)} + f(2100)\frac{(\ell nT-\ell n300)(\ell nT-\ell n900)}{(\ell n2100-\ell n300)(\ell n2100-\ell n900)} \qquad (D.1)$$

$$f(T) = f(300)\frac{\ell n\frac{T}{900}\ell n\frac{T}{2100}}{\ell n\frac{1}{3}\ell n\frac{1}{7}} + f(900)\frac{\ell n\frac{T}{300}\ell n\frac{T}{2100}}{\ell n3\,\ell n\frac{3}{7}} + f(2100)\frac{\ell n\frac{T}{300}\ell n\frac{T}{900}}{\ell n7\,\ell n\frac{7}{3}} \qquad (D.2)$$

D.2 σ_0-INTERPOLATION AT A FIXED T.

(a) The empirical σ_0-interpolation is:

$$f(\sigma_0) = A\tanh B(\ell n\sigma_0 + C) + D \tag{D.3}$$

Constants A and D can be found by inspection of the range and magnitude of the self-shielding factors - namely:

$$A + D = f\ max \tag{D.4}$$

$$A - D = f\ min \tag{D.5}$$

where

f max = maximum self-shielding factor

f min = minimum self-shielding factor

To find B and C we need two tabulated points $(f(\sigma_0), \sigma_0)$ nearest the point of interest. Equation (D.3) can be cast in the following form:

$$\alpha(\sigma_0) \equiv \frac{f(\sigma_0)-D}{A} = \tanh B(\ell n\sigma_0+C) \equiv \tanh x(\sigma_0) \tag{D.6}$$

$$\tanh x(\sigma_0) = \frac{e^{2x} - 1}{e^{2x} + 1} \tag{D.7}$$

where $x(\sigma_0) \equiv B(\ell n\sigma_0+C)$, see Eq. (D.6)

or

$$x(\sigma_0) = \ell n\left|\frac{1 + \alpha(\sigma_0)}{1 - \alpha(\sigma_0)}\right|^{1/2} \tag{D.8}$$

Now using two values of $(f(\sigma_0), \sigma_0)$, say $(f(\sigma_1), \sigma_1)$ and $(f(\sigma_2), \sigma_2)$ we get:

$$x(\sigma_1) = B\ell n\sigma_1 + BC \tag{D.9}$$

$$x(\sigma_2) = B\ell n\sigma_2 + BC \tag{D.10}$$

Solving the simultaneous Eqs. (D.9) and (D.10) yields:

$$B = \frac{x(\sigma_1) - x(\sigma_2)}{\ell n \frac{\sigma_1}{\sigma_2}} \tag{D.11}$$

where $x(\sigma_0) = \tanh^{-1}[\frac{f(\sigma_0)-D}{A}]$

$$C = \frac{x(\sigma_1) - B\ell n\sigma_1}{B} \tag{D.12}$$

(b) Segev's correlation is:

$$\frac{1}{1 - f^2(\sigma_0)} = A\sigma_0 + B$$

where A and B can easily be found using two tabulated points $(f(\sigma_0), \sigma_0)$ nearest the point of interest.

Appendix E

SAMPLE PROBLEM

In this Appendix a sample calculation is presented using the new equivalence relation given by Eq. (3.42). The example we have chosen is for U-238 capture in an oxide-fueled unit cell. Data pertinent to the present sample problem are summarized in Table E.1. Note that the calculations are done for Group 45 of LIB-IV (K6).

Recall the definition of σ_0, which is:

$$\sigma_0 = \frac{\sum_{j\neq i}^{j=N} \bar{\Sigma}_{tj}^{\infty}}{\bar{N}_i} \qquad (E.1)$$

where $\bar{\Sigma}_{tj}^{\infty}$ is the volume-weighted-homogenized infinite-dilution total cross section of isotope j;

$\bar{N}_i$ is the volume-weighted-homogenized concentration of nuclei of isotope i, here U-238.

Using the data* in Table E.1 in Eq. (E.1), in the order shown in the table (i.e., U-235, oxygen, ...):

$$\sigma_0 = \frac{0.0062+0.0683+0.0316+0.0093+0.0863+0.0147+0.0006+0.0005+0.0002}{0.009011} \qquad (E.2)$$

from which

$$\sigma_0 = \frac{0.2177}{0.00901} = 24 \text{ barns} \qquad (E.3)$$

---

* Cross-sections are taken from LIB-IV (K6).

Table E.1

Data Pertinent to Oxide-Fueled Blanket Unit Cell

Homogenized Atom Densities	
Element	Atom Densities (nuclei/barn-cm)
Uranium-28	9.011×10^{-3}
Uranium-25	1.00×10^{-4}
Oxygen	1.8222×10^{-2}
Sodium	9.927×10^{-3}
Chromium	2.055×10^{-3}
Iron	7.462×10^{-3}
Nickel	8.09×10^{-4}
Manganese	2.16×10^{-4}
Silicon	2.11×10^{-4}
Carbon	3.9×10^{-5}

Cell Dimensions

$r_f = 0.546$ (cm); $r_g = 0.564$ (cm); $r_{clad} = 0.635$ (cm); $r_{coolant} = 0.814$ (cm)

$$\frac{V_f}{V_{cell}} = 0.4506 \qquad \frac{V_{coolant}}{V_{cell}} = 0.5494$$

Temperature

T=300°K

Mean Lethargy Decrements for Elastic Moderation

$\xi_{28} = 0.00838$; $\xi_{25} = 0.00849$; $\xi_O = 0.11995$; $\xi_{Na} = 0.0845$; $\xi_{Cr} = 0.03797$;
$\xi_{Fe} = 0.03529$; $\xi_{Ni} = 0.03409$; $\xi_{Mn} = 0.03593$; $\xi_{Si} = 0.0674$; $\xi_C = 0.15777$

The mean energy decrement for the fuel is defined by

$$\bar{\xi}_f = \frac{\xi_{28}\Sigma_{es}^{28} + \xi_{25}\Sigma_{es}^{25} + \xi_O\Sigma_{es}^{O}}{\Sigma_{es}^{28} + \Sigma_{es}^{25} + \Sigma_{es}^{O}} = \frac{0.0019+0.00002+0.0179}{0.22673+0.00235+0.1496} \quad (E.4)$$

hence

$$\bar{\xi}_f = \frac{0.0198}{0.3787} = 0.0523 \quad (E.5)$$

where the elastic scattering cross sections are again taken from LIB-IV.

Similarly for the "coolant" (including the clad) region:

$$\bar{\xi}_c = \frac{\xi_O\Sigma_{es}^{O}+\xi_{Na}\Sigma_{es}^{Na}+\xi_{Cr}\Sigma_{es}^{Cr}+\xi_{Fe}\Sigma_{es}^{Fe}+\xi_{Ni}\Sigma_{es}^{Ni}+\xi_{Mn}\Sigma_{es}^{Mn}+\xi_{Si}\Sigma_{es}^{Si}+\xi_C\Sigma_{es}^{C}}{\Sigma_{es}^{O} + \Sigma_{es}^{Na} + \Sigma_{es}^{Cr} + \Sigma_{es}^{Fe} + \Sigma_{es}^{Ni} + \Sigma_{es}^{Mn} + \Sigma_{es}^{Si} + \Sigma_{es}^{C}} \quad (E.6)$$

and

$$\bar{\xi}_c = \frac{0.0001+0.0037+0.0014+0.0128+0.0012+0.0001+0.00003+0.00003}{0.0011+0.0439+0.0381+0.3628+0.0343+0.0017+0.0005+0.0002} \quad (E.7)$$

which yields:

$$\bar{\xi}_c = \frac{0.0194}{0.4826} = 0.0401 \quad (E.8)$$

Using Eqs. (E.6) and (E.8) one can find the fraction of the elastic slowing down source generated in the fuel using the following equation:

$$Q_f = \frac{\bar{\xi}_f \Sigma_{pf} \frac{V_f}{V_{cell}}}{\bar{\xi}_f \Sigma_{pf} \frac{V_f}{V_{cell}} + \bar{\xi}_c \Sigma_{pc} \frac{V_c}{V_{cell}}} \qquad (E.9)$$

where Σ_{pf}, Σ_{pc} are the macroscopic potential scattering cross sections(LIB-IV) in the fuel and the coolant regions, respectively.

Hence:

$$Q_f = \frac{(0.0523)(0.3619)(0.4506)}{(0.0523)(0.3619)(0.4506) + (0.0401)(0.4826)(0.5494)} \qquad (E.10)$$

$$Q_f = \frac{0.0085}{0.0192} = 0.444 \qquad (E.11)$$

and

$$Q_c = 1 - Q_f = 0.556 \qquad (E.12)$$

Next, we have to find various optical thicknesses* (here taken at the infinite dilution limit) and use them in Eqs. (2.84) through (2.89); they are recalled here to show the detailed step-by-step calculations.

$$\delta_{fg} = \tau_r^{28} + \tau_r^{25} + \tau_r^{0} \qquad (E.13)$$

where subscript r stands for removal, see Section 2.7.2 for detailed explanation.

$$\delta_{fg} = 5.7238 + 0.0073 + 0.0396 = 5.7707 \qquad (E.14)$$

* Cross-sections are taken from LIB-IV.

Similarly;

$$\delta_{mg} = \tau_r^{O} + \tau_r^{Na} + \tau_r^{Cr} + \tau_r^{Fe} + \tau_r^{Ni} + \tau_r^{Mn} + \tau_r^{Si} + \tau_r^{C} \qquad (E.15)$$

and

$$\delta_{mg} = 0.0003+0.0106+0.0062+0.0413+0.0139+0.0012+0.0004+0.0003$$
$$= 0.0742 \qquad (E.16)$$

Furthermore:

$$\alpha_{fg} = \frac{\frac{1}{3}\left[1 + \frac{0.24\delta_{fg}}{1+0.24\delta_{fg}}\right] + 0.24\delta_{mg}^{1/2}}{1 + 0.24\delta_{mg}^{1/2}} \qquad (E.17)$$

and,

$$\alpha_{mg} = \frac{\frac{1}{3}\left[1 + \frac{0.24\delta_{mg}}{1+0.24\delta_{mg}}\right] + 0.24\delta_{fg}^{1/2}}{1 + 0.24\delta_{fg}^{1/2}} \qquad (E.18)$$

Using Eqs. (E.14) and (E.16) in Eqs. (E.17) and (E.18), the following results will be obtained:

$$\alpha_{fg} = 0.556 \qquad (E.19)$$

and,

$$\alpha_{mg} = 0.581$$

Finally:

$$\beta_{gg} = 1 + 0.06\tau_{fgg} \qquad (E.20)$$

and,

$$\rho_{gg} = 1 + 0.06\tau_{mgg}$$

where the subscripts fgg and mgg stand for in-group scattering in fuel and moderator regions, respectively.

$$\beta_{gg} = 1 + 0.06[\tau^{28}_{fgg} + \tau^{25}_{fgg} + \tau^{O}_{fgg}] \tag{E.21}$$

or

$$\beta_{gg} = 1 + 0.06[0.0519+0.0026+0.1241] = 1.039 \tag{E.22}$$

Similarly;

$$\rho_{gg} = 1 + 0.06[\tau^{O}_{mgg} + \tau^{Na}_{mgg} + \tau^{Cr}_{mgg} + \tau^{Fe}_{mgg} + \tau^{Ni}_{mgg} + \tau^{Mn}_{mgg} + \tau^{Si}_{mgg} + \tau^{C}_{mgg}] \tag{E.23}$$

or

$$\rho_{gg} = 1 + 0.06[0.0011+0.0485+0.0468+0.4486+0.0332+0.0021+0.0022 + 0.0007] = 1.035 \tag{E.24}$$

Using Eqs. (E.11) through (E.24) we are able to find:

$$\bar{\gamma}_f = \alpha_{fg}\beta_{gg}\rho_{gg}Q_{cg} = 0.332 \tag{E.25}$$

and

$$\theta = 1 + \alpha_{mg}\beta_{gg}\rho_{gg}\delta_{mg}Q_{fg} = 1.021 \tag{E.26}$$

At this point we have enough information to evaluate the modified background cross-section σ_0' - namely:

$$\sigma_0' = \frac{\bar{\Sigma}_{tnf}}{\bar{N}_f} + \frac{1}{\theta+\bar{\gamma}_f\delta_{mg}} \cdot \frac{\bar{\Sigma}_{tm}}{\bar{N}_f} \tag{E.27}$$

$$\sigma_0' = 4.0 + \frac{1}{1.021 + (0.332)(0.0742)}\,(20.0) = 23 \text{ barns} \qquad (E.28)$$

Next, we have to use the empirical σ_0-interpolation scheme, discussed in Appendix D, which is:

$$f_{cg}(\sigma_0) = \text{AtanhB}(\ell n\sigma_0 + C) + D \qquad (E.29)$$

Using data points at $\sigma_0 = 10^4$, 10^2, 10^1, 10^{-1} barns and T=300°K, one gets (using the procedure given in Appendix D) the following values for the constants in Eq. (E.29):

$$f_{cg}(\sigma_0) = 0.3402\tanh 0.3990(\ell n\sigma_0 - 7.6715) + 0.3710 \qquad (E.30)$$

which can be used to obtain the self-shielding factors at σ_0=24 (barns) and σ_0' = 23 (barns).

$$f_{cg}(24) \simeq 0.0492 \qquad (E.31)$$

and

$$f_{cg}(23) \simeq 0.0486 \qquad (E.32)$$

Finally, we need to evaluate the following quantities:

$$\varepsilon = f_{cg}(\sigma_0')\sigma_{cg}^{\infty}\,\frac{\bar{\gamma}_f}{\theta}\,\frac{V_m}{V_{cell}}\,N_f\ell_f \qquad (E.33)$$

$$\eta = \frac{V_f}{V_{cell}} + \frac{1}{\theta}\,\frac{V_m}{V_{cell}} + \varepsilon'' f_{sg}(\sigma_0')\cdot\sigma_{sg}^{\infty} + \frac{\bar{\gamma}_f}{\theta}\,\frac{V_m}{V_{cell}}\cdot\tau_{ng} \qquad (E.34)$$

where we have neglected the small fission term - namely:

$$\varepsilon'' f_{fg}(\sigma_0') \cdot \sigma_{fg}^{\infty} .$$

Utilizing all the results obtained so far in Eqs. (E.33) and (E.34) yields:

$$\varepsilon = (0.0486)(261)\frac{0.332}{1.021}(0.549)(0.019)(1.09) = 0.047 \quad \text{(E.35)}$$

and

$$\eta = (0.4506)+\frac{1}{1.021}(0.5494)+(0.003)(0.360)(23) + \frac{0.332}{1.021}(0.5494)(0.17) = 1.044 \quad \text{(E.36)}$$

$$\frac{f^{het}(\sigma_0)}{f^{hom}(\sigma_0)} = \frac{1}{\eta + \varepsilon} \frac{f^{hom}(\sigma_0')}{f^{hom}(\sigma_0)} = 0.910$$

Note that the above result is for a hexagonal oxide-fueled unit cell and hence different from the corresponding results given in Tables 4.4 and 5.7 which are obtained using assembly-based homogenized atom densities.

Appendix F

REFERENCES

A1 "ANISN - A One Dimensional Discrete Ordinates Transport Code," RSIG Computer Code Collection, Oak Ridge National Laboratory, CCC-82.

B1 G.I. Bell, "A Simple Treatment for Effective Resonance Integrals in Dense Lattices," Nucl. Sci. Eng., 5, 138 (1959).

B2 G.L. Bell, S. Glasstone, Nuclear Reactor Theory, Van Nostrand Reinhold Co., New York (1970).

B3 I. Bondarenko et al., Group Constants for Nuclear Reactor Calculations, Consultants Bureau Enterprises, Inc., New York (1964).

C1 K.M. Case and P.F. Zweifel, Linear Transport Theory, Addison-Wesley (1976).

C2 N. Corngold, "Resonance Escape Probability in Slab Lattices," J. N. Energy I, 4, 293 (1957).

C3 K.M. Case et al., "Introduction to the Theory of Neutron Diffusion," Los Alamos Scientific Laboratory (1953).

D1 J.J. Duderstadt, L. Hamilton, Nuclear Reactor Analysis, John Wiley & Son, Inc.(1976).

D2 L. Dresner, Resonance Absorption in Nuclear Reactors, Pergamon Press (1960).

F1 Y. Fukai, "A Comparison of Some One-Velocity Transport Approximations in Lattices," BNL 669(T-222) (1961).

F2 I.A. Forbes et al., "LMFBR Blanket Physics Project Progress Report No. 2," COO-3060-5, MITNE-131 (1971).

F3 Y. Fukai, "New Analytical Formula for Dancoff Correction for Cylindrical Fuel Lattices," Nucl. Sci. Eng., 9, 370 (1961).

F4 F.L. Filmore, "Effective Group Absorption Cross-Section and Resonance Overlap," NAA-SR-11963, Atomics International (1966).

F5 S. Flugge, Neutrons and Related Gamma Ray Problems, Springer-Verlag, Berlin (1959).

F6 J.H. Ferziger, P.F. Zweifel, The Theory of Neutron Slowing Down in Nuclear Reactors, MIT Press (1966).

G1 M.V. Gregory, M.J. Driscoll, D.D. Lanning, "Heterogeneous Effects in Fast Breeder Reactors," COO-2250-1, MITNE-142 (1973).

G2 A.D. Galanin, Thermal Reactor Theory, Pergamon Press (1960).

G3 R. Goldstein, H. Brooks, "Intermediate Resonance Absorption in Nonhomogeneous System," Nucl. Sci. Eng., 20, 331 (1964).

G4 R. Goldstein, R. Cohen, "Theory of Resonance Absorptions of Neutrons," Nucl. Sci. Eng., 13, 132 (1962).

G5 A.J. Goodjohn and G.C. Pomraning, ed., "Intermediate Resonance Absorption," Reactor Physics in the Resonance and Thermal Region, Vol. II, 37, MIT Press (1966).

H1 A.F. Henry, Nuclear Reactor Analysis, MIT Press (1975).

H2 H.H. Hummel, R.N. Hwang, K. Philips, "Recent Investigation of Fast Reactor Reactivity Coefficients," ANL-7120, 413 (1965).

H3 H. Haggblom, "Computation of Resonance-Screened Cross Section by the Dorix-Speng System," AE-334, Stockholm, Sweden (1968).

H4 H. Henryson II et al., "A Code to Calculate Fast Neutron Spectra and Multigroup Cross Sections," ANL-8144 (1976).

H5 H. Honeck, "THERMOS, a Thermalization Transport Theory Code for Reactor Lattice Calculations," BNL-5826 (1961).

K1 O.K. Kadiroglu, M.J. Driscoll, I. Kaplan, "Uranium Self-Shielding in Fast Reactor Blankets," COO-2250-17, MITNE-178 (1976).

K2 K.D. Kirby, R.A. Karam, "A General Method for Generating Resonance Cross Sections for Heterogeneous Media." Nucl. Sci. Eng., 59, 215 (1976).

K3 C.N. Kelber, "An Extended Equivalence Relation," Nucl. Sci. Eng., 16, 329 (1963).

K4 R.B. Kidman et al., "The Shielding Factor Method of Generating Multigroup Cross-Sections for Fast Reactor Analysis," Nucl. Sci. Eng., 48, 189 (1972).

K5 R.B. Kidman et al., "Resonance Cross Shielding in Reactor Analysis," BNWL-1509, Battelle Northwest Laboratory (1970).

K6 R.B. Kidman, R.E. MacFarlane, "LIB-IV, A Library of Group Constants for Nuclear Reactor Calculations," LA-6260-MS, Los Alamos Scientific Laboratory (March 1976).

L1 T.C. Leung, M.J. Driscoll, I. Kaplan, and D.D. Lanning, "Neutronics of an LMFBR Blanket Mock-Up," COO-3060-1, MITNE-127 (1972).

L2 M.M. Levine, "Resonance Integral Calculations for U^{238} Lattices," Nucl. Sci. Eng., 16, 271 (1963).

L3 D.C. Leslie, J.G. Hill, A. Jonsson, "Improvements to the Theory of Resonance Escape in Heterogeneous Fuel," Nucl. Sci. Eng., 22, 78 (1965).

L4 J.R. Lamarsh, Introduction to Nuclear Reactor Theory, Addison-Wesley, Reading (1965).

L5 "LEOPARD - A Spectrum Dependent Non-Spatial Depletion Code," Westinghouse Electric Corporation WCAP-3269-26 (1963).

M1 G.I. Marchuk, V.P. Il'in, "Neutron Resonance Capture in an Annular Lump," in Theory and Methods of Nuclear Reactor Calculations, Consultants Bureau, New York, 147 (1964).

M2 R. Meghreblian, D. Holmes, Reactor Analysis, McGraw-Hill, New York (1960).

M3 J.C. Mougniot et al., "Breeding Gains of Sodium-Cooled Oxide-Fueled Fast Reactors," European Nuclear Conf. April 1975, Paris, translation: ORNL-tr-2994.

N1 D.A. Newmarch, "Errors Due to the Cylindrical Cell Approximation in Lattice Calculations," AEEW-R34, Atomic Energy Establishment Winfrith (1960).

O1 D. Okrent et al., ed., Computing Methods in Reactor Physics, Gordon & Breach, New York (1968).

P1 S. Pearlstein, ed., "Seminar on ^{238}U Resonance Capture," BNL-NCS-50451, Brookhaven National Laboratory (March 1975).

S1 G. de Saussure, R.B. Perez, "Present Status of Cross Section Data of the Fissile and Fertile Isotopes for Fast Reactors," Advanced Reactors: Physics, Design and Economics, Pergamon Press (1975).

S2 A. Sauer, "Approximate Escape Probabilities," Nucl. Sci. Eng., 16, 329 (1963).

S3 E.R. Seghal and R. Goldstein, "Intermediate Resonance Absorption in Heterogeneous Media," Nucl. Sci. Eng., 25, 174 (1966).

S4 P. Silvennoinen, Reactor Core Fuel Management, Pergamon Press, New York (1976).

S5 M. Segev, "Systematic Errors in Analytically Formulated Resonance Integrals," FRA-TML-80 (1975).

S6 M. Segev, "The σ Ambiguity in the Method of Self-Shielding Factors," Trans. Am. Nucl. Soc., 18, 555 (1974).

S7 M. Segev, "A Theory of Resonance-Group Self-Shielding," Nucl. Sci. Eng., 56, 72 (1975).

S8 J.R. Stehn, ed., The Physics of Intermediate Spectrum Reactors, Vol. III, Naval Reactors Physics Handbook, AEC (1958).

S9 A. Santamarina, "Effects De Protection Mutuelle Dans Les Interactions ^{238}U-^{235}U Et ^{238}U-^{239}Pu," Annals of Nucl. Energy, 3, 1 (1976).

T1 H. Takahashi, "Resonance Escape Probabilities in Circular Cylindrical Cell System," J.N. Energy, Part A: Reactor Science, 12, 26 (1960).

W1 C.R. Weisbin et al., "Fast Reactor Cross Section Processing Codes - Is There A Dollars Worth of Difference Between Them?" Advanced Reactors: Physics, Design and Economics, Pergamon Press (1975).

W2 G.L. Woodruff et al., "A Study of the Spatial Distributions of Fast Neutrons in Lattices of Slightly Enriched Uranium Rods Moderated by Heavy Water," AT(30-1)2344, MITNE-67 (1965).

Z1 P.F. Zweifel, "Neutron Self-Shielding," Nucleonics, 174, (1960).